

COORDINATION OF G PROTEIN AND MITOGEN-ACTIVATED PROTEIN KINASE
SIGNALING PATHWAYS BY BRANCHED-CHAIN AMINO ACID METABOLITE
SECOND MESSENGERS DURING OSMOTIC STRESS

James Paul Shellhammer

A dissertation submitted to the faculty at the University of North Carolina at Chapel Hill in partial fulfillment of the requirements for the degree of Doctor of Philosophy in the Department of Pharmacology in the School of Medicine.

Chapel Hill
2017

Approved by:

Henrik G. Dohlman

Lee M. Graves

Robert A. Nicholas

Jay E. Brenman

Michael J. Emanuele

© 2017
James Paul Shellhammer
ALL RIGHTS RESERVED

ABSTRACT

James Paul Shellhammer: Coordination of G Protein and Mitogen-Activated Protein Kinase Signaling Pathways by Branched-Chain Amino Acid Metabolite Second Messengers during Osmotic Stress

(Under the direction of Henrik G. Dohlman)

Cells experience a variety of environmental signals, often simultaneously. These signals may encode opposing effects, so the response must be coordinated in a manner that promotes cell and organismal well-being. The expression of surface receptors, such as G protein-coupled receptors (GPCRs), aids in the detection of bioactive molecules. Once perceived by the cell, the signal is transduced to intracellular signaling components that carry out the appropriate response. Mitogen-activated protein kinase (MAPK) cascades are commonly activated in response to external stimuli that range from growth factors to environmental stresses. The budding yeast *S. cerevisiae* employs MAPK pathways to respond to mating pheromones and environmental stresses. The pheromone response pathway is a MAPK pathway regulated by a GPCR, and the high osmolarity glycerol (HOG) pathway is a parallel MAPK pathway that shares some components with the pheromone response pathway. Signal fidelity is maintained during simultaneous activation of these and other MAPK pathways through mechanisms including signal strength and duration, feedback regulation, and cross-pathway inhibition. In this dissertation, I identify a new means by which parallel MAPK pathways are regulated. I show that activation of the HOG pathway promotes the production of second messenger molecules derived from branched-chain amino acids. These new second messengers promote phosphorylation of the α subunit regulating the pheromone response pathway, and lead to reduced downstream

transcriptional output. I also compare conventional and recently developed methods for analyzing MAPK activation and gene transcription. This work adds to our understanding of how signaling pathway cross-talk can maintain signal fidelity, and provides an update on the methods that can be used to best study these pathways for future discoveries.

To all first-generation graduate students, be proud of what you have done, and have faith in what you can achieve.

ACKNOWLEDGMENTS

The pursuit of a PhD is no easy task, and there are many people who have made the journey much more manageable and memorable. I think it is appropriate to first thank the man who encouraged me to embark on this journey to begin with, my undergraduate genetics professor and friend, Dr. Robert Hinrichsen. Next, I would like to thank my advisor, Dr. Henrik Dohlman for his fantastic mentorship throughout my time as a graduate student. He has always been supportive of my ideas and ambitions, provided excellent counsel, and taught me to be a better writer, presenter, and scientist. I will always admire his level-headed leadership and extraordinary patience. I would also like to thank my dissertation committee, Dr. Lee Graves, Dr. Rob Nicholas, Dr. Mike Emanuele, and Dr. Jay Brenman for their thoughtful and helpful guidance in completing this work. Thank you to Guowei Yin and Sharon Campbell for conducting the protein NMR experiments in Chapter 2, and to Beverly Errede for helpful conversations, plasmids, and teaching me how to do tetrad dissections.

The difference between a good graduate experience and a great one depends heavily on the people one associates with on a day-to-day basis. Thanks to the past and current members of the Dohlman lab, mine has been a great one. Special thanks to Dan Isom, who taught me many of the experimental techniques that I have learned, and also became much like an older brother with whom I could share my troubles and jublations. I would also like to thank Justin English, who was my first mentor in the Dohlman lab, and is someone with no shortage of scientific ideas. Thanks also to Sarah Clement and Gauri Dixit, my former cubicle buddies, with whom I've had some great chats, some more scientific than others.

During my time in graduate school, I have met hundreds of people. Some were passing acquaintances and a few have become my very good friends. I would especially like to thank Marissa Cann and Garrett Berry for their friendship since week one. I am glad it has remained strong throughout graduate school, and I hope it remains so afterward. I would also like to thank one of my oldest friends, Jim Zewe, with whom I attended high school and college, and have talked to nearly every day of graduate school. Thanks for keeping things in perspective, and being available for late-night Skype hangouts. Thank you also to Joe Zewe for advice on graduate school and coming out for annual hockey game trips.

They say you can pick your friends, but you can't pick your family. Given the choice, I wouldn't trade mine. Thank you to my parents, sisters, grandparents, and extended family, who have always been supportive and undoubting of my ability to succeed in graduate school.

Odd as it may be, I would like to thank my cat, Crouton, for being my companion while I sat at home writing this document. Though she spent most of the time asleep next to me, she also forced me to take necessary breaks to play with her or add more food to her bowl. Also, a cat is always willing to listen.

Last, but certainly not least, thank you to my loving fiancée Erin Soule, with whom I have shared half of my graduate school journey. She has always given an ear to listen to stories of lab trials and triumphs, and a shoulder to lean on during the inevitable slump. Her support for me through the final stages of graduate school has made all the difference. She has also shown me that not all Dookies are bad.

TABLE OF CONTENTS

LIST OF TABLES	x
LIST OF FIGURES	xi
LIST OF ABBREVIATIONS AND SYMBOLS	xiii
CHAPTER 1 – INTRODUCTION	1
Heterotrimeric G Protein Signaling	2
Second Messenger Signaling	6
Mitogen-Activated Protein Kinase Signaling	8
Osmotic Stress adaptation	9
Yeast as a Model Organism to Study Cell Signaling	11
The Yeast Pheromone Response Pathway: A Model for G Protein and MAPK Signaling	12
The High Osmolarity Glycerol Pathway: A Model for Stress Response Signaling	14
Metabolomics	16
Dissertation Summary	17
CHAPTER 2 – AMINO ACID METABOLITES THAT REGULATE G PROTEIN SIGNALING DURING OSMOTIC STRESS	19
Summary	19
Introduction	20
Results	23
Discussion	46
Materials and Methods	49

CHAPTER 3 – COMPARATIVE METHODS ANALYSIS FOR MEASURING MAPK- AND TRANSCRIPTIONAL ACTIVATION IN THE YEAST PHEROMONE RESPONSE PATHWAY.....	61
Summary.....	61
Introduction.....	62
Materials and Methods.....	63
Results and Discussion	69
Conclusions.....	89
CHAPTER 4 – GENERAL DISCUSSION AND CONCLUSIONS	91
Future Directions	93
Broader applications of this research.....	99
Concluding remarks	103
REFERENCES	104

LIST OF TABLES

Table 2.1 Metabolite fold-change values for Figure 2.3 heatmap.....	31
Table 2.2 Yeast strains used in this study.....	50
Table 2.3 Plasmids used in this study.....	51

LIST OF FIGURES

Figure 1.1 Heterotrimeric G protein activation cycle.	4
Figure 1.2 G protein signaling through effectors specific to G α subclasses.....	7
Figure 1.3 The yeast pheromone response pathway.	13
Figure 1.4 The yeast High Osmolarity Glycerol (HOG) pathway.	15
Figure 2.1 Phosphorylation of Gpa1 in response to osmotic stress occurs in a Hog1-dependent, pH-independent manner.	26
Figure 2.2 Additional stress conditions promote Gpa1 phosphorylation with differing effects on intracellular pH.....	27
Figure 2.3 Global metabolomics analysis identifies candidate second messengers for osmotic stress.	30
Figure 2.4 BCAA derivatives are necessary for a full response to osmotic stress.	34
Figure 2.5 Bat1 and Bat2 phosphorylation and abundance are unaffected by osmotic stress.	37
Figure 2.6 BCAA derivatives promote Gpa1 phosphorylation in the absence of osmotic stress.	39
Figure 2.7 BCAA derivatives do not bind directly to G proteins.	41
Figure 2.8 The AMPK kinase Elm1 phosphorylates Gpa1 upon BCAA derivative addition.	42
Figure 2.9 The AMPK kinase Elm1 phosphorylates Gpa1 upon osmotic stress or BCAA derivative addition.	43
Figure 2.10 BCAA derivatives diminish MAPK-dependent gene transcription.	45
Figure 3.1 Phosphorylation of Fus3 by conventional SDS-PAGE and immunoblotting with phospho-p44-42 antibodies.	72
Figure 3.2 Phosphorylation of Kss1 by conventional SDS-PAGE and immunoblotting with phospho-p44-42 antibodies.	75
Figure 3.3 Phosphorylation of Fus3 by Phos-tag SDS-PAGE and immunoblotting with Fus3 antibodies.....	79
Figure 3.4 Phosphorylation of Kss1-Myc by Phos-tag SDS-PAGE and immunoblotting with Myc-Tag antibodies.....	83

Figure 3.5 Pheromone-induced gene transcription assays.....	87
Figure 4.1 Model of BCAA derivatives as second messengers for osmotic stress.....	92
Figure 4.2 Osmotic stress-dependent, Hog1-dependent gene transcription.	98

LIST OF ABBREVIATIONS AND SYMBOLS

°C	Degrees Celsius
¹⁵ N	Nitrogen-15
¹ H	Proton
2D	2-dimensional
A or Ala	Alanine
ABC	ATP-binding cassette
ALD2	Aldehyde dehydrogenase 2
ALD4	Aldehyde dehydrogenase 4
AMPK	Adenosine monophosphate-activated kinase
ARI1	Aldehyde reductase intermediate 1
BAR1	Barrier to the alpha-factor response 1
BAT1	Branched-chain amino acid transaminase 1
BAT2	Branched-chain amino acid transaminase 2
BCAA	Branched-chain amino acid
BCAT	Branched chain aminotransferase
BCKDH	Branched-chain keto acid dehydrogenase
BirA	Bifunctional ligase/repressor A
CaMK	Calcium/calmodulin-dependent kinase
cAMP	Cyclic adenosine monophosphate
Cdc42	Cell division cycle 42
cGMP	Cyclic guanosine monophosphate
CVD	Cardiovascular disease

DAG	Diacylglycerol
DNA	Deoxyribonucleic acid
EC ₅₀	Half-maximal effective concentration
EGOC	Exit from G ₀ complex
EDTA	Ethylenediaminetetraacetic acid
ELM1	Elongated morphology 1
ERK	Extracellular signal-regulated kinase
FDG	Fluorescein-di-β-D-galactopyranoside
fQCR	Fast quantitative cysteine reactivity
FUS1	Cell fusion 1
FUS3	Cell fusion 3
g	Gram or force of gravity
G protein	Guanine nucleotide binding protein
G ₀	Quiescent state of the cell cycle
G ₁	Gap 1 phase of the cell cycle
G6PDH	Glucose-6-phosphate dehydrogenase
GABA	Gamma-aminobutyric acid
GAL1	Galactose metabolism 1
GAP	GTPase accelerating protein
GATOR	GAP activity towards Rags
GC-MS	Gas chromatography mass spectrometry
GDP	Guanosine diphosphate
GEF	Guanine nucleotide exchange factor

GFP	Green fluorescent protein
Glc	Glucose
GLC7	Glycogen 7
GPA1	G protein alpha subunit 1
GPCR	G protein-coupled receptor
GRX1	Glutaredoxin 1
GRX7	Glutaredoxin 7
GST	Glutathione S-transferase
GTP	Guanosine triphosphate
GTPase	Guanosine triphosphate hydrolase
G α	G protein alpha subunit
G $\beta\gamma$	G protein beta-gamma heterodimer
HCl	Hydrochloric acid
HIC	2-hydroxyisocaproate
HIV	2-hydroxyisovalerate
HKR1	<i>Hansenula mrakii</i> killer toxin resistant 1
HMVA	2-hydroxy-3-methylvaleric acid
HOG	High osmolarity glycerol
HOG1	High osmolarity glycerol 1
HSQC	Heteronuclear spin quantum correlation
IP ₃	Inositol 1, 4, 5-trisphosphate
IRI	Ischemia reperfusion injury
ITC	Isothermal titration calorimetry

JNK	c-Jun N-terminal kinase
K or Lys	Lysine
KCl	Potassium chloride
KSS1	Kinase suppressor of sst2 1
L	Liter
L or Leu	Leucine
LacZ	Lactose operon Z, β -galactosidase gene
LC-MS/MS	Liquid chromatography tandem mass spectrometry
m	Milli-
M	moles/Liter, molar
mAb	Monoclonal antibody
MAPK	Mitogen-activated protein kinase
MAPKK	Mitogen-activated protein kinase kinase
MAPKKK	Mitogen-activated protein kinase kinase kinase
MgCl ₂	Magnesium chloride
MI	Myocardial infarction
mRNA	Messenger ribonucleic acid
MSB2	Multicopy suppression of a budding defect 2
MSUD	Maple syrup urine disease
mTOR	Mammalian target of rapamycin
N	Nitrogen
NaCl	Sodium chloride
NaN ₃	Sodium azide

NFAT5	Nuclear factor of activated T-cells 5
NMR	Nuclear magnetic resonance
NSCLC	Non-small cell lung cancer
OD ₆₀₀	Optical density at 600 nanometers
OPY2	Overproduction-induced pheromone-resistant yeast 2
p21	Protein of 21 kilodaltons, small GTP binding protein
p38	Protein of 38 kilodaltons, mammalian stress response MAPK
p44/42	Proteins of 44 and 42 kilodaltons, ERK2 and ERK1
PBS2	Polymyxin B sensitivity
PDAC	Pancreatic ductal adenocarcinoma
PDR12	Pleiotropic drug resistance 12
pH	Negative logarithm of the proton concentration
pH _i	Intracellular pH
Phos-tag	Phosphate-binding tag
PKA	Protein kinase A
pK _a	Acid dissociation constant
PKC	Protein kinase C
PP1	Protein phosphatase 1
PVDF	Polyvinylidene fluoride
PX(S/T)P	MAPK consensus phosphorylation motif
R or Arg	Arginine
REG1	Resistance to glucose repression 1
RGS	Regulator of G protein signaling

ROS	Reactive oxygen species
RSD	Relative standard deviation
SAK1	Snf1-activating kinase
SAPK	Stress-activated protein kinase
SCD	Synthetic complete dextrose medium
SDS	Sodium dodecyl sulfate
SDS-PAGE	Sodium dodecyl sulfate polyacrylamide gel electrophoresis
SEA	Seh1 associated complex
SHO1	Synthetic, high osmolarity-sensitive
SLN1	Synthetic lethal of N-end rule
SNF1	Sucrose non-fermenting 1
SPR	Surface plasmon resonance
SSK1	Suppressor of sensor kinase
STE11	Sterile 11
T or Thr	Threonine
TAC	Transaortic constriction
TAP	Tandem-affinity purification
TBS-T	Tris-buffered saline with Tween 20
TCA	Trichloroacetic acid or tricarboxylic acid cycle
THI4	Thiamine metabolism
TIF	Tagged image file
TKL2	Transketolase 2
T _m	Mean temperature of unfolding

TORC	Target of rapamycin complex
TOS3	Target of Sbf 3
tRNA	Transfer ribonucleic acid
UPLC	Ultra-performance liquid chromatography
UV	Ultraviolet
V	Volts
WT	Wild-type
YPD1	Tyrosine phosphatase dependent 1
Zn(NO ₃) ₂	Zinc nitrate
Δ	Deletion
μ	micro

CHAPTER 1 – INTRODUCTION

The environment in which a cell exists is ever changing. To survive, the cell must be able to take in information about its environment, process this information, and execute a response that permits adaptation to the changes. This is true throughout all of life, but here the focus is on eukaryotic systems. Eukaryotes have evolved sophisticated cellular signaling systems that are used to relay information about the surroundings of the cell to the inside of the cell, where adaptive changes are executed. Among the most studied molecules responsible for detecting extracellular signals are G protein-coupled receptors (GPCRs). These cell membrane proteins serve crucial functions in maintaining homeostasis, and regulate critical processes including heart rate, blood pressure, and neurotransmission. As such, GPCRs are molecular targets for drugs that regulate these and other processes.

In addition to maintaining homeostasis, cells must respond to signals that promote cell growth and proliferation, as well as signals that are detrimental to the well-being of the cell or organism. For these processes, cells employ an extremely well-conserved intracellular signaling module called the mitogen-activated protein kinase (MAPK) cascade. MAPKs are serine/threonine kinases that are activated in response to extracellular cues, such as growth factors, hormones, and cytokines that promote cell growth, proliferation, or motility. MAPKs are also activated in response to cell stressors, such as ultraviolet irradiation, oxidative stress, and osmotic stress, and serve to increase production of proteins that can help the cell to overcome the stressful environment [1].

These are but two examples of many types of signaling pathways that exist in eukaryotic cells, and even within GPCR and MAPK pathways there are several classes of each protein, and MAPKs are activated downstream of a variety of receptor types, including GPCRs [2]. At any given time, the extracellular environment may contain hundreds of potential ligands for membrane receptors, in addition to any physical stimuli that can exert a cellular response. As such, many signaling cascades are active simultaneously, and some components of these cascades are shared among other pathways. In order to properly process the information that is presented to a cell, it must have mechanisms in place to maintain signaling fidelity. Cell-type-specific expression of proteins and compartmentalization of molecules help to greatly reduce the potential for aberrant signaling. Crosstalk between signaling pathways is another mechanism by which cells maintain signaling fidelity [3]. In this work, I identify a new means by which one MAPK pathway can regulate a parallel MAPK pathway by promoting the production of new second messenger molecules that regulate upstream G protein signaling. This work adds to a growing body of work from the Dohlman lab that serves to highlight the importance of signaling pathway crosstalk in maintaining signal fidelity in the face of a complex environment [4, 5].

Heterotrimeric G Protein Signaling

The most prominent class of druggable molecules is comprised of G protein-coupled receptors (GPCRs). Currently, an estimated 30% of all prescription drugs target members of the GPCR family [6]. These receptors are seven-transmembrane-spanning molecules that serve to transmit an extracellular cue, such as light [7], smell [8] or taste [9], or the presence of hormones or neurotransmitters, to the inside of the cell, where an appropriate physiological response can then be executed [10].

The first step in executing the response to an activated GPCR is the activation of the associated heterotrimeric G protein. G proteins are so-named for their ability to bind guanine nucleotides. The specific guanine nucleotide that is bound to the G protein dictates its state of activity. A G protein bound to guanosine diphosphate (GDP) is inactive, whereas a G protein bound to guanosine triphosphate (GTP) is considered to be active. In addition to its ability to bind to guanine nucleotides, a G protein also possesses the ability to hydrolyze the gamma phosphate on GTP to yield GDP. In this way, G proteins act as molecular switches that cycle between the “on” and “off” states. While G proteins can intrinsically convert from the “on” state to the “off” state, and subsequently release GDP and bind a new GTP molecule, the rates for these processes are very slow [11]. Cells have evolved the ability to use the switch-like properties of G proteins to control when particular effector molecules are activated. This is achieved by accelerating the rates of GDP exchange and GTP hydrolysis in a four-stage G protein signaling cycle (Figure 1.1), beginning with an inactive, GDP-bound G protein.

The role of the GPCR is to act as guanine nucleotide exchange factor (GEF) to facilitate the exchange of GDP for GTP, and thereby turn the switch to the “on” position. Upon agonist binding, the GPCR undergoes a conformational change that is transmitted through the entire protein to alter the three-dimensional structure of the intracellular domain. This altered structure is preferred for association with the heterotrimeric G protein, and subsequent nucleotide exchange. A G protein heterotrimer consists of the $G\alpha$ subunit, which possesses the guanine nucleotide binding and hydrolytic functions, and the obligate heterodimer, $G\beta\gamma$. The $G\alpha$ subunit is composed of two domains—the Ras-like domain (so-called because of its structural similarity to the small GTPase, Ras), and the α -helical domain [12-14]. Upon GTP binding to $G\alpha$, conformational changes in three “switch regions” in the Ras-like domain promote dissociation of

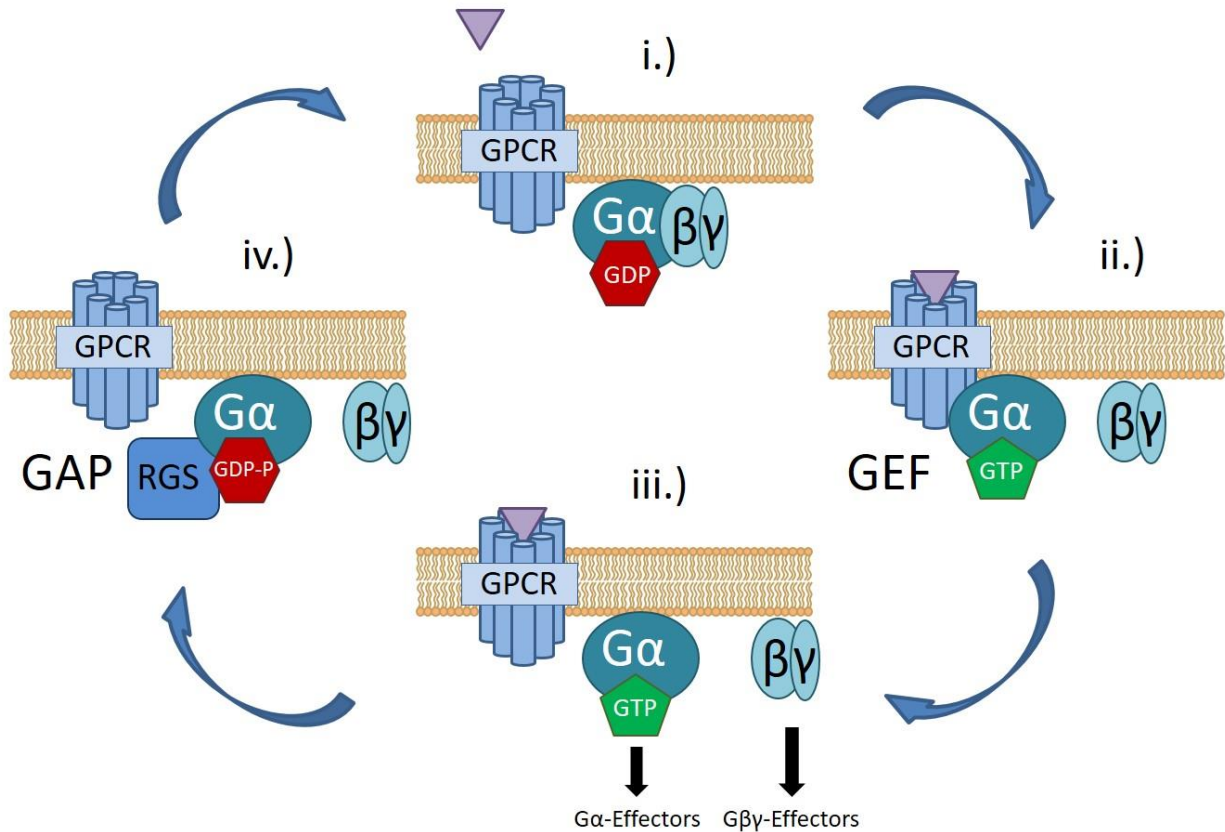


Figure 1.1 Heterotrimeric G protein activation cycle.

i.) In the absence of a GPCR-activating ligand, the G protein is in the inactive, GDP-bound state, with all three subunits ($G\alpha$ and $G\beta\gamma$) in complex. ii.) Upon agonist binding, the GPCR acts as a guanine nucleotide exchange factor for the $G\alpha$ subunit, promoting exchange of GDP for GTP and dissociation of $G\beta\gamma$ from $G\alpha$. iii.) Activated, GTP-bound $G\alpha$ and dissociated $G\beta\gamma$ are free to interact with downstream effectors to transmit the GPCR-activating signal. iv.) Regulator of G protein signaling proteins interact with $G\alpha$, and act as GTPase accelerating proteins to by stabilizing the transition state (GDP-P) of nucleotide hydrolysis. Hydrolysis of GTP to GDP returns $G\alpha$ to the inactive state, promoting re-association with $G\beta\gamma$ and termination of the signal.

G $\beta\gamma$ from G α . Both dissociated subunits can then go on to bind effector molecules in the next step of G protein signal transduction. Signaling events following activation of the G protein serve to regulate the duration for which the G protein remains in the “on” state. One way that G protein signaling is terminated is through interaction with members of the Regulator of G protein Signaling (RGS) family of proteins. RGS proteins act as GTPase accelerating proteins (GAPs) to increase the rate of GTP hydrolysis [15] by stabilizing the hydrolytic transition state, and thus serve to turn the switch to the “off” position [16]. The re-formation of a GDP-bound G α and reassociation with G $\beta\gamma$ completes the cycle of G protein activation.

In addition to this canonical scheme, G proteins can be regulated through phosphorylation and other post-translational modifications, including myristoylation [17], palmitoylation [18], and ubiquitination [19, 20]. The lipid modifications serve to localize G proteins to the plasma membrane, and therefore promote closer proximity to the GPCRs that activate them. The role of G α phosphorylation is more complex, and less understood.

The work in this dissertation is primarily focused on phosphorylation of the yeast G α subunit, Gpa1. As the goal for conducting research in model organisms, such as yeast, is to be able to translate those findings to the human system, here I will briefly introduce what is known about phosphorylation of mammalian G proteins, and details on Gpa1 phosphorylation will be covered in the next chapter. Several G α family members have been identified as being modified by phosphorylation. The kinases responsible for these phosphorylation events were identified as protein kinase A (PKA) [21, 22], protein kinase C (PKC) [23], calcium/calmodulin-dependent protein kinase (CaMK) [24], and Src [25]. The consequences of phosphorylation vary and include reduced affinity for guanine nucleotides [22], inhibition of interaction with G $\beta\gamma$ [23], reduced binding with RGS proteins [26], and inhibition of interaction with downstream effectors

[21]. However, conclusive consequences of $G\alpha$ phosphorylation on overall signaling in mammals are still poorly understood.

Second Messenger Signaling

There are 16 mammalian $G\alpha$ subunits, and they can be divided into four classes based on the main effector molecules with which they interact [27]. These sub-type based classes are $G\alpha_s$, $G\alpha_i$, $G\alpha_q$, and $G\alpha_{12/13}$. The first three of these four classes work to control second messenger production, while the fourth is involved in cell polarity (Figure 1.2) [27, 28]. The concept of second messenger signaling originates from work by Earl Sutherland in 1957 [29] when he discovered that liver phosphorylase was stimulated indirectly by hormones, requiring a “heat-stable factor” that was later identified as cyclic adenosine monophosphate (cAMP) [30]. Second messenger signaling is now recognized as an entire paradigm of cell signaling. In this paradigm, signaling is initiated by a first messenger (e.g., hormone or neurotransmitter) that activates a cell surface receptor (canonically a GPCR). Activation of the receptor leads to activation of intracellular effector molecules (e.g., adenylate cyclase) that produce the second messenger molecule (e.g., cAMP). The production of second messengers greatly amplifies the original signal, promoting a rapid and robust intracellular response [31]. Over the years, many additional second messengers have been identified. These include cGMP [32], inositol trisphosphate (IP_3) [33, 34], diacylglycerol (DAG) [35], and calcium [36]. The work in this dissertation presents a new class of second messengers produced not by G protein signaling, but through activation of the stress-response mitogen-activated protein kinase (MAPK) pathway. I find that these second messengers promote phosphorylation of the yeast $G\alpha$, Gpa1, and serve to regulate a parallel MAPK pathway that is controlled by the G protein.

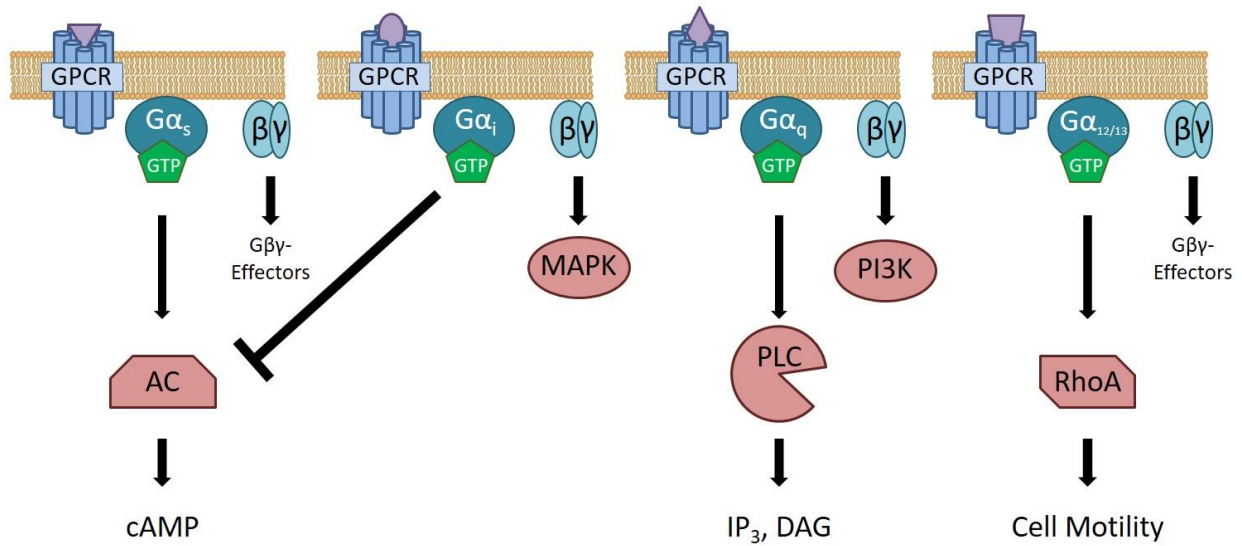


Figure 1.2 G protein signaling through effectors specific to $G\alpha$ subclasses.

$G\alpha_s$, $G\alpha_i$, and $G\alpha_q$ subclasses regulate second messenger production, while $G\alpha_{12/13}$ has roles in cytoskeletal rearrangement and cell motility. From left, $G\alpha_s$ family proteins increase cAMP through activation of adenylate cyclase (AC). $G\alpha_i$ family proteins decrease cAMP through inhibition of AC. $G\alpha_q$ family proteins increase IP_3 and DAG through activation of phospholipase C (PLC). $G\alpha_{12/13}$ family members promote cell motility through small GTPases, such as RhoA. $G\beta\gamma$ subunits have signaling effects including activation of PI3 kinase and indirect activation of MAPK pathways.

Mitogen-Activated Protein Kinase Signaling

Mitogen-activated protein kinases (MAPKs) are a class of cytoplasmic enzymes that are activated by various extracellular signaling cues, ranging from mitogens (as the name suggests), growth factors, cytokines and signals activating GPCRs, to environmental stress stimuli. MAPKs are the terminal component of a three-tiered kinase cascade module consisting of the MAP kinase kinase kinase (MAPKKK), the MAP kinase kinase (MAPKK) and the MAPK, as well as a scaffolding protein to bring the three kinase components together. The MAPK module has been highly conserved throughout evolution among all eukaryotes, emphasizing the efficiency of such a protein complex in signal transduction. The MAPK is activated via phosphorylation by the MAPKK on conserved tyrosine and threonine residues. In turn, the activated MAPK recognizes and phosphorylates the serine or threonine in a specific PX(S/T)P motif on protein substrates in the cytoplasm and nucleus to regulate functions such as cell proliferation and adaptation to stressful or damaging stimuli. Deactivation of MAPKs is regulated by dephosphorylation by specific MAPK phosphatases [1].

Humans possess four major MAPK pathways—the extracellular signal-regulated kinase (ERK)1/2 pathway, the p38 MAPK pathway, the c-Jun N-terminal kinase (JNK) pathway, and the ERK5 pathway [1]. The ERK1/2 pathway is activated by a range of growth factors and cytokines, and is involved in cell growth and proliferation. The p38 MAPK and JNK pathways, also called stress-activated protein kinases (SAPKs), are activated in response to environmental stressors, such as oxidative stress, ultraviolet irradiation, osmotic stress, and heat shock, as well as inflammatory cytokines [1]. ERK5, like ERK1/2, responds to growth factors and carries out many similar functions in cell-cycle regulation, but also has specific roles in cardiovascular development, angiogenesis, and neuronal differentiation [37].

The modular design of MAPK pathways helps to increase the versatility of MAPK systems, but also increases the potential for aberrant signaling. Despite only four main pathways, there exist at least 20 MAPKKKs, 7 MAPKKs, and 11 MAPKs. Thus, different MAPK modules can be assembled in response to different activating signals to achieve different functions, including transcription, proliferation, cell motility, cell death, and development [38]. In order to maintain signal fidelity, cells have developed multiple regulatory mechanisms. Part of this regulation is achieved through cell-type-specific expression of the different isoforms. Regulation in cells expressing the same isoforms is achieved through multiple mechanisms, localization, docking domain specificity, signal duration and intensity, and feedback phosphorylation by activated MAPKs [3, 4]. In this work, I identify another means by which MAPK signaling specificity can be regulated through pathway crosstalk; production of second messenger molecules is initiated by one MAPK pathway to control the activity of a parallel MAPK pathway.

Osmotic Stress adaptation

The response to different physical or chemical stresses is mediated by MAPK pathways networks. For example, ultraviolet irradiation and oxidative damage, inflammatory cytokines, and osmotic shock promote signaling through activation of the p38 and JNK MAPK pathways [39-41]. While much progress has been made in understanding the intracellular response to conditions such as oxidative stress and ultraviolet radiation damage, the processes involved in osmotic stress are often overlooked in relation to human health.

Osmotic stress occurs when the solute concentration (osmolarity) in the extracellular space deviates from the osmolarity of the intracellular space. A higher osmolarity in the

extracellular space relative to the intracellular space is considered a hyperosmotic stress, and a lower osmolarity in the extracellular space relative to the intracellular space is a hypo-osmotic stress. Hereafter, osmotic stress will refer to hyperosmotic stress. Upon encountering osmotic stress, cells rapidly lose water through osmosis in order to normalize the osmotic balance between the intracellular and extracellular space. The loss of intracellular water results in cell shrinkage. In cases of severe osmotic stress, this cell shrinkage can lead to macromolecular crowding and, thus, a hampered ability for biochemical processes to occur [42]. Under less-severe osmotic stress, cells initiate signaling events that promote reactive oxygen species (ROS) production, DNA damage, cell cycle arrest, and apoptosis [43].

In addition to these negative effects, cells also initiate signaling events that promote adaptation to osmotic stress by activating p38 MAPK. Upon activation, p38 MAPK phosphorylates the transcription factor NFAT5, which promotes the transcription of osmoprotective target genes. These include genes associated with the synthesis and transport of osmolytes, antioxidants, and molecular chaperones [44-46].

Several tissues routinely experience osmotic stress, and can develop disease if osmoregulation is impaired. For example, osmotic stress in ocular tissue can promote dry eye disease [47] and diabetic retinopathy [48], and high osmolarity in the vasculature can lead to hyperosmolar hyperglycemic state in diabetics [49], and various cardiovascular complications caused by hypertension and changes in erythrocyte deformability [50, 51]. The pathways used to activate the cellular response to osmotic stress appear to be, in some ways, cell type specific [51], emphasizing the need for a more complete understanding of the osmotic stress response to aid in developing treatment strategies for associated pathologies.

Yeast as a Model Organism to Study Cell Signaling

Studying the mechanisms of pathway cross-talk and coordination is often challenging due to the expression of multiple protein isoforms, and differences in the expression of these isoforms among various cell types and tissues. Researchers often seek ways to simplify the complex human system by using model organisms that retain many of the desired features for study, but offer a more manageable number of components. This allows us to gain a basic understanding of how a given system works that can be built upon by moving into higher, more complex systems of study. The budding yeast, *Saccharomyces cerevisiae*, has been one of Nature's greatest gifts to mankind. In addition to its uses for hundreds of years in baking and brewing, yeast offer scientists the ability to study signaling pathways and processes in the simplest of eukaryotic systems.

Yeast exists stably in both diploid and haploid states. Using haploid cells affords a high degree of genetic tractability, making studies involving gene deletion or point mutation much easier than in a diploid system. Strain libraries are available that contain strains harboring individual deletion of each non-essential gene [52] and inducible knock-down of essential genes [53], as well as epitope-tagged versions of each protein with TAP [54] or GST [55] for purification or identification by immunoblotting, and GFP [56] for determining cellular localization or expression levels by microscopy or flow cytometry. Yeast also grow and reproduce quickly, with a cell division cycle that lasts roughly two hours, reducing the time scale necessary for completing experiments. Finally, and perhaps most importantly, yeast possess well-characterized signaling pathways whose component proteins have been highly conserved throughout evolution. Two such pathways are the G protein signaling and MAPK pathways [57, 58]. In contrast to mammals, which possess ~800 GPCRs, 16 G α subunits, and 11 MAPKs, yeast

possess 3 GPCRs, 2 G α subunits, and 5 MAPKs, thus greatly simplifying the task of understanding how these pathways operate and coordinate. Two yeast MAPK pathways are most similar to mammalian MAPK pathways. The yeast pheromone response pathway is highly homologous to the mammalian ERK1/2 pathway in its roles in cell growth and proliferation, and the yeast high osmolarity glycerol pathway is homologous to the p38 MAPK pathway in its role in responding to environmental stress. These pathways are described below.

The Yeast Pheromone Response Pathway: A Model for G Protein and MAPK Signaling

Yeast exist in two haploid mating types: **a**-type and α -type. To form a diploid **a**/ α cell, the two haploid types must mate. Much like higher eukaryotic organisms, yeast use pheromones to attract a mate. The **a**-type cells secrete a peptide pheromone called **a**-factor, and α -type cells secrete a pheromone called α -factor. These pheromones act as chemotropic agents; upon sensing the pheromone from the opposite mating type, cells will form a mating projection, or “shmoo”, toward the source of the pheromone gradient (a.k.a. a mating partner), until the two cells ultimately fuse to form a diploid cell. Mating pheromones also act to arrest the cell cycle in the G1 stage, and to promote transcription of genes necessary for the mating response and cell fusion. The signaling pathway responsible for sensing and carrying out the mating response, called the pheromone response pathway, is a canonical GPCR signaling pathway that regulates a prototypical MAPK cascade (Figure 1.3) [59].

The pheromone response pathway is activated upon binding of mating pheromone to a GPCR (Ste2 in **a**-cells, Ste3 in α -cells) [60]. As described above, GPCRs act as GEFs for heterotrimeric G proteins, promoting the exchange of GDP for GTP in the G α subunit (Gpa1) and subsequent dissociation of G $\beta\gamma$ (Ste4/Ste18). Once dissociated from Gpa1, Ste4/Ste18

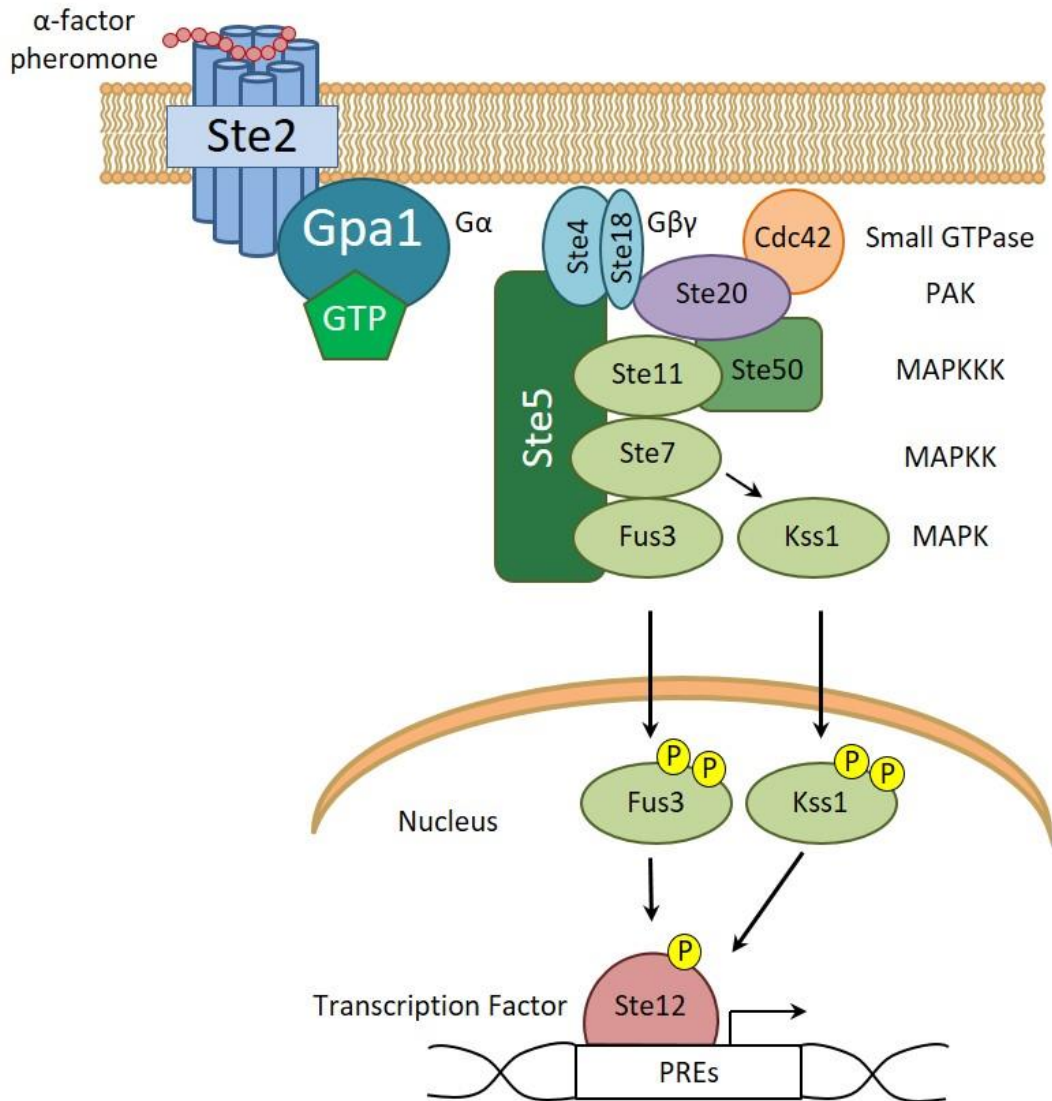


Figure 1.3 The yeast pheromone response pathway.

Yeast detect mating pheromone from opposite mating types by a GPCR. Here, the GPCR Ste2 expressed on an **a**-type cell detects α -factor secreted by an α -type cell. Exchange of GTP for GDP in the Gpa1(G α) promotes dissociation of Ste4/Ste18 (G $\beta\gamma$). Free G $\beta\gamma$ recruits the MAPK scaffold protein Ste5 and the PAK Ste20 (membrane-localized by Cdc42) into complex. The MAPKKK Ste11 is recruited to Ste5, and then brought into activation proximity to Ste20 by the adapter protein Ste50. The MAPKK Ste7 and MAPK Fus3 are recruited to Ste5. Activation of Ste11 by Ste20 promotes activation of Ste7, and subsequently, Fus3. The MAPK Kss1 is activated by Ste7, but does not require scaffolding. Activated Fus3 and Kss1 translocate to the nucleus, where they phosphorylate the transcription factor Ste12, promoting transcription of pheromone response elements (PREs). Kinases in the MAPK module are shown in light green.

recruits and binds to the MAPK scaffolding protein Ste5, and the p21-activated kinase Ste20. The adapter protein Ste50 is associated with Ste20, and serves to recruit the MAPKKK, Ste11 to the scaffold, where upon activation by Ste20, Ste11 activates the MAPKK, Ste7. Subsequently, the MAPK, Fus3 is activated upon binding with Ste5 [57, 61]. A second MAPK, Kss1 is also activated by Ste7, but does not require scaffolding by Ste5 [62]. Once activated, Fus3 and Kss1 translocate to the nucleus and phosphorylate the pathway-specific transcription factor Ste12, which then promotes transcription of genes required for cell mating (Figure 1.3) [63, 64].

The High Osmolarity Glycerol Pathway: A Model for Stress Response Signaling

Yeast use a MAPK pathway parallel to the pheromone response pathway to respond to osmotic stress. The High Osmolarity Glycerol, or HOG, pathway is activated upon increases in extracellular osmolarity [65]. Unlike the pheromone response pathway, the HOG pathway can be activated by two distinct branches that later converge on the MAPKK, Pbs2 (Figure 1.4). In addition to its role as MAPKK, Pbs2 serves as the scaffold protein for the HOG MAPK module [66]. The MAPK, Hog1 is the yeast ortholog of mammalian p38 MAPK [58].

The first branch of the HOG pathway is the Sho1 branch. Increased extracellular osmolarity is detected by two osmosensor proteins, Hkr1 and Msb2 [67]. The signal is then transmitted to the inside of the cell by another transmembrane protein, Sho1. The detailed mechanism by which this is achieved is unknown. However, Sho1 and an associated membrane protein Opy2 appear to have important functions in scaffolding the p21-activated kinase, Ste20 and the activated small G protein Cdc42. These two proteins are also employed in the pheromone response pathway, and similarly, recruit the MAPKKK Ste11 and the adapter protein Ste50 to the cell membrane. Sho1 also serves as a scaffold for the MAPKK, Pbs2. Hog1 is then recruited

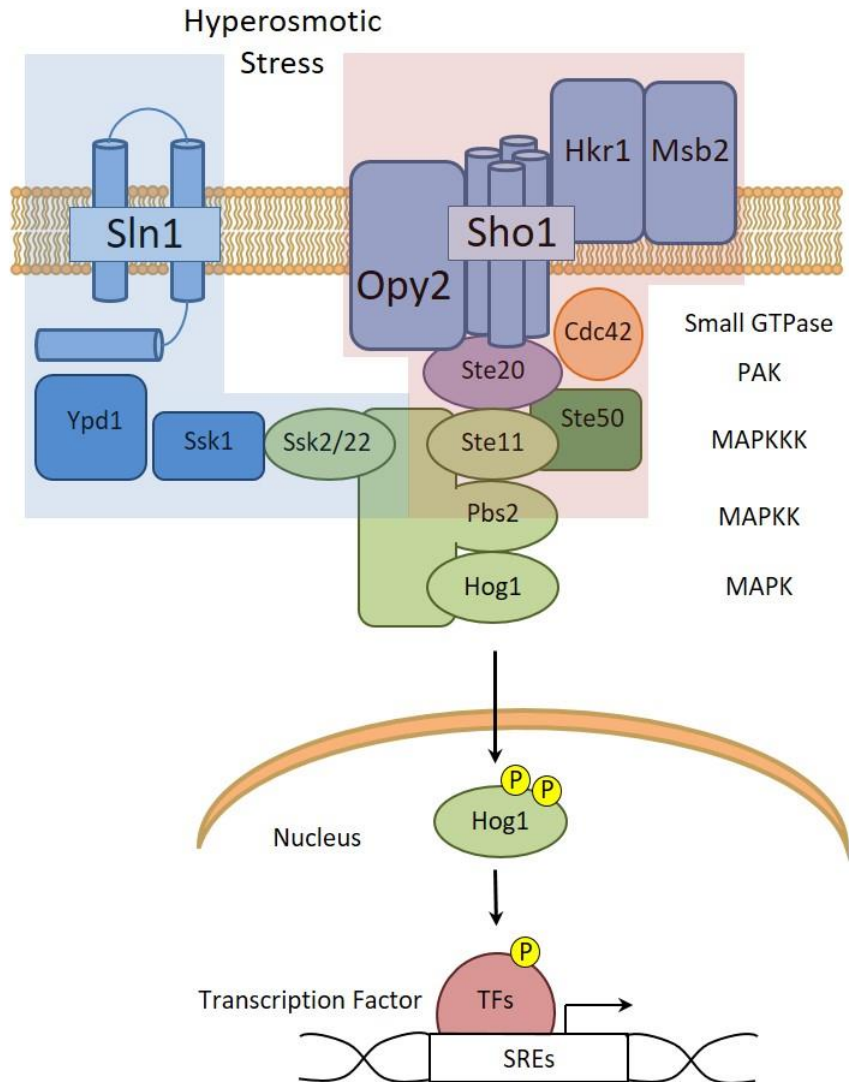


Figure 1.4 The yeast High Osmolarity Glycerol (HOG) pathway.

The response to hyperosmotic stress is mediated by a MAPK pathway with two upstream input branches that converge on the MAPKK, the Sln1 branch (left shaded) and the Sho1 branch (right shaded). The Sln1 branch uses a histidine kinase/receiver protein (Sln1) and phospho-relay system through Ypd1 and Ssk1 to maintain pathway deactivation. Hyperosmotic stress disrupts Sln1 histidine kinase activity and releases inhibiting phosphorylation on Ssk1, promoting activation of the MAPKKKs Ssk2/22. The Sho1 branch uses mucin-related proteins Hkr1 and Msb2 to sense hyperosmotic stress. The signal is transmitted across the cell membrane by Sho1 and Opy2, which recruit Active Cdc42 and associated Ste20 to the membrane. As with the pheromone response pathway, Ste20 activates the MAPKKK Ste11. MAPKKK activation by either branch results in activation of the scaffold/MAPKK Pbs2, and subsequent activation of the MAPK Hog1. Active Hog1 translocates to the nucleus to phosphorylate transcription factors, promoting transcription of stress response elements (SREs). Hog1 also phosphorylates cytoplasmic proteins to promote stress adaptation.

to and activated by Pbs2 (Figure 1.4) [65].

The second branch of the HOG pathway is the Sln1 branch. A loss in turgor pressure associated with increased extracellular osmolarity is sensed by the histidine kinase/receiver protein, Sln1, that is similar to the two-component systems in prokaryotes [68]. Sln1, Ypd1, and Ssk1 form a phospho-relay system that is active during normal conditions. Phosphorylation of Ssk1 is inhibitory to its catalytic function. Upon sensing osmotic stress, The Sln1 two-component system is disrupted, and the phospho-relay is deactivated. Ssk1 inhibition is relieved, and Ssk1 phosphorylates the redundant MAPKKKs Ssk2/Ssk22 [65]. These MAPKKKs then activate the MAPKK, Pbs2, which phosphorylates and activates Hog1. Upon activation, Hog1 phosphorylates cytoplasmic and nuclear proteins to aid in the restoration of osmotic equilibrium through synthesis of osmolytes, such as glycerol and trehalose, export of ions, and stress response gene transcription (Figure 1.4) [69].

Metabolomics

In the on-going search for a more-complete understanding of how physiological systems function and how these systems develop disease, “-omics” technologies have come to take the foreground. Omics approaches allow the functional monitoring of many cellular pathways simultaneously. Systems biology methods have been developed to conduct global analyses of each component of the central dogma of biology—DNA (genomics), mRNA (transcriptomics), and protein (proteomics)—and extended one step further to examine the small-molecule products of enzymatic reactions, metabolites (metabolomics) [70]. One goal for these approaches is to be able to characterize the networks that regulate cell function in an unbiased and systematic description way. Once we truly understand how a cell functions on the global scale, we can

better develop treatments for when these networks are compromised. A long-term goal for these approaches then is to develop personalized medicine, where treatment is designed based on the specific disease state of an individual. While we still may be far from achieving this goal, -omics technologies have contributed to great leaps forward.

Metabolomics presents the ability to examine a nearly complete complement of small molecules present in a given cell type through mass spectrometry- and NMR-based approaches. After extraction of metabolites from cell lysates, supernatants, body fluids, or tissues, samples can be analyzed by LC-MS/MS [71], GC-MS [72], and/or NMR [73]. The spectra are compared to a library of spectra of known metabolites, and the metabolome of the sample is identified. Metabolomes from different mutants and/or cells subjected to different treatment conditions can be compared to answer a variety of scientific questions. In this way, progress has been made in identifying biomarkers and metabolic signatures for diseases such as obesity [74], diabetes [75], heart failure [76], and differential effects of disease in hosts of altered microbiomes have been mapped [77-79]. Here, we use a metabolomics approach to identify 2-hydroxy branched-chain amino acid derivatives as second messengers of osmotic stress.

Dissertation Summary

The remaining sections of this dissertation are presented in three chapters. In Chapter 2, “Amino Acid Metabolites that Regulate G Protein Signaling during Osmotic Stress”, I present the identification of a new class of second messenger molecules derived from the three branched-chain amino acids, valine, leucine, and isoleucine. I identified these second messengers by a comprehensive metabolomics screen, and found that they are produced in a manner dependent upon osmotic stress, and requiring the yeast stress-response MAPK, Hog1. Through functional

studies, I found that these second messengers are necessary and sufficient to promote the phosphorylation of the yeast G α , Gpa1, and serve to diminish the output of the pheromone response MAPK pathway. Through this work, I propose that in addition to its canonical role as a regulator of second messenger production, the G protein can be regulated by second messengers produced through activation of the stress-responsive MAPK pathway in a new mechanism of pathway coordination.

In Chapter 3, I present a methods update for studying MAPK pathways, focusing on phosphorylated MAPK western blotting and pathway-specific transcriptional reporter assays. I compare conventional immunoblot analysis using standard SDS-PAGE, followed by probing with phospho-specific antibodies, and the recently developed Phos-tag immunoblotting method, where individual phosphorylated species are separated in proportion to the number of phosphorylation sites. To analyze transcriptional output, I compare an enzyme-based β -galactosidase assay and a fluorescent protein based GFP assay. These assays are compared in the yeast pheromone response pathway, but can be adapted for use in studying MAPK pathways in other organisms.

Finally, in Chapter 4, “General Discussion and Conclusions”, I discuss the broader impacts of my dissertation research, offer future directions for this research, and speculate on the future directions of the field.

CHAPTER 2 – AMINO ACID METABOLITES THAT REGULATE G PROTEIN SIGNALING DURING OSMOTIC STRESS

Summary

All cells respond to osmotic stress by implementing molecular signaling events to protect the organism. Failure to properly adapt can lead to pathologies such as hypertension and ischemia-reperfusion injury. Many signaling nodes, including mitogen-activated protein kinases (MAPKs), are activated in response to osmotic stress and by signals acting through G protein-coupled receptors (GPCRs). For proper adaptation, the action of these kinases must be coordinated. To identify second messengers of stress adaptation, we conducted mass spectrometry-based global metabolomics profiling analysis, quantifying nearly 300 metabolites in the yeast *S. cerevisiae*. We show that three branched-chain amino acid (BCAA) metabolites increase in response to osmotic stress and require the MAPK Hog1. Ectopic addition of BCAA derivatives promotes phosphorylation of the G protein α subunit and dampens G protein-dependent transcription, similar to that seen in response to osmotic stress. Conversely, genetic ablation of Hog1 activity or the BCAA-regulatory enzymes leads to dampened phosphorylation of $G\alpha$ and increased gene transcription. Taken together, our results define a new class of second messengers that regulate a novel cross-talk mechanism for adapting to osmotic stress.

Introduction

Cells routinely experience changing and often unfavorable conditions in their environment. The ability to adapt to environmental stress and re-establish homeostasis is essential not only to the survival of a cell, but also to the well-being of the organism. The response to such physical or chemical stresses is mediated by well-defined signaling networks. For example, changes in nutrient availability switch signaling between the opposing mammalian target of rapamycin (mTOR) and AMP-activated protein kinase (AMPK) pathways [80, 81] and promote signaling through the ERK2 mitogen-activated protein kinase (MAPK) [82]. Stressors such as UV irradiation, inflammatory cytokines, and osmotic shock promote signaling through activation of the p38 and c-Jun N-terminal Kinase (JNK) MAPK pathways [39-41]. While much is known about the mechanisms of stress-dependent signaling, less is known about the mechanisms of cross-pathway signal coordination. In this study, we report the regulatory effects of signaling cross-talk between osmotic stress and G protein-coupled receptor (GPCR) signaling pathways.

Hyperosmotic stress causes water efflux and cell shrinkage in order to normalize the osmotic balance between the intracellular and extracellular space. Depending on the severity of the stress, cell shrinkage can lead to macromolecular crowding and alterations in cellular protein activity [42], the production of reactive oxygen species (ROS), DNA damage, cell cycle arrest, and apoptosis [43]. In addition to these negative effects, cells also initiate signaling events that promote adaptation. Most prominently, in eukaryotes osmotic stress activates homologs of the stress response MAPK p38, which in turn phosphorylates myriad downstream targets that coordinate osmotic stress adaptations. This includes targets such as the transcription factor NFAT5, which promotes the transcription of osmoprotective target genes, including those

associated with the synthesis and transport of osmolytes, antioxidants, and molecular chaperones [44-46]. These changes ensure the survival of the cell, and they are likely to have important consequences for other signaling pathways via cross-talk mechanisms.

Previously, we have shown that cross-talk between nutrient sensing and GPCR pathways causes phosphorylation of the $G\alpha$ subunit [5], the principle transducer of GPCR signals. As the largest receptor family in humans [4], GPCRs respond to a wide variety of homeostatic cues, such as hormones and neurotransmitters, as well as to environmental signals such as odors and light through intracellular heterotrimeric G proteins, comprised of $G\alpha$ and $G\beta\gamma$ subunits. G proteins in turn serve to transmit signals between activated GPCRs and downstream effectors. Activation of effector proteins promotes production of second messenger molecules such as calcium or cAMP, which bind to and activate intracellular protein kinases. Another mechanism of GPCR signaling entails the direct activation of protein kinases upstream of MAPKs [10]. The $G\alpha$ subunit is a molecular on/off switch for signaling processes. As such, it is likely to be a critical target for post-translational modifications that regulate GPCR signaling, whether by intra-pathway mechanisms or by cross-talk with other pathways. In fact, several studies have shown that $G\alpha$ proteins are phosphorylated, resulting in altered affinity for $G\beta\gamma$ subunits or guanine nucleotides [21-25, 83]. In some cases, phosphorylation is the direct result of pathway activation, and thus constitutes a positive or negative feedback. In other cases, phosphorylation is triggered by parallel pathways and thus constitutes a mechanism of signal coordination or cross-talk. Our focus here is cross-talk regulation of G protein and osmotic stress response MAPK pathways.

Identifying how environmental stress can promote post-translational modification of $G\alpha$ subunits is necessary to fully understand the mechanisms by which the pathways are coordinated

and integrated. Studying the response to environmental stress is often challenging, however, due to the expression of multiple protein isoforms and differences in expression among various tissues and cell types. Given these complexities, much can be learned from the analysis of orthologous signaling processes in simpler eukaryotes.

The budding yeast *Saccharomyces cerevisiae* has a stress response pathway and a GPCR signaling pathway with component proteins that are evolutionarily conserved across eukaryotes [57, 58]. The High Osmolarity Glycerol, or HOG, pathway is comprised of a MAPK (Hog1), a MAPK kinase (Pbs2), and MAPK kinase kinases (Ste11, Ssk2/Ssk22). Upon activation, Hog1 phosphorylates cytoplasmic and nuclear proteins to aid in the restoration of osmotic equilibrium through osmolyte synthesis and the induction of stress response genes [69]. Hog1 is the yeast ortholog of mammalian p38.

Yeast use another, parallel MAPK pathway to initiate haploid cell fusion, or mating. This pathway is activated by pheromone binding to a GPCR to initiate exchange of GDP for GTP in the G α subunit (Gpa1) and subsequent dissociation of G $\beta\gamma$. G $\beta\gamma$ activates a MAPKKK (Ste11, shared by the HOG pathway), a MAPKK (Ste7) and a MAPK (Fus3). Once activated, Fus3 promotes transcription of genes to initiate cell mating [57]. Fus3 is the yeast ortholog of mammalian ERK1 and ERK2.

In the present study, we use yeast as a model system to investigate how crosstalk regulates G protein signaling in response to environmental stress. We have shown previously that osmotic stress dampens the pheromone response pathway, but the mechanism has not been explored [4]. We have also shown that glucose limitation dampens the pheromone response pathway, and does so by reducing intracellular pH [84]. The increase in proton concentration is detected by the G protein directly, resulting in increased phosphorylation of Gpa1. Additionally,

we have identified a family of three kinases (Elm1, Sak1, and Tos3) and a PP1 phosphatase complex (Reg1/Glc7) as the molecular machinery responsible for phosphorylating and dephosphorylating Gpa1 [5]. We show here that Gpa1 is likewise phosphorylated in response to osmotic stress, and that phosphorylation of Gpa1 requires the same protein kinases, but does not entail any changes in intracellular pH. In an unbiased metabolomics screen, we determine that 2-hydroxy branched chain amino acid metabolites are produced in a salt- and Hog1-dependent manner. Finally, we show that these metabolites are necessary and sufficient to promote Gpa1 phosphorylation and dampen downstream signaling. We propose that these metabolites represent a new class of second messengers of the stress-responsive HOG pathway.

Results

Gpa1 is phosphorylated in response to environmental stress

To understand how cells adapt to environmental stresses, we sought to identify conditions that impact pheromone signaling through the phosphorylation of Gpa1. We recently established that Gpa1 is phosphorylated by a family of three AMPK kinases (Elm1, Sak1, and Tos3), and dephosphorylated by the phosphatase complex Reg1/Glc7 [5]. These proteins were previously shown to phosphorylate and dephosphorylate the yeast AMPK, Snf1 [85-87]. Snf1, is phosphorylated and activated in response to nutrient limitation, as well as heat shock, hyperosmotic shock, reactive oxygen species, ethanol, and changes in extracellular pH [88]. Accordingly, we asked whether the same environmental stressors would lead to phosphorylation of Gpa1. We treated wild-type cells with the indicated stressor in a 2-hour time-course (see Materials and Methods), and cell lysates were analyzed by western blot. As shown in Figure 2.1, Gpa1 and Snf1 were phosphorylated in all stress conditions tested (see also Figure 2.2).

However, among the stressors there were differences in the both the magnitude and duration of phosphorylation. In glucose-limiting conditions, approximately 90% of Gpa1 was phosphorylated by 2 minutes, with a gradual decline after 10 minutes (Figure 2.1A). Heat shock (30 minutes at 42°C) also promoted rapid phosphorylation but slow dephosphorylation. Osmotic stress promoted slow phosphorylation, but fast dephosphorylation. Heat and osmotic stress also promoted the phosphorylation of Snf1, but the effects were comparatively weak and transient (Figure 2.1B, C) [88]. These data reveal that Gpa1, like Snf1, is phosphorylated in response to various stress signals. More broadly, the results indicate that physico-chemically distinct stimuli have a common ability to promote phosphorylation of two functionally distinct proteins, Snf1 and Gpa1.

It is well-established that the MAPK Hog1 is phosphorylated and activated in response to osmotic stress. Hog1 is also activated by heat shock [89], cold stress [90], oxidative stress [91], and hypoxia [92]. Given that many of these conditions also lead to phosphorylation of Gpa1 and Snf1, we asked if Hog1 activation was required in either case. To this end, we replaced Hog1 with a mutant that lacks catalytic activity, *hog1^{K52R}* [93], and treated the cells with 0.5 M KCl. Whereas Snf1 phosphorylation was unperturbed, the phosphorylation of Gpa1 was almost completely abrogated in the *hog1^{K52R}* strain (compare Figure 2.1C, blue curve vs. red curve). These data indicate that osmotic stress-induced phosphorylation of Gpa1, but not Snf1, is dependent upon Hog1 catalytic activity. More broadly, these results implicate at least two distinct signaling pathways, and potentially two distinct second messengers, that mediate the response to osmotic stress.

One potential second messenger is pH. Indeed, it is well established that glucose limitation leads to a substantial decrease in intracellular pH (pH_i). We have shown recently that

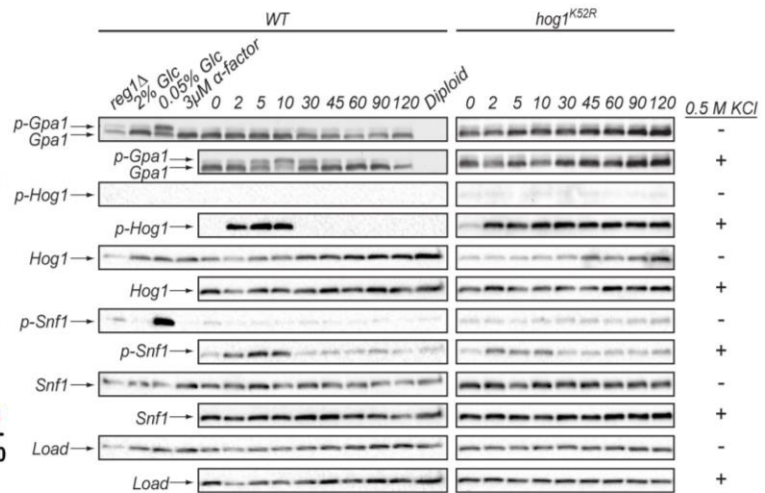
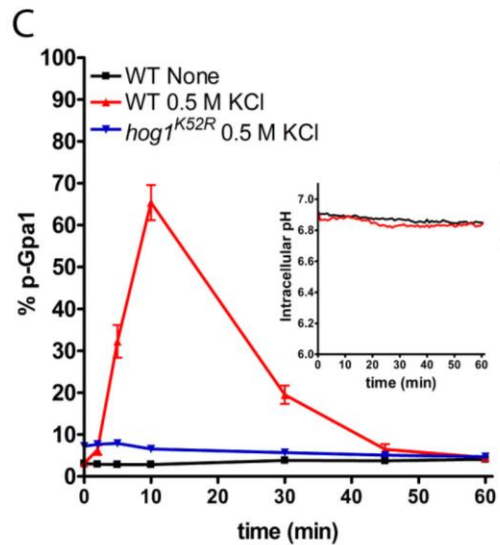
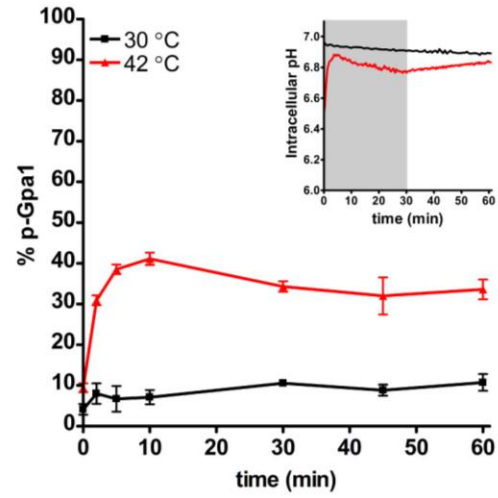
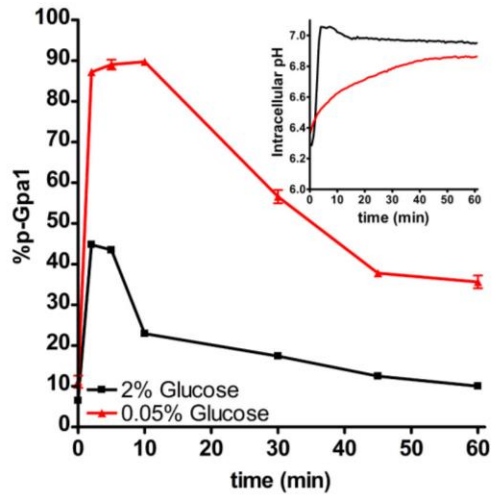
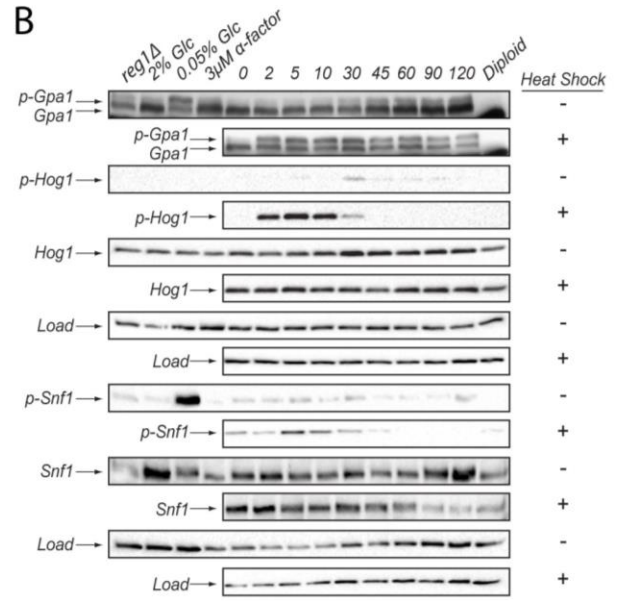
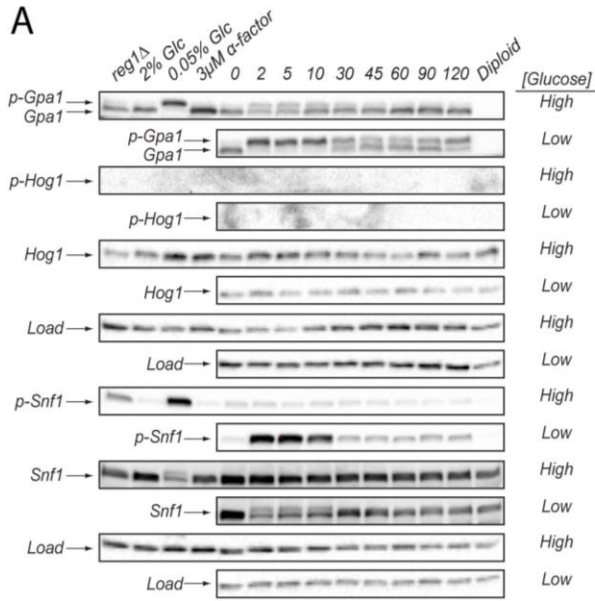


Figure 2.1 Phosphorylation of Gpa1 in response to osmotic stress occurs in a Hog1-dependent, pH-independent manner.

Western blot analysis reveals that Gpa1 and Snf1 are phosphorylated (p-Gpa1 and p-Snf1) in response to (A) glucose (Glc) limitation (“High” = 2% glucose, “Low” = 0.05% glucose), (B) heat shock (42 °C, 30 minutes), or (C) osmotic stress (0.5 M KCl). Note that Hog1 is phosphorylated (p-Hog1) in response to heat shock or osmotic stress, but not glucose limitation. Intracellular pH (insets) decreases in response to glucose limitation or heat shock, but not osmotic stress. Hog1 catalytic activity (*hog1^{K52R}*) is required for phosphorylation of Gpa1 but not Snf1. Diploid, control cells lacking Gpa1. *reg1*Δ, control cells lacking Gpa1 phosphatase. Hog1, Snf1, and Load correspond to gels probed with Hog1, Snf1 and G6PDH antibodies, respectively. Data presented as mean ± standard deviation, N = 3.

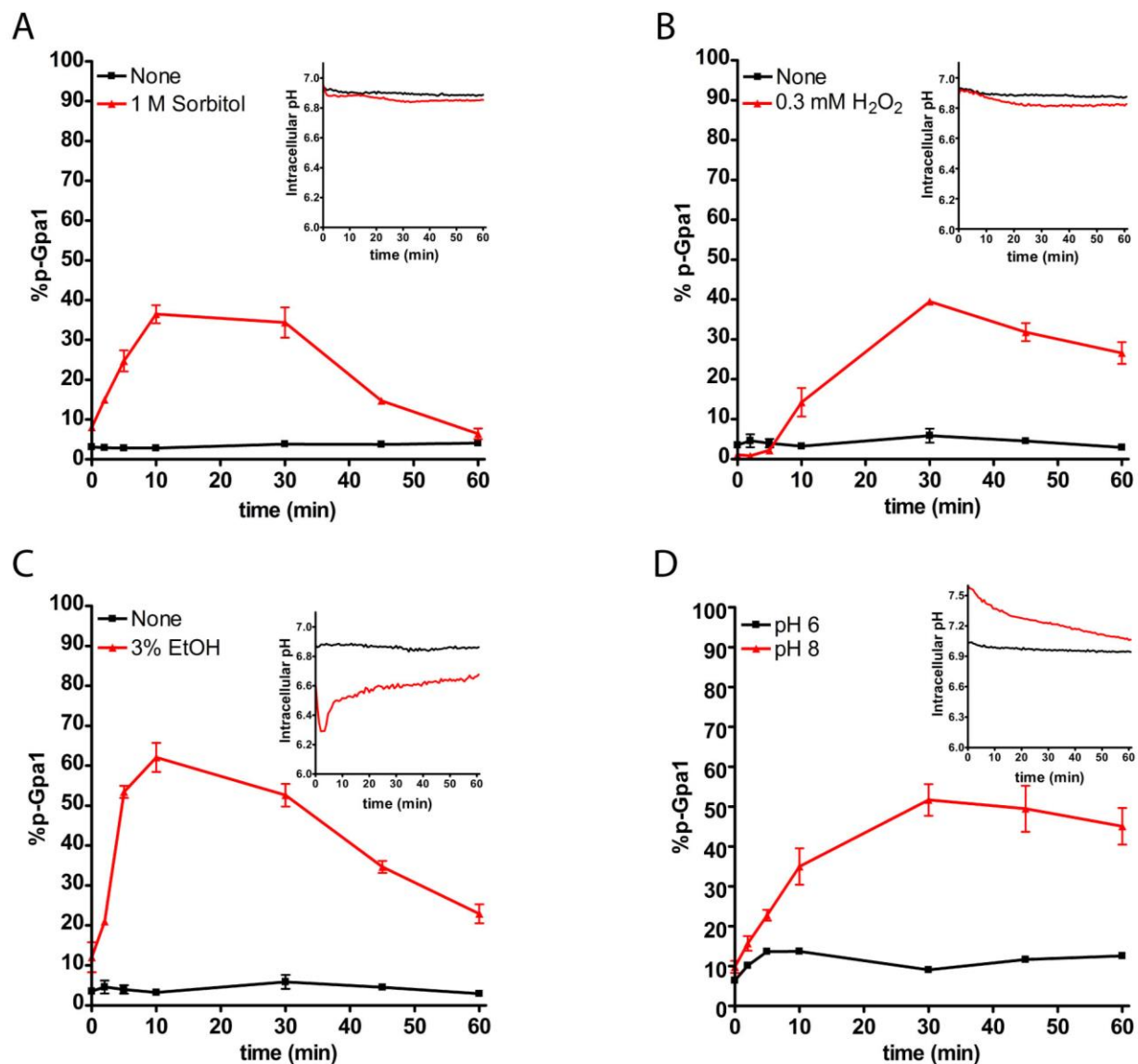


Figure 2.2 Additional stress conditions promote Gpa1 phosphorylation with differing effects on intracellular pH.

In addition to salt, heat and glucose stress, Gpa1 is phosphorylated in response to (A) non-ionic osmotic stress, (B) oxidative stress, (C) ethanol stress, and (D) alkaline pH. (A-D, insets) Intracellular pH decreases in response to oxidative- and ethanol stress, but not non-ionic osmotic stress, and increases in response to alkaline pH. Data presented as mean \pm standard deviation, N = 3.

Gpa1 is a pH sensor, and that pH-dependent changes in conformation result in phosphorylation of the protein [84]. Since other stressors trigger phosphorylation of Gpa1, we asked whether any of those conditions also cause a change in pH_i . To that end we expressed the ratiometric fluorescent pH biosensor, pHluorin, in wild-type cells [84, 94, 95]. Consistent with earlier studies [84], we observed a decrease in pH_i from 7.0 to 6.4 upon glucose limitation (Figure 2.1A, inset). In contrast, cells subjected to osmotic stress exhibited no change in pH_i over the course of 60 minutes (Figure 2.1C and Figure 2.2). These data indicate that low glucose and osmotic stress each promote Gpa1 phosphorylation, but glucose alone affects pH_i . We therefore postulated the existence of an additional second messenger of the osmotic stress response.

Global metabolomics analysis of second messengers for osmotic stress

The data presented above reveal that osmotic stress has no effect on pH_i , yet is a potent inducer of Gpa1 phosphorylation. To identify potential second messengers of osmotic stress, we conducted a global, unbiased metabolomics analysis [75, 96]. Based on results from the Gpa1 phosphorylation experiments above, we sought to identify metabolites that increased with osmotic stress and in a Hog1-dependent manner. To this end, we subjected wild-type and Hog1-deficient yeast cells to 0.5 M KCl for 20 minutes and then analyzed cell extracts by LC-MS/MS and GC-MS (Figure 2.3A). This analysis identified 296 distinct entities representing each major class of biochemical molecules— amino acids, peptides, carbohydrates, lipids, nucleic acids, vitamins and cofactors, and xenobiotics. Consistent with past findings, we found that the osmolytes trehalose [97] and glycerol [98] were induced substantially (32-fold and 2.5-fold, respectively) (Figure 2.3C, Table 2.1). Using a comparable (2-fold) cut off, we identified an additional 26 metabolites that increased in response to osmotic stress, and 13 that increased in the presence of Hog1. Of these, only three required osmotic stress and Hog1 together

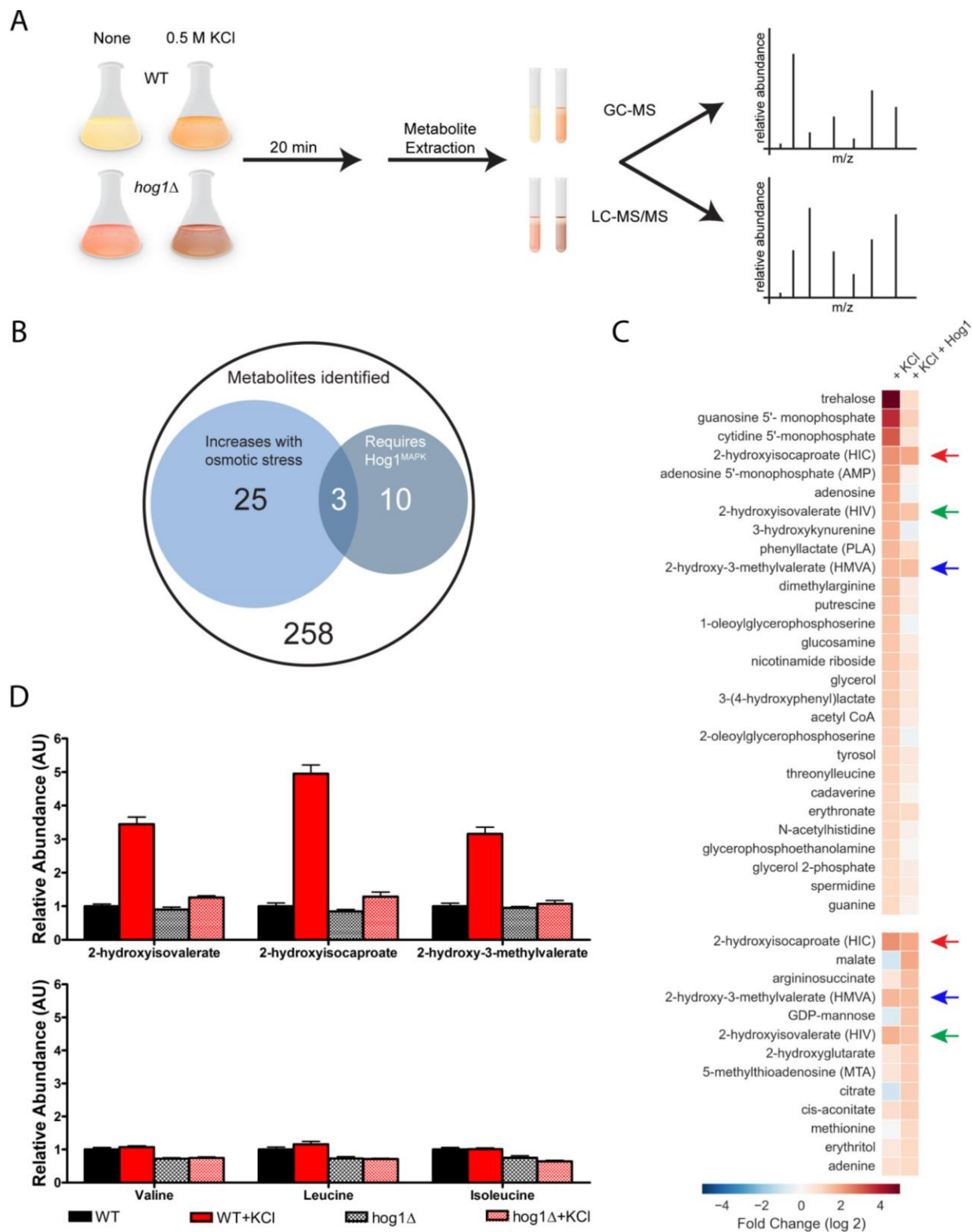


Figure 2.3 Global metabolomics analysis identifies candidate second messengers for osmotic stress.

(A) Metabolites from wild-type and *hog1Δ* cells, untreated or treated for 20 minutes with 0.5 M KCl, were extracted and analyzed by GC-MS and LC-MS/MS. (B) 296 unique metabolites were identified. Venn diagram of metabolites that increase >2-fold in response to osmotic stress (n=28), in cells that express Hog1 (n=13) or both (n=3). (C) Heat map of metabolites that increase in salt-treated wild-type compared to unstressed wild-type cells (left column, top), and increase in salt-treated wildtype, but not salt-treated *hog1Δ* cells(right column, bottom). Colored arrows indicate 2-hydroxy carboxylic acid derivatives of the BCAAs valine (HIV, green), leucine (HIC, red), and isoleucine (HMVA, blue). (D, Top) Relative abundance of the three BCAA derivatives and (D, Bottom) their parent amino acids. Data presented as mean ± standard deviation, N = 5.

Table 2.1 Metabolite fold-change values for Figure 2.3 heatmap.

Metabolite	Fold change with osmotic stress in wild-type vs. untreated wild-type	Fold change with osmotic stress in wild-type vs. <i>hog1Δ</i>
trehalose	32.28	1.96
guanosine 5'- monophosphate (5'-GMP)	13.27	2.27
cytidine 5'-monophosphate (5'-CMP)	8.38	1.61
2-hydroxyisocaproate (2-HIC)	4.95	3.85
adenosine 5'-monophosphate (AMP)	4.24	1.20
adenosine	3.75	0.85
2-hydroxyisovalerate (2-HIV)	3.45	2.70
3-hydroxykynurenine	3.23	0.78
phenyllactate (PLA)	3.21	1.96
2-hydroxy-3-methylvalerate (2-H3MP)	3.16	2.94
dimethylarginine (SDMA + ADMA)	3.05	1.32
putrescine	2.85	1.45
1-oleoylglycerophosphoserine	2.8	0.88
glucosamine	2.63	1.41
nicotinamide riboside*	2.59	1.75
glycerol	2.51	1.47
3-(4-hydroxyphenyl)lactate	2.5	1.52
acetyl CoA	2.42	1.35
2-oleoylglycerophosphoserine*	2.26	0.81
tyrosol	2.23	1.49
threonylleucine	2.2	1.39
cadaverine	2.17	1.11
erythronate*	2.16	1.96
N-acetylhistidine	2.15	1.22
glycerophosphoethanolamine	2.11	1.04
glycerol 2-phosphate	2.07	1.32
spermidine	2.06	1.39
guanine	2.05	1.20
2-hydroxyisocaproate (2-HIC)	4.95	3.85
malate	0.53	3.85
argininosuccinate	1.54	2.94
2-hydroxy-3-methylvalerate (2-H3MP)	3.16	2.94
GDP-mannose	0.62	2.78
2-hydroxyisovalerate (2-HIV)	3.45	2.70
2-hydroxyglutarate	1.58	2.38
5-methylthioadenosine (MTA)	1.57	2.33
citrate	0.5	2.33
cis-aconitate	1.84	2.33
methionine	0.95	2.08
erythritol	1.44	2.04
adenine	1.76	2.00

(Figure 2.3B, C): 2-hydroxyisovalerate (HIV), 2-hydroxyisocaproate (HIC), and 2-hydroxy-3-methylvalerate (HMVA). All three compounds are 2-hydroxy carboxylic acid derivatives of the branched-chain amino acids (BCAAs) valine, leucine, and isoleucine, respectively (Figure 2.3C, D). Thus, our analysis points to 2-hydroxy BCAA derivatives as candidate second messengers of osmotic stress.

Branched-chain aminotransferase null mutants exhibit reduced stress-induced phosphorylation of Gpa1

Our metabolomics study demonstrated that BCAA derivatives are produced in response to osmotic stress, and that their production requires Hog1 (Figure 2.3D). In principle, deleting Hog1 could alter the production of additional second messengers that may not have been detected in our metabolomics screen. However, as BCAA derivatives were the most robustly increased metabolites that met our criteria for osmotic stress, we examined the consequences of disrupting BCAA catabolism through the so-called Ehrlich pathway in yeast [99]. The first step in the pathway is transamination to an α -keto acid by the branched-chain amino acid transaminases, Bat1 and Bat2 (Figure 2.4A). The resulting α -keto acid is subsequently reduced to the 2-hydroxy acid (Figure 2.4A). Products of the Ehrlich pathway are exported from the cell by the ABC transporter Pdr12 [99, 100].

To test whether BCAA derivatives are required for phosphorylation of Gpa1 and/or Snf1, we deleted the *BAT1* and *BAT2* genes individually (Figure 2.4B). After osmotic stress, we observed a modest, but significant reduction in maximal phosphorylation of Gpa1 in the *bat1Δ* and *bat2Δ* mutants, as compared to wild-type cells (Figure 2.4B, C). As expected, Snf1 phosphorylation was maintained in the *bat1Δ* mutant (Figure 2.4B). Cells harboring deletion of both *BAT* genes are reported to be viable [101, 102]; however in our hands, *bat1Δbat2Δ* double

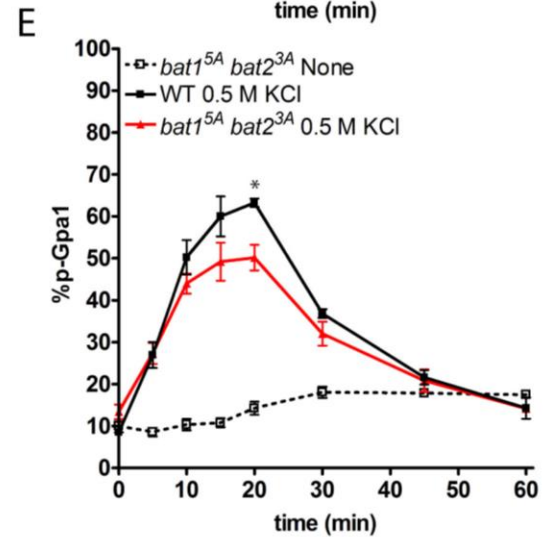
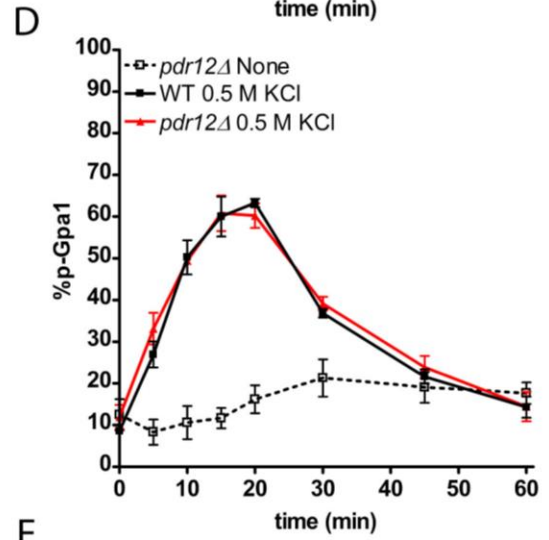
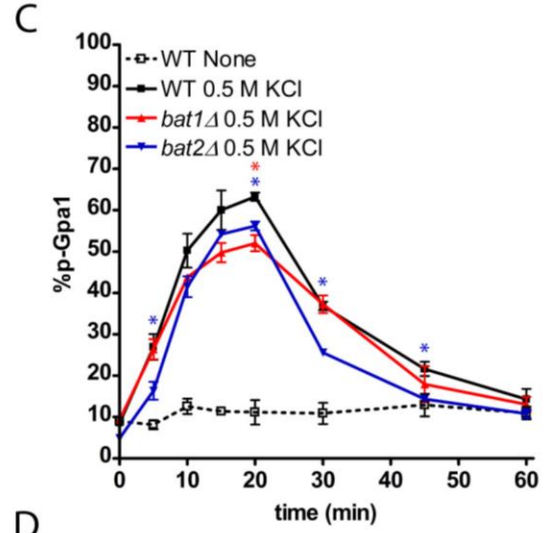
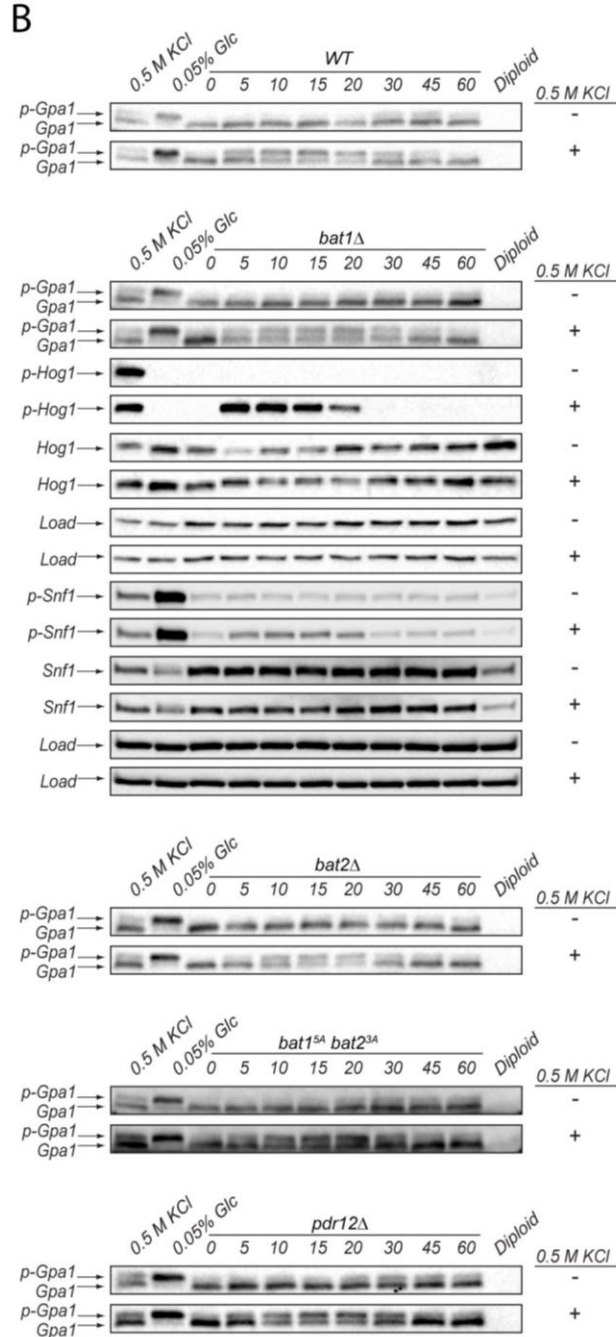
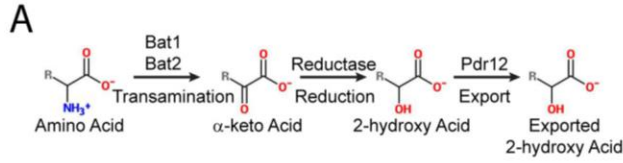


Figure 2.4 BCAA derivatives are necessary for a full response to osmotic stress.

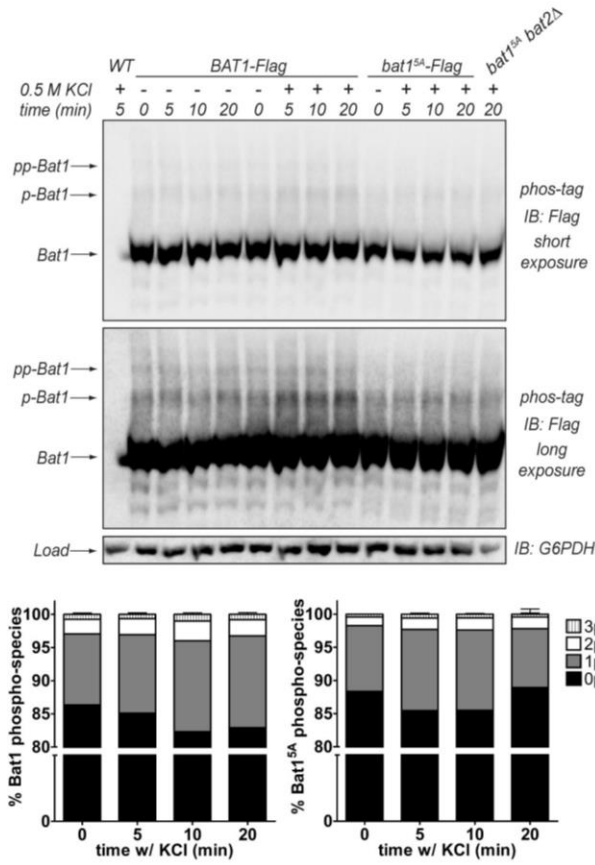
(A) BCAAs are converted to α -keto acids by the BCAA transaminases, Bat1 and Bat2. The α -keto acids are subsequently reduced to the 2-hydroxy acids, and ultimately exported by the fusel acid transporter, Pdr12. (B, C) Genetic ablation of *BAT1* or *BAT2*, or (B, E) loss of MAPK phosphorylation consensus sites (Bat1^{5A} Bat2^{3A}) leads to reduced Gpa1 phosphorylation. (B, D) Genetic ablation of *PDR12* does not affect Gpa1. Data presented as mean \pm standard deviation, * indicates $p \leq 0.05$, N = 3.

mutants arose at a lower-than-predicted frequency after tetrad dissection and likely harbored suppressor mutations. As an alternative approach, we attempted to use a tetracycline-repressible *BAT1* in a *bat2Δ* background. However, the doxycycline used to repress *BAT1* expression also promoted the phosphorylation of Gpa1. Gpa1 phosphorylation was unaffected by loss of the transporter gene *PDR12* (Figure 2.4D). Together these results indicate that either Bat1 or Bat2 is necessary for cell viability. Both proteins, as well as their catalytic products, are necessary for a full response to osmotic stress.

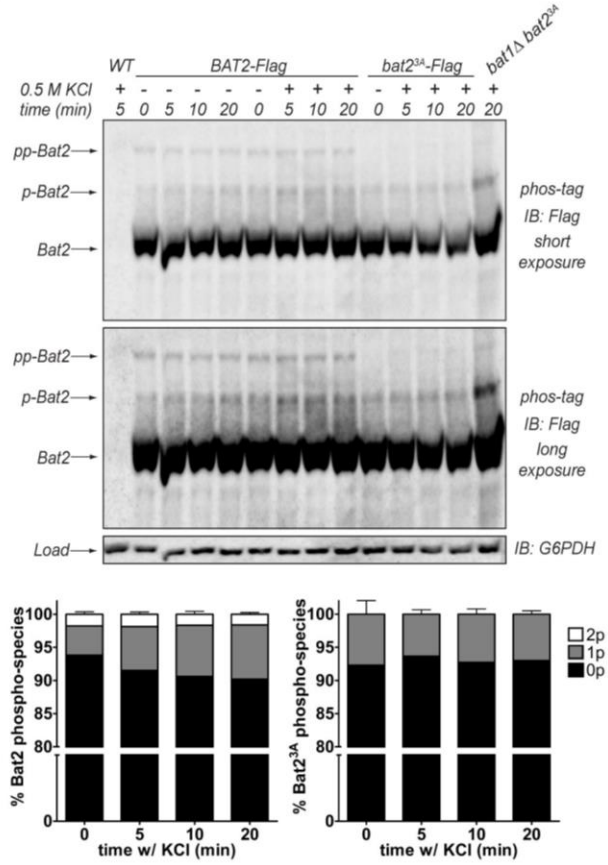
MAPK-dependent phosphorylation of branched-chain amino acid transaminases does not affect Gpa1 phosphorylation after osmotic stress

Our results indicate that Hog1 activity and BCAA catabolism are both needed for a full response to osmotic stress. In particular, we have shown that osmotic stress-dependent Gpa1 phosphorylation is reduced in mutants lacking Bat1 or Bat2, and is eliminated in cells lacking Hog1 catalytic activity. Based on these findings, we hypothesized that Hog1 phosphorylates one or more components of the Ehrlich pathway. Indeed, Bat1 possesses five MAPK consensus sites (S/TP), and Bat2 possesses three such sites. In support of our hypothesis, replacement of the MAPK consensus sites led to a significant reduction in Gpa1 phosphorylation (Figure 2.4B, E). However, there were no changes in the electrophoretic (phosphorylation-dependent) mobility of Bat1, Bat2, Bat1^{5A}, or Bat2^{3A}, either in the absence or presence of salt stress. There was also no effect of osmotic stress on Bat2^{3A} in cells lacking Bat1 (*bat1Δ* Bat2^{3A}) or Bat1^{5A} in the absence of Bat2 (Bat1^{5A} *bat2Δ*) (Figure 2.5). Taken together, these results suggest that Hog1 does not target the transaminases, and instead plays an indirect role in promoting the production of BCAA derivatives.

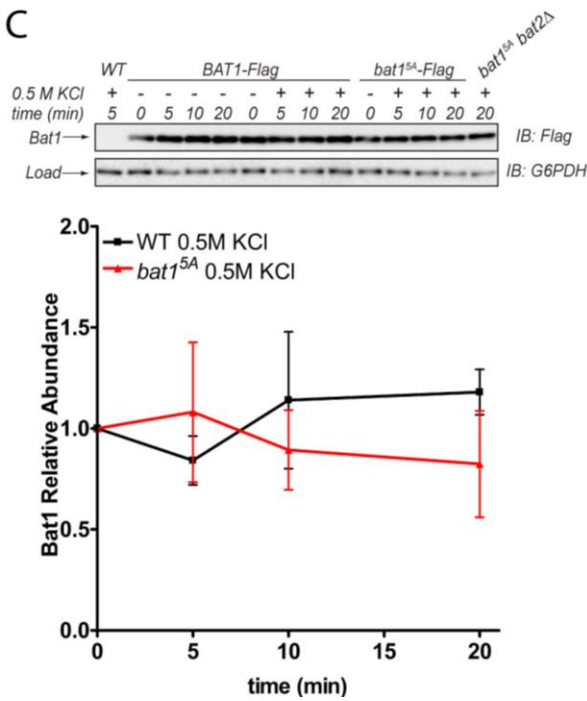
A



B



C



D

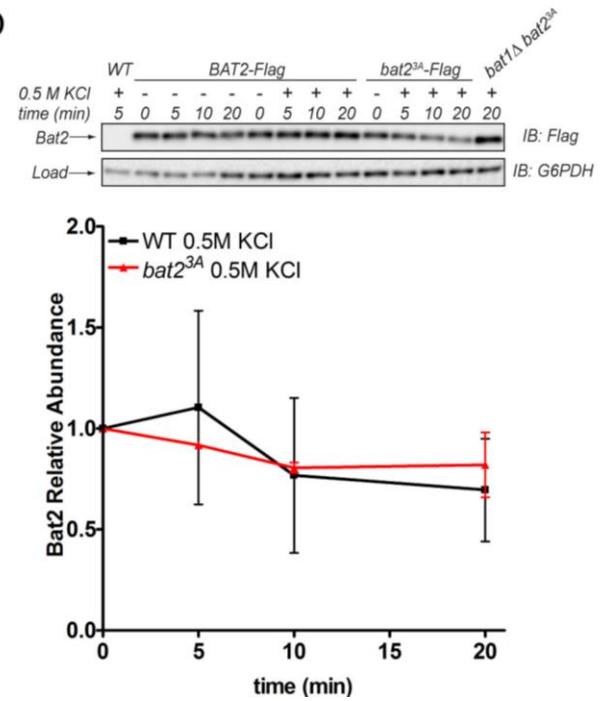


Figure 2.5 Bat1 and Bat2 phosphorylation and abundance are unaffected by osmotic stress.

Phos-tag western blots of (A) Bat1-Flag and Bat1^{5A}-Flag or (B) Bat2-Flag and Bat2^{3A}-Flag reveal no detectable changes in phosphorylation after osmotic stress. (C) Western blot analysis of (C) Bat1-Flag or (D) Bat2-Flag reveals no change in abundance after osmotic stress. Putative non-phosphorylated (Bat1, Bat2), mono-phosphorylated (p-Bat1, p-Bat2) and dual phosphorylated (pp-Bat1, pp-Bat2) species are indicated. WT, untagged control. Data presented as mean \pm standard deviation, N = 3.

Ectopic addition of BCAA derivatives promotes Gpa1 phosphorylation in the absence of osmotic stress

An intracellular second messenger should, by definition, be sufficient as well as necessary to evoke the response of the extracellular first messenger. Having demonstrated that BCAA derivatives are necessary for a full response to osmotic stress, we tested the ability of the BCAA derivatives to promote phosphorylation in the absence of the stimulus. To better enable these compounds to traverse the cell membrane, we grew the cells at pH 5, which is closer to the pK_a of the metabolites. By favoring the protonated, uncharged species, the BCAA derivatives can more easily traverse the plasma membrane. Importantly, the lower external pH does not change the intracellular pH [84]. Using this approach, we found that HIV, HIC, and HMVA promoted Gpa1 phosphorylation, but with varying efficacy. HIC showed the strongest effect while HIV had the weakest effect (Figure 2.6). Hog1 was not activated by BCAA derivatives, consistent with the idea that their production is a consequence of Hog1 activation. Snf1 was likewise unaffected, consistent with the idea that it is regulated by a distinct second messenger. Taken together, these experiments indicate that BCAA derivatives are sufficient to promote phosphorylation of Gpa1 and thus meet the criteria for second messengers of osmotic stress.

BCAA derivatives do not bind directly to G α proteins

Our results so far show that BCAA derivatives promote the phosphorylation of Gpa1. We next attempted to delineate the mechanism by which BCAA derivatives act. Our lab has demonstrated previously that protons directly interact with the G protein α subunit, causing a conformational change that promotes its phosphorylation. Moreover, the pH dependent change is conserved in yeast and human G α proteins [84]. We hypothesized that BCAA derivatives might likewise act by binding to the G α subunit. To test the potential mechanism, we employed NMR

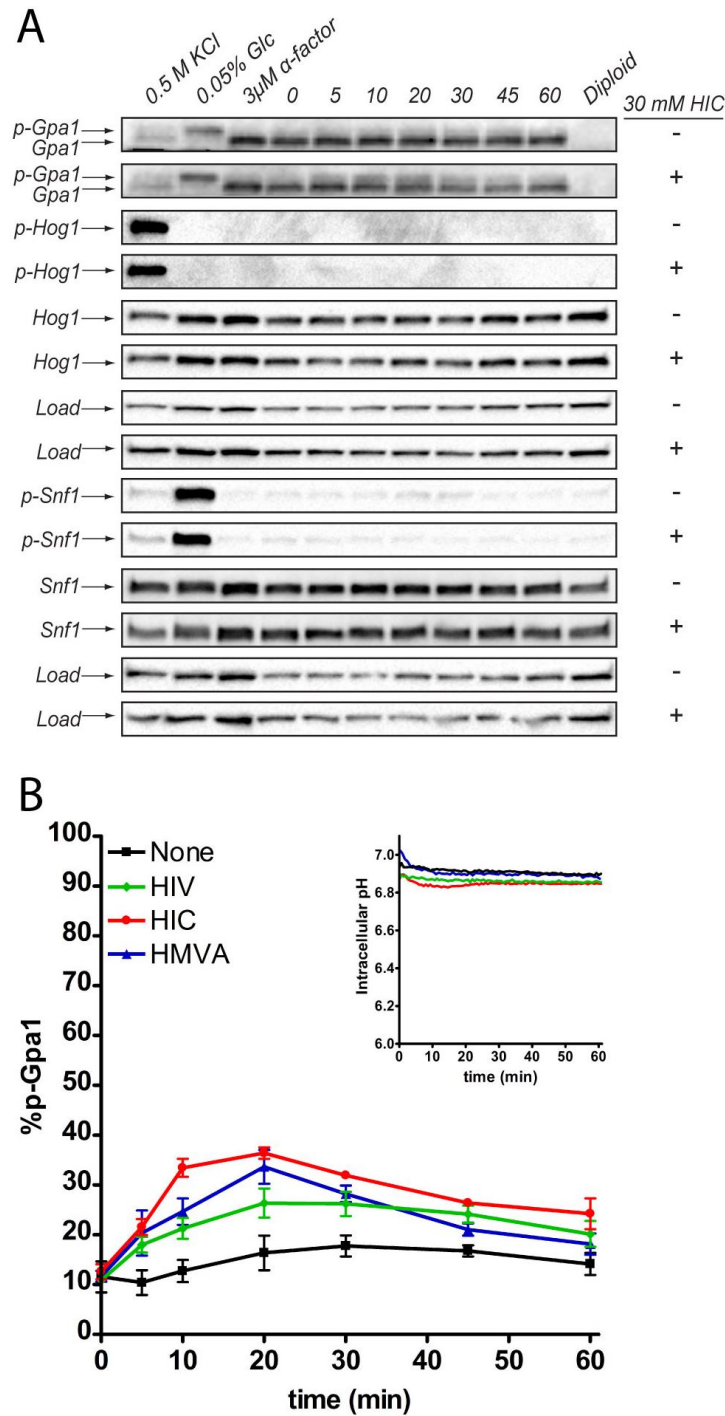


Figure 2.6 BCAA derivatives promote Gpa1 phosphorylation in the absence of osmotic stress.

(A) Ectopic addition of HIC promotes phosphorylation of Gpa1 but not Hog1 or Snf1. (B) Ectopic addition of the BCAA derivatives promote Gpa1 phosphorylation while intracellular pH is unaffected (inset). Data presented as mean \pm standard deviation, N = 3.

spectroscopy. ^1H - ^{15}N 2D heteronuclear NMR spectra of ^{15}N -enriched G α were collected in the absence and presence of BCAA derivatives. These spectra allow for the detection of protons directly bonded to a ^{15}N , including both backbone and side-chain NH resonances. As an NH resonance can be detected for every residue, with the exception of proline, the spectrum contains a “fingerprint” of the protein backbone and allows perturbations resulting from interactions to be detected on a per-residue basis. This approach is widely considered as a definitive method for detecting low- to intermediate-affinity binding of ligands to proteins [103]. Accordingly, we acquired the NMR spectra of G α i in its GDP-bound state, alone or in the presence of a 25-fold excess of individual BCAA derivatives. As shown in Fig. 5, there were no significant peak shifts when BCAA derivatives were present (Figure 2.7A-C). As a positive control, we acquired NMR spectra of G α i-GDP at pH 6 and at pH 7. As shown in Figure 2.7D, a substantial number of peaks are shifted at the lower pH, consistent with proton-dependent conformational changes in G α i. These results indicate that BCAA derivatives likely target another component of the G protein signaling pathway.

The AMPK kinase Elm1 phosphorylates Gpa1 in response to osmotic stress and BCAA derivative production

Gpa1 is phosphorylated by the AMPK kinases Elm1, Sak1, and Tos3 [5]. Whereas Elm1 phosphorylates Gpa1 in a cell-cycle-dependent manner [83], Sak1 is responsible for phosphorylation during glucose limitation [5]. Our data presented above indicate that Gpa1 is likewise phosphorylated in response to osmotic stress. To determine which, if any, of the AMPK kinases mediates the response to osmotic stress, we compared Gpa1 phosphorylation in cells lacking each of the three kinases, alone or in combination. As shown in Figure 2.9, deletion of *ELM1* resulted in the greatest reduction of Gpa1 phosphorylation, while deletion of *SAK1* had a

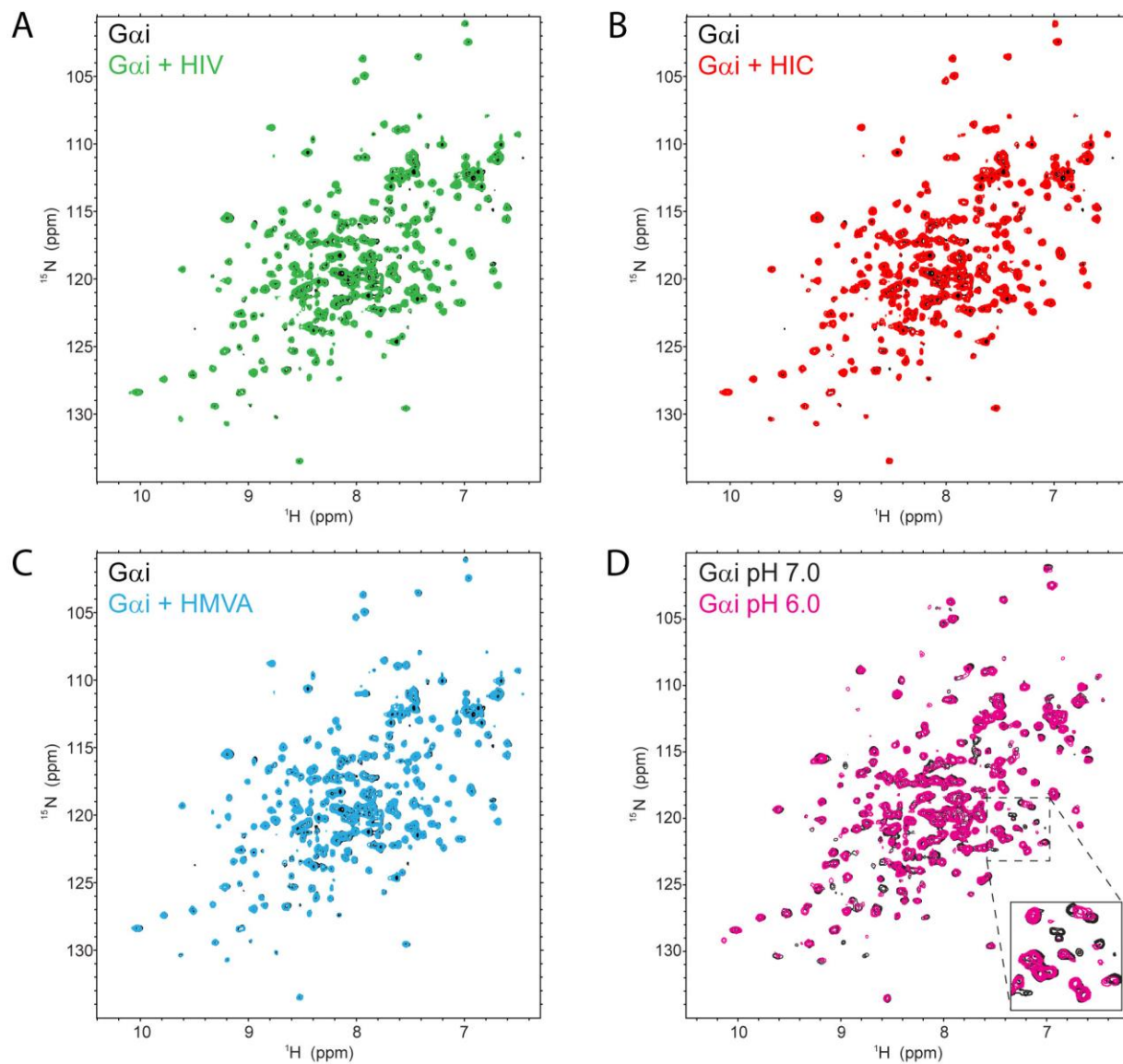


Figure 2.7 BCAA derivatives do not bind directly to G proteins.

^1H - ^{15}N 2D HSQC NMR spectra of *Gai*-GDP alone (black) or in the presence of 25-fold excess (A) HIV, (B) HIC, or (C) HMVA (color) reveal no discernable peak shifts. (D) Spectral overlay of *Gai*-GDP at pH 6.0 (magenta) and pH 7.0 (black) is presented as a positive control. Inset, magnified view of a subset of resonances showing pH-dependent spectral changes.

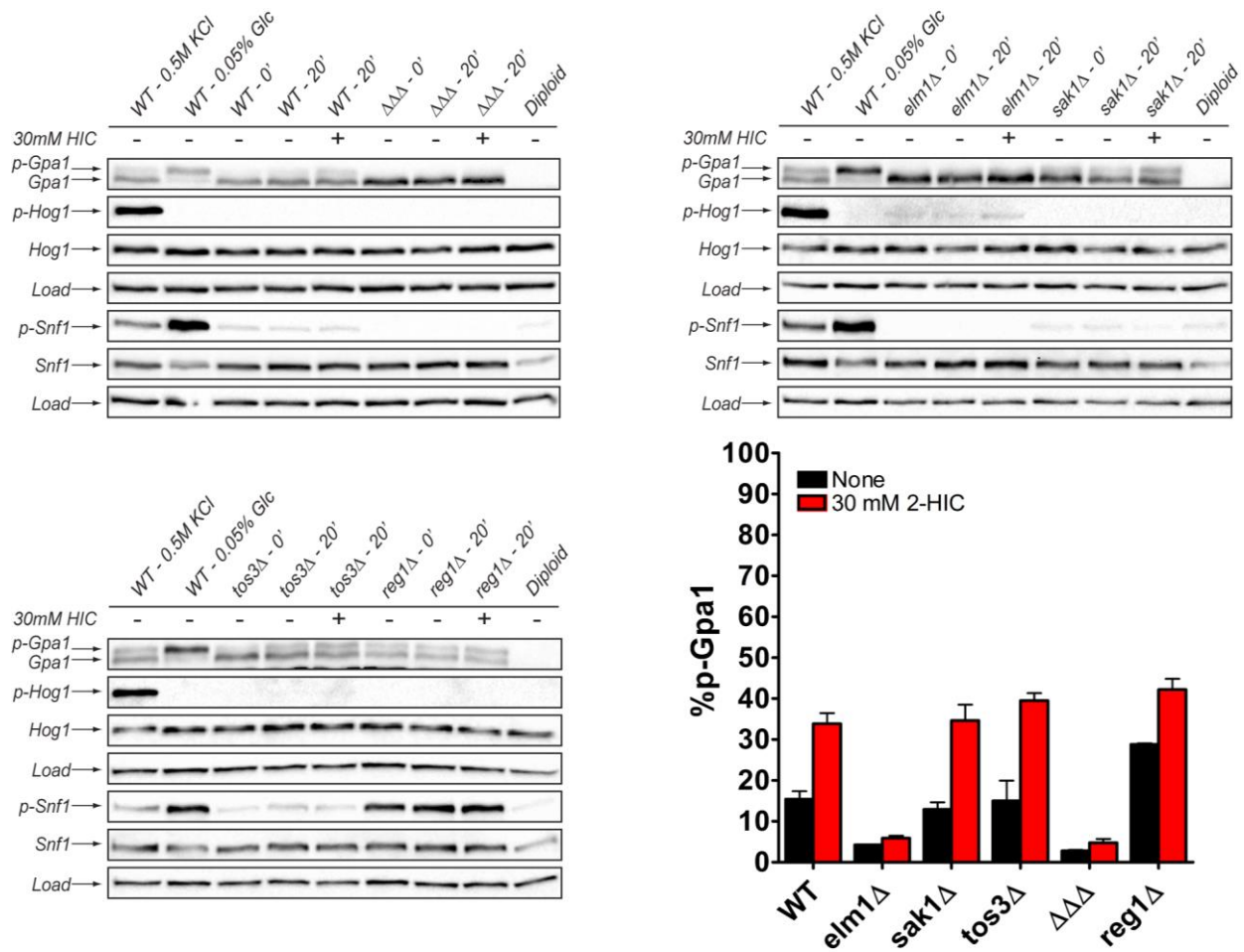


Figure 2.8 The AMPK kinase Elm1 phosphorylates Gpa1 upon BCAA derivative addition. Gpa1 phosphorylation after ectopic addition of 30 mM HIC is abrogated in cells lacking the AMPK kinase *ELM1*, or all three AMPK kinases ($\Delta\Delta\Delta$). Data presented as mean \pm standard deviation, N = 3.

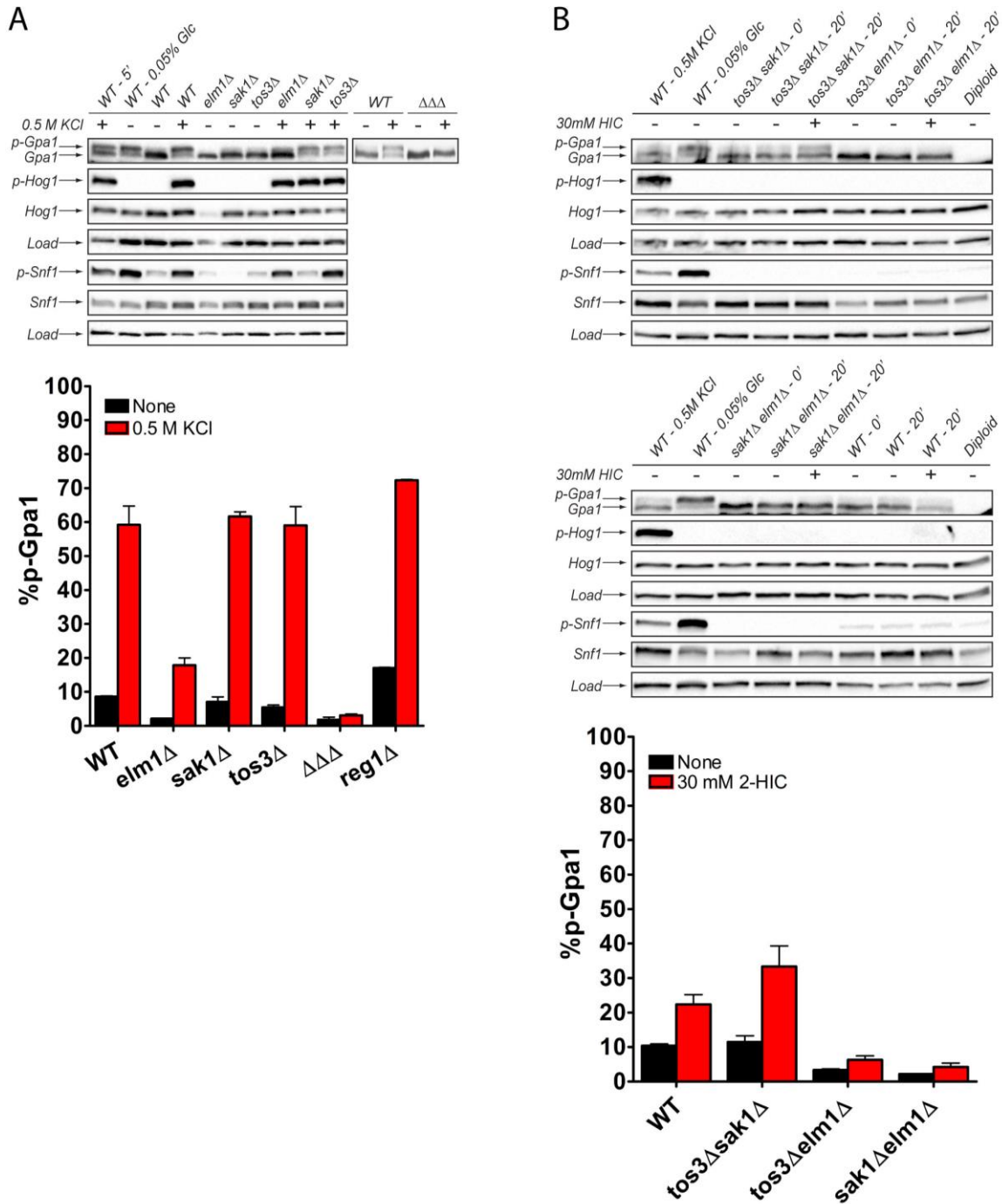


Figure 2.9 The AMPK kinase Elm1 phosphorylates Gpa1 upon osmotic stress or BCAA derivative addition.

(A) Gpa1 phosphorylation after addition of 0.5 M KCl is diminished in cells lacking *ELM1* and abrogated in cells lacking all three AMPK kinases ($\Delta\Delta\Delta$). In contrast to Gpa1, phosphorylation of Snf1 requires Sak1 but not Elm1. (B) Gpa1 phosphorylation after ectopic addition of 30 mM HIC is abrogated in cells lacking the AMPK kinases *TOS3* and *ELM1* or *SAK1* and *ELM1*. Data presented as mean \pm standard deviation, N = 3.

comparatively small effect. We then performed the same experiment using BCAA metabolites in place of osmotic stress. As with salt stimulation, HIC promoted the phosphorylation of Gpa1 in cells, and phosphorylation was diminished in the *elm1Δ* mutant (Figure 2.8 and Figure 2.9). Taken together, these results indicate that both the primary messenger (osmotic stress) and the putative second messenger (the BCAA derivatives) act through Elm1. More broadly, these results confirm a fundamental difference between glucose- and salt-dependent changes in the cell. While both conditions lead to Gpa1 phosphorylation, they lead to the production of two distinct second messengers (protons and BCAA derivatives) and to phosphorylation by two distinct protein kinases (Sak1 and Elm1).

Osmotic stress and BCAA derivatives dampen the pheromone response MAPK pathway

We have shown that osmotic stress leads to a diminished pheromone response [4] and phosphorylation of the $G\alpha$ protein (this work). Based on our model, the BCAA derivatives are responsible for many of the intracellular effects of osmotic stress signaling including $G\alpha$ phosphorylation. According to our proposed mechanism, the same metabolites should also dampen the response to pheromone. To test this hypothesis, we employed a transcriptional reporter assay using GFP under control of the *FUS1* promoter, which is specific to the pheromone response pathway [104]. We then measured fluorescence in response to increasing concentrations of the α -factor mating pheromone, alone or in combination with KCl or the BCAA derivatives. Consistent with previous reports [4], osmotic stress dampened the pheromone response by approximately 40%. Consistent with our present model, the addition of HIV, HIC, or HMVA also led to a diminished response of up to 40% (Figure 2.10A). The capacity of each BCAA derivative to dampen transcription correlated directly with its ability to promote Gpa1 phosphorylation (figure 2.6B). Deletion of the Gpa1 kinases confers an elevated

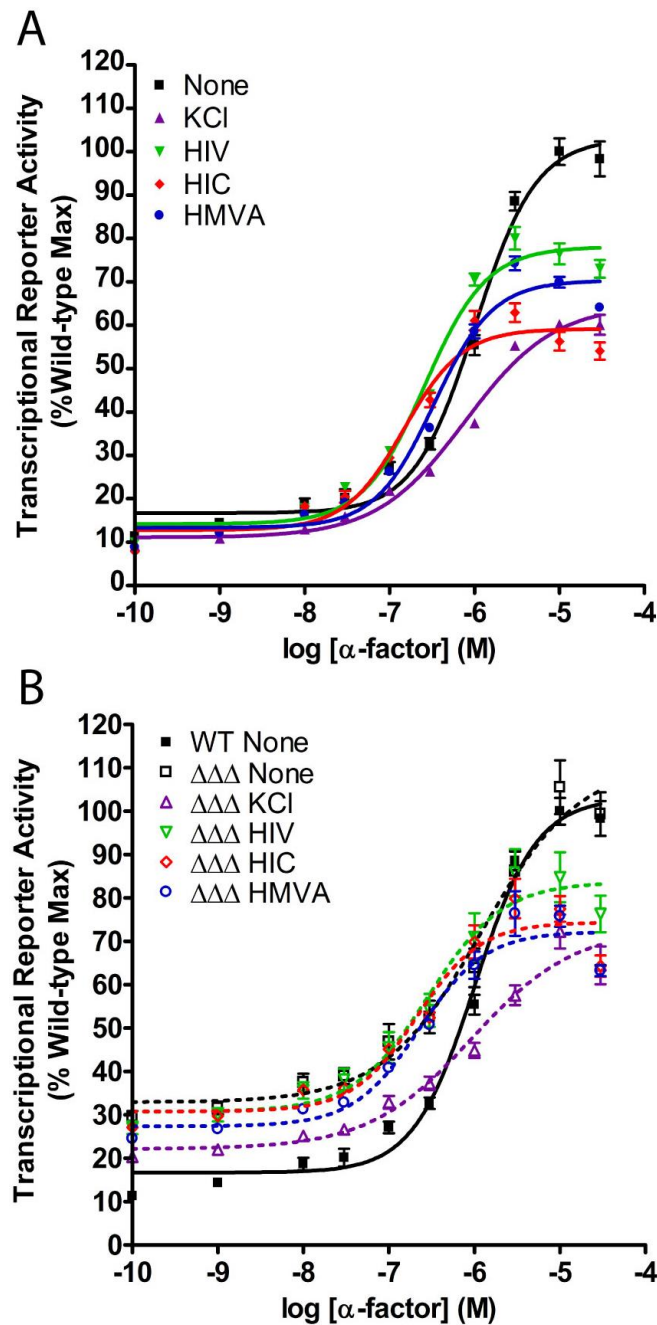


Figure 2.10 BCAA derivatives diminish MAPK-dependent gene transcription.

(A) Addition of BCAA derivatives, or KCl, dampens α -factor pheromone-induced gene transcription (P_{FUS1} -GFP). The dampening capacity of each BCAA derivative is correlated with Gpa1 phosphorylation (see Fig. 4). (B) Genetic ablation of the AMPK kinases increases basal gene transcription, consistent with reduced Gpa1 phosphorylation. Correspondingly, the kinase mutants abrogate any ability of the metabolites to suppress basal signaling and limit their ability to suppress pheromone signaling (41% reduction in wildtype vs. 26% reduction in the kinase mutant strain). Data are presented as mean \pm standard deviation, N = 4.

signal at all but the highest concentrations of pheromone. At 10 μ M pheromone the mutant strain was less sensitive to KCl and HIC (a reduction of 27% and 26%) compared to wild type (35 and 41%, respectively). At low and intermediate concentrations, the mutant strain was less responsive to salt and largely unresponsive to the BCAA derivatives (Figure 2.10B). Thus, BCAA derivatives are produced in response to an osmotic stress stimulus and, by every measure used, appear to mimic the biochemical effects of the osmotic stress signal. By these criteria the BCAA derivatives function as second messengers of the osmotic stress response pathway.

Discussion

Here, we present several novel features of the pheromone response pathway that we believe will be generally applicable to other MAPK signaling systems. First, we show that multiple environmental stressors lead to G protein phosphorylation. Phosphorylation of Gpa1 is accompanied by attenuated signaling through the effector MAPK, Fus3 [4, 5, 84]. Second, we show that many of these same stressors trigger the activation of another MAPK, Hog1. When Hog1 is activated, Fus3 signaling is inactivated. Third, we present the results of a comprehensive screen of small molecule metabolites, and show that 2-hydroxy BCAA derivatives are generated in response to osmotic stress and Hog1 activation. We show further that these metabolites are sufficient to trigger Gpa1 phosphorylation and dampening of the Fus3 pathway. Finally, we show that the protein kinase Elm1 is responsible for phosphorylating Gpa1 in response to osmotic stress and by addition of the metabolites. While the target of these metabolites remains to be identified, we have largely excluded the kinase and G protein substrate as candidates.

Based our findings, we propose that BCAA metabolites represent a newly described “second messenger” of stress-activated signaling. The concept of second messenger signaling

stems from the work of Earl Sutherland in 1957 [29] when he discovered that the activity of liver phosphorylase is stimulated indirectly by hormones, requiring a “heat-stable factor” that was later identified as cAMP [30]. That work established a paradigm of cell signaling whereby a first messenger (e.g., hormone or neurotransmitter) activates a receptor on the cell surface (canonically a GPCR) and activation of an intracellular effector molecule that produces the second messenger molecule. This process serves to greatly amplify the intracellular response since activation of just one receptor can lead to the production of multiple second messenger molecules. Since the discovery of cAMP, several other second messengers have been identified, including cGMP [32], inositol trisphosphate [33, 34], diacylglycerol [35], and calcium [36, 105]. Each of these molecules was painstakingly identified through rudimentary biochemical methods. With advances in metabolomics technologies however, we now have the ability to examine a broad complement of small molecules in a single experiment.

In yeast, BCAAs are catabolized through the Ehrlich pathway. The end products of this pathway are fusel alcohols or fusel acids [99]. Much like the catabolism of BCAAs by the Ehrlich pathway in yeast, BCAAs in mammals are metabolized to 2-keto acids by the branched-chain amino acid transaminases (BCATs). The 2-keto acids primarily undergo oxidative decarboxylation by branched-chain keto acid dehydrogenase (BCKDH) to yield substrates for further oxidation and generation of anaplerotic compounds for the TCA cycle [106]. Alternatively, 2-keto acids can be reduced to form the 2-hydroxy acids that are the subject of this research. Excess levels of 2-hydroxy acids are found in human patients with maple syrup urine disease (MSUD), also known as branched-chain ketoaciduria. This is an autosomal recessive disorder caused by a deficiency in BCKDH activity. Without this enzyme, 2-keto acids accumulate and are shunted towards formation of 2-hydroxy acids [107]. Accumulation of 2-keto

and 2-hydroxy acids often results in brain damage due to impaired neurotransmitter function caused by inhibition of glutamate uptake [108, 109], and neuronal energy metabolism dysfunction [110, 111]. Although 2-hydroxy acids are produced, the accumulation of BCAAs and 2-keto acids seems to have the greater impact on the pathophysiology of MSUD [112].

Previously we showed that osmotic stress dampens and delays the mating pheromone response in yeast [4]. Here we describe potential mechanisms of this cross-pathway regulation. While our analysis focused on yeast, several tissues routinely experience osmotic stress, and can develop disease if osmoregulation is impaired. For example, osmotic stress can promote dry eye disease [47] and diabetic retinopathy [48]. High osmolarity in the vasculature can lead to hypertension [51] and a hyperosmolar hyperglycemic state in diabetics [49]. Importantly, BCAA metabolism is also conserved in humans [113]. Reduced levels of the BCAAs are observed in heart failure, sepsis, trauma, and burn injury [114]. Moreover, a reduction in the expression of BCATs and BCKDH, as well as an increase in the levels of 2-keto acids, have been identified as hallmarks of heart failure [115]. However the connection between osmotic stress signaling and BCAA metabolism is not clearly understood. Collectively, these examples highlight the need for a more complete understanding of the osmotic stress response and of BCAA metabolism.

In summary, we identified 2-hydroxy BCAA derivatives as candidate second messengers of the osmotic stress pathway. As second messengers, these molecules are likely used to amplify the osmotic stress response and coordinate responses to hormones and neurotransmitters. A challenge for the future is to determine the mechanism by which Hog1 (or p38) promotes BCAA derivative accumulation, their cellular target(s) in both yeast and humans, as well as their potential as lead molecules for pharmacological control of the stress response in a mammalian system.

Materials and Methods

Strains and Plasmids

All strains were generated from the BY4741 wild type strain (*MATa his3Δ1 leu2Δ0 met15Δ0 ura3Δ0*) [116]. Gene deletion strains were generated by homologous recombination of PCR-amplified drug resistance genes from the pFA6a-KanMX6 [117] or pFA6a-hphMX6 plasmids [118], with flanking sequence homologous to the gene of interest [119], or by the delitto perfetto method, leaving no selection marker [120]. Similarly, Flag-tagged strains were generated by homologous recombination of the PCR-amplified cassette from pFA6a-6xGly-3xFlag-HIS3MX6 [121], with flanking sequence homologous to either side of the stop codon of the gene of interest. *Bat1*^{5A} *Bat2*^{3A} non-phosphorylatable mutants were generated using the delitto perfetto method. *BAT1* was replaced with the CORE cassette and then with synthesized *BAT1-5A*. The same steps were then used to replace *BAT2* with *BAT2-3A*. All cells were grown at 30°C unless otherwise noted.

The pRS426-P_{FUS1}-YeGFP3 plasmid was generated by subcloning the YeGFP3 gene [122] under control of the yeast *FUS1* promoter from pDS30 (from Daria Siekhaus, University of California, Berkeley) [123] into pRS426 [124], by digestion with BamHI and XhoI, and ligation of gel-purified products. pYEplac181-pHluorin (*2μ*, *amp*^R, *LEU2*⁺) was the gift of Rajini Rao (Johns Hopkins University) [84, 94, 95].

Environmental Stress Timecourses

Cells were grown to saturation overnight in SCD medium, diluted to OD₆₀₀ = 0.10, grown to OD₆₀₀ ~0.6-0.8, then diluted again and grown to OD₆₀₀ ~1.0. Aliquots were mixed 19:1 with 6.1 N trichloroacetic acid (TCA) and placed on ice. SCD or SCD containing 3x stress stimulus was added to the experimental cell cultures. Aliquots were collected at the times indicated, added

Table 2.2 Yeast strains used in this study.

Strain Name	Genotype	Source
BY4743	<i>MATa/α leu2Δ₀/ leu2Δ₀ LYS2/lys2Δ₀ met15Δ₀/MET15 his3-1/ his3-1 ura3Δ₀/ ura3Δ₀</i>	(Brachmann et al. 1998)
BY4741 ^a	<i>MATa leu2Δ₀ met15Δ₀ his3-1 ura3Δ₀</i>	(Brachmann et al. 1998)
<i>hog1Δ</i>	<i>MATa hog1Δ₀</i>	This study
<i>hog1^{K52R}</i>	<i>MATa hog1^{K52R}</i>	(Hao et al. 2007)
<i>bat1Δ</i>	<i>MATa bat1::KanMX4</i>	This study
<i>bat2Δ</i>	<i>MATa bat2::HphMX6</i>	This study
<i>TetO₇-BAT1-FLAG bat2Δ</i>	<i>MATa CMV-tTA-URA3 KanMX4-TetO₇-P_{BAT1} BAT1::6xGly-3xFLAG-HIS3MX6 bat2::HphMX6</i>	This study
<i>pdr12Δ</i>	<i>MATa pdr12::KanMX4</i>	This study
<i>bat1^{5A} bat2^{3A}</i>	<i>MATa bat1^{T68A, T101A, T175A, S186A, S339A} bat2^{T51A, T158A, S322A}</i>	This study
<i>BAT1-Flag</i>	<i>MATa BAT1-6xGly-3xFLAG-HIS3MX6</i>	This study
<i>bat1^{5A}-Flag</i>	<i>MATa bat1^{T68A, T101A, T175A, S186A, S339A}-6xGly-3xFLAG-HIS3MX6</i>	This study
<i>bat1^{5A}-Flag bat2Δ</i>	<i>MATa bat1^{T68A, T101A, T175A, S186A, S339A}-6xGly-3xFLAG-HIS3MX6 bat2::HphMX6</i>	This study
<i>BAT2-Flag</i>	<i>MATa BAT2-6xGly-3xFLAG-HIS3MX6</i>	This study
<i>bat2^{3A}-Flag</i>	<i>MATa bat2^{T51A, T158A, S322A}-6xGly-3xFLAG-HIS3MX6</i>	This study
<i>bat1Δ bat2^{3A}-Flag</i>	<i>MATa bat1::KanMX4 bat2^{T51A, T158A, S322A}-6xGly-3xFLAG-HIS3MX6</i>	This study
<i>elm1Δ</i>	<i>MATa elm1::KanMX4</i>	(Clement et al. 2013)
<i>sak1Δ</i>	<i>MATa sak1::KanMX4</i>	(Clement et al. 2013)
<i>tos3Δ</i>	<i>MATa tos3::KanMX4</i>	(Clement et al. 2013)
<i>elm1Δ sak1Δ</i>	<i>MATa elm1::URA3 sak1::KanMX4</i>	(Clement et al. 2013)
<i>elm1Δ tos3Δ</i>	<i>MATa elm1::URA3 tos3::KanMX4</i>	(Clement et al. 2013)
<i>sak1Δ tos3Δ</i>	<i>MATa sak1::URA3 tos3::KanMX4</i>	(Clement et al. 2013)
<i>elm1Δ sak1Δ tos3Δ</i>	<i>MATa elm1Δ₀ sak1::URA3 tos3::KanMX4</i>	This study
<i>elm1Δ sak1Δ tos3Δ</i>	<i>MATa elm1Δ::URA3 sak1::LEU2 tos3::KanMX4</i>	(Clement et al. 2013)
<i>reg1Δ</i>	<i>MATa reg1::KanMX4</i>	(Clement et al. 2013)

^aAll strains were derived from BY4741

Table 2.3 Plasmids used in this study.

Plasmid Name	Description	Source
pYEplac181	2 μ , amp ^R , LEU2+, P _{TEF1} -pHluorin	(Isom et al. 2013) Dr. Rajini Rao, Johns Hopkins
pRS426-P _{FUS1} -YeGFP3	2 μ , amp ^R , URA3+, P _{FUS1} -YeGFP3	This Study

to TCA, and placed on ice. Cell pellets were collected by centrifugation at 1962 x g for 2 minutes, and resuspended in 10 mM NaN₃. Cells were collected by centrifugation at 16,060 x g for 1 minute, the supernatant was removed, and cell pellets were stored at -80°C until use.

Heat shock experiments were carried out by growing cells as indicated above, then transferring the cultures to a 42°C water bath incubator/shaker and adding 1/3 final volume of SCD medium pre-warmed to 42°C.

For glucose limitation experiments, wild-type cells were grown as above to an OD₆₀₀ ~0.8, collected by centrifugation at 1962 x g for 2 minutes, resuspended with one-quarter volume of glucose-free SCD medium, centrifuged again and resuspended in original volume SCD medium containing either 2% or 0.05% glucose. Note that centrifugation alone leads to partial Gpa1 phosphorylation (Figure 1A, 2% Glucose curve).

Standard SDS-PAGE and Immunoblotting

Cell Lysis and Protein Quantification

Cell pellets were thawed on ice, and resuspended in ice cold TCA buffer (10 mM Tris-HCl, pH 8.0, 10% TCA, 25 mM ammonium acetate, 1 mM ethylenediaminetetraacetic acid). Cells were vortexed for 10 minutes, then collected by centrifugation at 16,060 x g for 10 minutes at 4°C. Pellets were reconstituted in resuspension buffer (100 mM Tris-HCl, pH 11.0, 3% sodium dodecyl sulfate (SDS)), heated at 99°C for 10 minutes, cooled to room temperature for 10 minutes, and centrifuged at 16,060 x g for 1 minute. Lysates were transferred to new tubes and 5 µL was used in a Bio-Rad DC Protein Assay (Bio-Rad #5000112), carried out according to the manufacturer's protocol, and compared against a bovine serum albumin standard curve. Lysates were normalized to 2 µg/µL with resuspension buffer and 6x SDS sample buffer (350

mM Tris-HCl, pH 6.8, 30%(v/v) glycerol, 10%(w/v) SDS, 600 mM dithiothreitol, 0.012%(w/v) bromophenol blue), and used immediately or stored at -80°C.

Immunoblotting

Cell lysates were heated at 99°C for 10 minutes, then 40 µg of protein was loaded onto 10% SDS-PAGE gels. Gels were then run in SDS electrophoresis buffer (25 mM Tris base, 20 mM glycine, 0.1%(w/v) SDS) at room temperature for 20 minutes at 20 mA/gel after which, current was increased to 25 mA/gel for 110 minutes. Electrophoresed proteins were then transferred to nitrocellulose membranes at 100 V for 90 minutes at 4°C in transfer buffer (20% methanol, 25 mM Tris Base, 200 mM glycine). Membranes were blocked in TBS-T (100 mM Tris Base, 150 mM NaCl, 0.1% Tween-20, pH 7.5) containing 5% (w/v) milk and 10 mM NaN₃ for 1 hour unless otherwise indicated. Western blots were probed with antibodies raised against Gpa1 (in-house rabbit polyclonal antibody, 1:1,000 ratio) [125], phospho-Snf1 (phospho-AMPKα (Thr172) 40H9 Rabbit mAb, Cell Signaling Technology #2353, 1:2,000 ratio), Snf1 (poly histidine HIS-1 mouse mAb, Sigma-Aldrich #H1029, 1:3,000 ratio), Hog1 (Santa Cruz Biotechnology #sc-6815, 1:500 ratio), phospho-Hog1 (phospho-p38 MAPK (Thr180/Tyr182) 28B10 Mouse mAb, Cell Signaling Technology #9216, 1:500 ratio), and Glucose-6-phosphate dehydrogenase as a loading control (G6PDH, Sigma # A9521, 1:50,000 ratio). Blots were incubated with primary antibodies for 1 hour to overnight, washed 3 x 5 minutes with TBS-T, then incubated with horseradish peroxidase-conjugated secondary antibodies raised against rabbit (Bio-Rad #1662408), mouse (Bio-Rad #1721011), or goat (Santa Cruz Biotechnology #sc-2768) at a 1:10,000 ratio in TBS-T containing 5% (w/v) milk, and washed 3 x 5 minutes with TBS-T. Blots were imaged on a Bio-Rad ChemiDoc MP imaging system after a 5 minute incubation with Clarity ECL Western Blotting Substrate (Bio-Rad #1705061).

Phos-tag SDS-PAGE and Immunoblotting

Cell Lysis and Protein Quantification

Frozen cell pellets were collected as described above. Cell pellets were thawed on ice, and resuspended in ice cold TCA buffer without EDTA (10 mM Tris-HCl, pH 8.0, 10% TCA, 25 mM ammonium acetate). Cells were lysed and lysate protein content was determined by the Bio-Rad DC Protein Assay as described above. Lysates were normalized to 1.5 µg/µL with resuspension buffer and 2x SDS sample buffer (500 mM Tris-HCl, pH 8.5, 20%(v/v) glycerol, 2%(w/v) SDS, 200 mM dithiothreitol, 0.01%(w/v) bromophenol blue), and used immediately or stored at -80°C.

Phos-tag bis-tris acrylamide gel preparation and transfer for immunoblotting

8% bis-tris SDS-PAGE gels containing 20 µM Phos-tag and 40 µM Zn(NO₃)₂ were prepared, run and transferred as described previously [126]. Briefly, protein samples were heated at 70°C for 10 minutes, then 15 µg of protein per lane was loaded onto Phos-tag gels. Gels were then run in phos-tag SDS-PAGE electrophoresis buffer (50 mM Tris base, 50 mM MOPS, 0.1%(w/v) SDS, 5mM sodium bisulfite, pH 7.2) at room temperature 150V for 90 minutes. Resolving layers were removed and equilibrated in transfer buffer (1x NuPAGE transfer buffer (Life Technologies # NP0006-1), 20%(v/v) methanol, 2.5 mM sodium pyrophosphate, 5 mM sodium bisulfite) for 15 minutes at room temperature with shaking to release phospho-proteins from Phos-tag. Electrophoresed proteins were then transferred to polyvinylidene difluoride (PVDF) membranes (Millipore # IPVH00010) 20 V for 20 hours at 4°C.

Immunoblotting

Membranes were blocked in TBS-T (100 mM Tris Base, 150 mM NaCl, 0.1% Tween-20, pH 7.5) containing 5% (w/v) milk and 10 mM NaN₃ for 1 hour. Membranes were then probed for

Flag-tagged proteins using the anti-Flag M2 primary antibody (Sigma # F3165) at a 1:10,000 ratio in blocking buffer, and Glucose-6-phosphate dehydrogenase as a loading control (G6PDH, Sigma # A9521, 1:50,000 ratio). Blots were incubated with primary antibodies for 1 hour, washed 3 x 5 minutes with TBS-T, then incubated with horseradish peroxidase-conjugated secondary antibodies raised against rabbit (Bio-Rad #1662408), or mouse (Bio-Rad #1721011) at a 1:10,000 ratio in TBS-T containing 5% (w/v) milk for 1 hour, and washed 3 x 5 minutes with TBS-T. Blots were imaged on a Bio-Rad ChemiDoc MP imaging system after a 5 minute incubation with Clarity ECL Western Blotting Substrate (Bio-Rad #1705061).

Intracellular pH Measurements

Wild type yeast were transformed with plasmid pYEplac181-pHluorin [84, 94, 95] and grown in SCD-Leu medium. For cells treated with BCAA derivatives (30 mM) the medium was titrated to pH 5.0 with HCl. Experiments and pH_i calculations were carried out as in [84] using the indicated stressor or metabolite at 3x stock concentration.

Metabolomics

Wild type and *hog1Δ* cells were grown to saturation overnight, diluted to $\text{OD}_{600} = 0.10$ grown to $\text{OD}_{600} \sim 0.6$, diluted again to $\text{OD}_{600} = 0.00075$, incubated overnight at to $\text{OD}_{600} \sim 0.9$. Cultures were then split in half and grown to $\text{OD}_{600} \sim 1.0$ and mixed 1:4 with SCD or SCD plus 2.5M KCl. After 3 minutes the cultures were transferred to 250 mL conical bottles (Corning #430776) and centrifuged for 3 minutes at 2,500 rpm (1819.3 x g) in a Sorvall RC3C Plus centrifuge using an H6000A swinging bucket rotor. After aspirating the supernatant the cell pellets were snap-frozen in place with liquid nitrogen and stored at -80°C . The cells were exposed to KCl for a total of 20 minutes. Frozen pellets were submitted to Metabolon, Inc. for GC-MS and LC-MS/MS analysis of metabolites.

Sample Preparation

Samples were stored at -70°C until processed. Sample preparation was carried out as described previously [71] at Metabolon, Inc. Briefly, recovery standards were added prior to the first step in the extraction process for quality control purposes. To remove protein, dissociate small molecules bound to protein or trapped in the precipitated protein matrix, and to recover chemically diverse metabolites, proteins were precipitated with methanol under vigorous shaking for 2 min followed by centrifugation. The resulting extract was divided into four fractions: one for analysis by ultra high performance liquid chromatography-tandem mass spectrometry (UPLC-MS/MS; positive mode), one for analysis by UPLC-MS/MS (negative mode), one for analysis by gas chromatography–mass spectrometry (GC-MS), and one sample was reserved for backup.

Three types of controls were analyzed in concert with the experimental samples: samples generated from a pool of each experimental sample served as technical replicates throughout the metabolomics platform run; extracted water samples served as process blanks; and a cocktail of standards spiked into every analyzed sample allowed instrument performance monitoring. Instrument variability was determined by calculating the median relative standard deviation (RSD) for the standards that were added to each sample prior to injection into the mass spectrometers (median RSD = 5; $n = 29$ standards). Overall process variability was determined by calculating the median RSD for all endogenous metabolites (i.e., non-instrument standards) present in 100% of the pooled yeast technical replicate samples (median RSD = 9%; $n = 296$ metabolites). Experimental samples and controls were randomized across the platform run.

Mass Spectrometry Analysis

Non-targeted MS analysis was performed at Metabolon, Inc. Extracts were subjected to either GC-MS [127] or UPLC-MS/MS[71]. The chromatography was standardized and once the method was validated, and no further changes were made. As part of Metabolon's general practice, all columns were purchased from a single manufacturer's lot at the outset of experiments. All solvents were similarly purchased in bulk from a single manufacturer's lot in sufficient quantity to complete all related experiments. For each sample, vacuum-dried samples were dissolved in injection solvent containing eight or more injection standards at fixed concentrations, depending on the platform. The internal standards were used both to assure injection and chromatographic consistency. Instruments were tuned and calibrated for mass resolution and mass accuracy daily.

The UPLC-MS/MS platform utilized a Waters Acquity UPLC and a ThermoFisher LTQ mass spectrometer, which included an electrospray ionization source and a linear ion-trap mass analyzer. The instrumentation was set to monitor for positive ions in acidic extracts or negative ions in basic extracts through independent injections. The instrument was set to scan 99–1000 m/z and alternated between MS and MS/MS scans. The scan speed was approximately six scans per s (three MS and three MS/MS scans). MS/MS scans were collected using dynamic exclusion, a process in which after an MS/MS scan of a specific m/z has been obtained, then that m/z is placed on a temporary MS/MS exclude list for a user-set period of time to allow greater MS/MS coverage of ions present in the MS scan because the instrument will not trigger an MS/MS scan of the same ion repeatedly. Extracts were loaded onto columns (Waters UPLC BEH C18-2.1×100 mm, 1.7 μm) and gradient-eluted with water and 95% methanol containing

0.1% formic acid (acidic extracts) or 6.5 mM ammonium bicarbonate (basic extracts). Columns were washed and reconditioned after every injection.

The samples destined for analysis by GC-MS were dried under vacuum desiccation for a minimum of 18 h prior to being derivatized under dried nitrogen using bistrimethylsilyltrifluoroacetamide. Derivatized samples were separated on a 5% phenyldimethyl silicone column with helium as carrier gas and a temperature ramp from 60° to 340°C within a 17-min period. All samples were analyzed on a Thermo-Finnigan Trace DSQ MS operated at unit mass resolving power with electron impact ionization and a 50–750 atomic mass unit scan range.

Compound Identification, Quantification, and Data Curation

Metabolites were identified by automated comparison of the ion features in the experimental samples to a reference library of chemical standard entries that included retention time, molecular weight (m/z), preferred adducts, and in-source fragments as well as associated MS spectra and curated by visual inspection for quality control using software developed at Metabolon [128]. Identification of known chemical entities is based on comparison to metabolomic library entries of purified standards. Over 4,000 commercially available purified standard compounds have been acquired and registered into LIMS for distribution to both the LC/MS and GC/MS platforms for determination of their detectable characteristics. Peaks were quantified using area under the curve.

NMR Spectroscopy

For NMR measurements, ¹⁵N-enriched Gai-Δ31 produced as in [129] was exchanged into NMR buffer (20 mM sodium phosphate, pH 7.0, 50 mM NaCl, 2 mM MgCl₂, 200 μM GDP, 5% D₂O). Each NMR sample contained 50 μM Gai-Δ31 and 1.25 mM ligand. NMR spectra were acquired at 25 °C on a Bruker Avance 850 NMR spectrometer. Two-dimensional ¹H–¹⁵N HSQC

experiments were recorded with 1024 and 128 complex points in the direct and indirect dimensions, respectively, 44 scans per increment and a recovery delay of 1.0 s. Spectral widths used were 13586.957 Hz (^1H) and 3015.682 (^{15}N) Hz. Spectra were processed and analyzed using NMRPipe (NIDDK, NIH) and Sparky (UCSF).

Transcriptional Reporter Assay

Four colonies of the same strain transformed with plasmid pRS426- P_{FUS1} -YeGFP3 and one colony of the untransformed background strain (to use for background fluorescence subtraction) were grown to $\text{OD}_{600} \sim 1.0$. Cells were added in duplicate to black clear-bottomed 96-well plates containing 10x stocks of serially diluted α -factor mating pheromone ranging in concentration from $1 \times 10^{-4.5}$ M to 1×10^{-10} M prepared in sterile water, and 5x stocks of stimulus solution prepared in growth medium. The OD_{600} for each well was measured for cell number normalization. After 3 hours GFP fluorescence was measured at an excitation wavelength of 485 nm, and emission wavelength of 538 nm, using a cutoff of 530 nm, in a Molecular Devices Spectramax M5 plate reader. For data presentation, raw fluorescence values from each well were normalized to the number of cells in that well (represented by the OD_{600}) using the shorthand Taylor Series $\frac{1}{1+x}$ where $x = \text{OD}_{600}$. Normalized values of each technical duplicate were averaged, and normalized values from the background strain (containing no fluorescence reporter) were subtracted. Finally, each well was normalized as a percent to the average maximum fluorescence value in the α -factor only treated positive control. Dose-response curves were fitted using a nonlinear Boltzmann function.

Statistical Analysis

All data are reported as mean \pm the standard deviation. Statistical significance was determined by an unpaired two-sided student's t-test. In all cases, a p-value ≤ 0.05 was considered to be statistically significant.

CHAPTER 3 – COMPARATIVE METHODS ANALYSIS FOR MEASURING MAPK- AND TRANSCRIPTIONAL ACTIVATION IN THE YEAST PHEROMONE RESPONSE PATHWAY

Summary

The pheromone response pathway of the yeast *S. cerevisiae* is a well-established model for the study of G proteins and mitogen-activated protein kinase (MAPK) cascades. Our long-standing ability to combine gene editing with quantitative activity assays has provided a thorough understanding of pathway function and regulation. The pheromone response pathway has been used as a workhorse in drug screening platforms seeking to identify new therapeutics that target mammalian G protein signaling pathways. Additionally, assays monitoring phospho-MAPK levels and pathway-specific transcriptional reporters are routinely used to study perturbations to upstream G protein signaling. The long-standing methods used to measure these signaling events are immunoblotting with phospho-specific antibodies for MAPK activation, and pathway-specific β -galactosidase assays for transcriptional activation. Recent technological advances have garnered new, alternative methods to probe the pheromone response pathway at the level of MAPK activation and transcription, specifically Phos-tag immunoblotting and GFP-based transcriptional activity assays. Here, we compare gold-standard methods with these newer and alternative technologies in wild-type yeast and a *bar1 Δ* mutant strain with increased sensitivity to pheromone. We highlight important differences between newer and established methodologies, and compare the advantages and disadvantages of each as applied to the yeast model.

Introduction

The pheromone response pathway of the budding yeast *Saccharomyces cerevisiae* is a mitogen-activated protein kinase (MAPK) pathway that is regulated by a G protein-coupled receptor (GPCR) and heterotrimeric G protein, and thus serves as an ideal system in which to study both G protein and MAPK signaling. Indeed, the first MAPKs [130, 131] and MAPK signaling cascades were identified in yeast [132-135]. Additionally, yeast serves as a model system for studying fundamental mechanisms of GPCR signal regulation. In addition to its use as a simple system for studying cell signaling, the yeast pheromone response pathway has been modified and employed for use as a screening platform for directed evolution of designer receptors [136, 137], identifying new human GPCR agonists, antagonists, and modulators [138, 139] (reviewed in [140]), as well as studying the effects of toxicants on GPCR pathways [141].

The pheromone response pathway initiates events necessary for mating of haploid **a**- and α cells. These cells secrete specific pheromones, **a**-factor and α -factor, which bind to cognate receptors on cells of the opposite type. Since **a**-factor is prenylated and difficult to isolate, most work is done with α -factor and the GPCR Ste2. Once activated, the receptor promotes the exchange of GDP for GTP in the G α subunit, Gpa1, and subsequent dissociation of the G $\beta\gamma$ complex, Ste4/18. Ste4/18 then binds to the p21-activated kinase (PAK), Ste20, and the scaffold protein, Ste5 recruiting the components of the MAPK signaling cascade— the MAPKKK Ste11, the MAPKK Ste7, and the MAPK Fus3 [142, 143]. A homologous MAPK, Kss1, is also activated by Ste7, but binds poorly to Ste5, and this interaction is not required for Kss1 activation [62, 144, 145]. Either MAPK phosphorylates the transcription factor Ste12, which promotes transcription of pheromone-specific genes, including *FUS1*, to prepare the cell for mating [63, 64].

A comprehensive understanding of any signaling pathway requires quantitative measures of pathway activation. High-throughput assays, such as those used to screen for drugs acting on GPCRs, have also taken advantage of transcriptional reporters using the *FUS1* promoter fused to reporter genes including LacZ (encoding β -galactosidase), fluorescent proteins (e.g. GFP), drug resistance genes, and auxotrophic marker genes.

Here, we compare two methods for measuring the phosphorylation of the MAPKs Fus3 and Kss1 by immunoblotting—phospho-specific antibodies, and Phos-tag immunoblot analysis. We also compare two different transcriptional reporters—the enzyme-based P_{FUS1} -LacZ (or β -galactosidase) assay, and the fluorescent protein-based P_{FUS1} -GFP assay. We compare the advantages and disadvantages of each method, provide experimental data to illustrate their use, and discuss experimental scenarios where each method is favored.

Materials and Methods

Strains and Plasmids

All strains were generated from the BY4741 wild-type background [116]. Genetic deletion of *BARI* was achieved by homologous recombination of the PCR-amplified G418 drug resistance gene from the pFA6a-KanMX6 [117] plasmid, with flanking sequence homologous to the *BARI*, transformed by lithium acetate transformation [119]. Similarly, Kss1-9xMyc-tagged wild-type and *bar1* Δ strains were generated by homologous recombination of the PCR-amplified 9xMyc cassette with resistance to hygromycin B from the pYM20 plasmid (pYM-9xMyc-hphNT1) [146], with flanking sequence homologous to either side of the stop codon of *KSS1*. The pRS426- P_{FUS1} -YeGFP3 plasmid was generated by subcloning the YeGFP3 gene [122] under control of the yeast *FUS1* promoter from pDS30 (from Daria Siekhaus, University of California,

Berkeley) [123] into pRS426 [124] by digestion with BamHI and XhoI, and subsequent ligation of gel-purified products. The pRS423-P_{FUS1}-LacZ plasmid was generated previously [147].

Phospho-MAPK Time Courses

Cells were grown to saturation overnight in SCD medium at 30°C. Cultures were diluted with SCD medium to OD₆₀₀ = 0.10 and grown until OD₆₀₀ ~0.6-0.8, then diluted again and grown to an OD₆₀₀ ~1.0. An aliquot was collected for the 0 minute time point, added to 6.1 N trichloroacetic acid (TCA) to achieve 5% final TCA concentration, and placed on ice. For pheromone stimulation, 1000x α -factor was added to a final concentration of 3 μ M or 0.3 μ M (diluted from the same stock). Cultures were incubated at 30°C, and aliquots were collected at 5, 15, 30, 60, and 90 minutes, added to TCA, and placed on ice. Cell pellets were collected by centrifugation at 1962 x g for 2 minutes, and then washed with 10 mM NaN₃. Pellets were recollected by centrifugation at 16,060 x g for 1 minute, supernatant was removed, and pellets were stored at -80°C until use.

Cell Lysis and Protein Quantification

The same cell lysates were used for both conventional- and Phos-tag SDS-PAGE, and were prepared using optimal conditions for Phos-tag SDS-PAGE as described previously [126]. Cell pellets were thawed on ice, and resuspended in ice cold TCA buffer without EDTA (10 mM Tris-HCl, pH 8.0, 10% TCA, 25 mM ammonium acetate). Cells were vortexed for 10 minutes at 4°C, then pelleted by centrifugation at 16,060xg for 10 minutes at 4°C. Pellets were resuspended in resuspension buffer (100 mM Tris-HCl, pH 11.0, 3% sodium dodecyl sulfate (SDS)), then heated at 99°C for 10 minutes, cooled to room temperature for 10 minutes, and centrifuged at 16,060xg for 1 minute.

Lysates were transferred to new tubes and 5 μL were used in a Bio-Rad DC Protein Assay (Bio-Rad # 5000112) carried out per the manufacturer's protocol. Absorbance values were compared against a bovine serum albumin standard curve ranging from 0-10 $\mu\text{g}/\mu\text{L}$ prepared in resuspension buffer. Lysates were normalized to 2 $\mu\text{g}/\mu\text{L}$ with resuspension buffer and 2x SDS sample buffer (500 mM Tris-HCl, pH 8.5, 20% (v/v) glycerol, 2% (w/v) SDS, 200 mM dithiothreitol, 0.01% (w/v) bromophenol blue), and used immediately or stored at -80°C . For use, samples were heated at 70°C for 10 minutes prior to loading.

Conventional SDS-PAGE and Immunoblotting

30 μg of protein sample were loaded onto 10% SDS-PAGE gels. Gels were then run in SDS electrophoresis buffer (25 mM Tris base, 20 mM glycine, 0.1% (w/v) SDS) at room temperature for 20 minutes at 20 mA/gel for even migration of protein into the stacking layer, after which, current was increased to 25 mA/gel for 110 minutes. Electrophoresed proteins were then transferred to nitrocellulose membranes at 100 V for 90 minutes at 4°C in transfer buffer (20% methanol, 25 mM Tris Base, 200 mM glycine).

Membranes were blocked in TBS-T (100 mM Tris Base, 150 mM NaCl, 0.1% Tween-20, pH 7.5) containing 5% (w/v) non-fat dry milk and 10 mM NaN_3 for 1 hour. Western blots were probed with antibodies specific for phospho-p44/42 MAPK, raised against a phosphorylated MAPK peptide (Cell Signaling # 4370, 1:500 ratio), total Fus3 MAPK (Santa Cruz Biotechnology # 6773 ,1:500 ratio), total Kss1-Myc (Myc-Tag (9B11) Mouse mAb, Cell Signaling Technology # 2276, 1:1,000 ratio), and glucose-6-phosphate dehydrogenase (G6PDH) as a loading control (Sigma # A9521, 1:50,000 ratio). Blots were incubated with primary antibodies diluted in blocking buffer overnight with shaking, except for G6PDH, which was incubated for 1 hour. Blots were washed 3 x 5 minutes with TBS-T, then incubated with

horseradish peroxidase-conjugated secondary antibodies raised against rabbit (goat anti-rabbit, Bio-Rad # 1662408), mouse (donkey anti-mouse, Jackson ImmunoResearch # 715-035-151), or goat (donkey anti-goat, Santa Cruz Biotechnology # sc-2020) at a 1:10,000 ratio in TBS-T containing 5% (w/v) non-fat dry milk for 1 hour, and then washed 3 x 5 minutes with TBS-T. Blots were imaged on a Bio-Rad ChemiDoc MP imaging system after a 5 minute incubation with Clarity ECL Western Blotting Substrate (Bio-Rad # 1705061). Blots were stripped of antibodies between probing for phospho-MAPK and total MAPK (combined anti-Fus3 and anti-Myc-Tag), and between probing for total MAPK and G6PDH loading control in stripping buffer (62.5 mM Tris-HCl (pH 6.8), 2% (w/v) SDS, 100 mM β -mercaptoethanol) at 65°C for 30 minutes in a dry oven with occasional agitation by hand. Stripped blots were rinsed thoroughly with distilled water, and then washed with TBS-T 3x10 minutes before re-probing.

Phos-tag SDS-PAGE and Immunoblotting

10% bis-tris SDS-PAGE gels containing 50 μ M Phos-tag and 100 μ M Zn(NO₃)₂ were prepared, ran and transferred as described previously [126]. Briefly, 15 μ g of protein sample were loaded onto Phos-tag gels. Gels were then run in phos-tag SDS-PAGE electrophoresis buffer (50 mM Tris base, 50 mM MOPS, 0.1% (w/v) SDS, 5mM sodium bisulfite, pH 7.2) at room temperature 150V for 90 minutes. Resolving layers were removed and equilibrated in transfer buffer (1x NuPAGE transfer buffer (Life Technologies # NP0006-1), 20% (v/v) methanol, 2.5 mM sodium pyrophosphate, 5 mM sodium bisulfite) for 15 minutes at room temperature with shaking to release phopho-proteins from Phos-tag. Electrophoresed proteins were then transferred to polyvinylidene difluoride (PVDF) membranes (Millipore # IPVH00010) at 20 V for 20 hours at 4°C.

Membranes were blocked in TBS-T (100 mM Tris Base, 150 mM NaCl, 0.1% Tween-20, pH 7.5) containing 2% (w/v) fish gelatin (to reduce background fluorescence) and 10 mM NaN₃ for 1 hour. Membranes were then probed for total Fus3 MAPK and total Kss1-Myc simultaneously, diluted as above in TBS-T containing 0.5% fish gelatin and 10 mM NaN₃, and for G6PDH as above. Blots were washed 3 x 5 minutes with TBS-T, then MAPK blots were incubated with fluorescent-conjugated secondary antibodies raised against donkey (Fus3: donkey anti-goat Alexa-647, Thermo Life Sciences # A-21447, 1:1,000 ratio; Kss1-Myc: donkey anti-mouse Alexa-555, Thermo Life Sciences # A-31570, 1:1,000 ratio) diluted in TBS-T containing 0.5% fish gelatin for 1 hour, and then washed 3 x 5 minutes with TBS-T. Membranes probed for G6PDH were probed with horseradish peroxidase-conjugated secondary antibodies raised against rabbit (Bio-Rad # 1662408, 1:10,000 ratio) in TBS-T containing 5% (w/v) milk for 1 hour, and washed 3 x 5 minutes with TBS-T. MAPK blots were imaged on a Bio-Rad ChemiDoc MP imaging system using multichannel acquisition mode (Fus3, Alexa 647 channel; Kss1-Myc, Alexa546 channel) optimizing for intense bands after washing off excess secondary antibodies. G6PDH blots were imaged on a Bio-Rad ChemiDoc MP imaging system after a 5 minute incubation with Clarity ECL Western Blotting Substrate (Bio-Rad # 1705061). Blots were stripped as described above between probing for MAPK proteins (combined anti-Fus3 and anti-Myc-Tag) and G6PDH loading control.

Image Densitometry

Densitometry analysis of band intensities was carried out in ImageJ [148] as described in [149]. Briefly, 16-bit raw TIF files were exported from the Bio-Rad Image Lab software and opened in ImageJ. Images were rotated to align bands horizontally, and the rectangle tool was used to select each lane for analysis. Rectangles were drawn to cover the entire width of the band

in one lane without causing overlap in other lanes, and were drawn long enough to sample the background pixel intensities surrounding the band(s) of interest. Upon selection of all lanes of interest, pixel intensity profiles were plotted, and background was subtracted by connecting the adjacent background intensities surrounding the peak corresponding to the band of interest using the line tool. The left and right sides of the peaks of interest were connected to the horizontal line created for background subtraction, effectively isolating roughly 95% of the Gaussian distribution. The magic wand tool was then used to obtain the area under the curve as the raw densitometry value.

Transcriptional Reporter Assays

Wild-type Kss1-Myc and *bar1Δ* Kss1-Myc strains were transformed with pRS423-P_{FUS1}-LacZ or pRS426-P_{FUS1}-YeGFP3 by lithium acetate transformation as above and plated on SCD – His or SCD –Ura selection medium, respectively, and incubated at 30°C for 2 days. Four colonies from each transformation were grown to saturation overnight in selection medium, then diluted to OD₆₀₀ = 0.2 the following day and grown to OD₆₀₀ ~0.6-0.8. These cultures were diluted to OD₆₀₀ = 0.002 (GFP) or OD₆₀₀ = 0.005 (LacZ) and grown overnight to an OD₆₀₀ ~0.8. Then, 90 μL of cells from each of the four cultures per strain were added per well in duplicate rows to black clear-bottomed 96-well plates containing 10 μL of 10x stocks of serially diluted α-factor mating pheromone ranging in final concentration from 1x10^{-4.5} M to 1x10⁻⁹ M prepared in sterile water, with one well per row containing 10 μL of sterile water only.

For P_{FUS1}-GFP assays, plates were incubated for 1.5 hours at 30°C, then the OD₆₀₀ for each well was measured to use for normalization, and GFP fluorescence was measured at an excitation wavelength of 483 nm, and emission wavelength of 518 nm. Plates were then read again for OD₆₀₀ and GFP fluorescence at 2, 2.5, and 3 hours, incubating at 30°C between reads.

For P_{FUS1}-LacZ assays were carried out as described previously [150]. Briefly, the OD₆₀₀ for each well was measured immediately after loading, and plates were incubated for 1.5 hours at 30°C. After incubation, 20 µL fluorescein di-β-D-galactopyranoside (FDG) solution (135 mM PIPES, 0.25% (v/v) Triton X-100, 0.5 mM FDG, pH 7.2) was added, and the plates were incubated at 37°C for 1.5 hours. The reaction was stopped by addition of 20 µL of 1 M sodium carbonate, and fluorescence was measured at an excitation wavelength of 485 nm, and emission wavelength of 580 nm. All measurements were taken using a Molecular Devices Spectramax i3x plate reader.

For data analysis and presentation, raw fluorescence values from each well were normalized to the number of cells in that well (represented by the OD₆₀₀) using the shorthand Taylor Series $\frac{1}{1+x}$ where $x = OD_{600}$. Normalized values of each technical duplicate were averaged. Finally, each well was normalized as a percent to the average maximum fluorescence value in the wild-type strain. Dose-response curves were fitted using a nonlinear Boltzmann function.

Results and Discussion

Our objective here is to disseminate methods that we use routinely to quantify the pheromone response in yeast. All of the assays are, in our experience, sufficiently robust and reliable for adoption in any well-equipped laboratory. The assays are downstream of the G protein, and include MAPK activation and MAPK-dependent gene transcription. To illustrate their ability to quantify differences in activity, we compare wild-type cells and mutants deficient in the secreted α-factor protease, Bar1. Cells lacking Bar1 (*bar1Δ*) exhibit elevated sensitivity to pheromone and sustained activation of the pathway [151-153]. Where activity is measured over

time, we compare the effects of two doses of pheromone—3 μM , and 0.3 μM , roughly 5-fold the EC_{50} of wild-type and *bar1 Δ* cells, respectively. Transcriptional reporter experiments are done over a range of pheromone concentrations.

MAPK activation measured by immunoblotting with phospho-MAPK antibodies

Upon pheromone binding to the GPCR, $\text{G}\beta\gamma$ promotes the activation of a protein kinase cascade that culminates with the phosphorylation and activation of the terminal MAPKs Fus3 and Kss1 [143]. In addition, *FUS3* gene transcription is induced, resulting in an increase in Fus3 protein levels over time [154]. Phosphorylation of MAPKs is commonly measured by immunoblotting using antibodies raised against a phosphorylated MAPK peptide (phospho-p44/42), which recognize both phospho-Fus3 and phospho-Kss1. To account for changes in Fus3 abundance, blots must then be stripped of phospho-specific antibodies and re-probed with antibodies against the total protein. Where commercial antibodies are unavailable, it is convenient to use an epitope-tagged version of the kinase of interest. In this case, we use commercial polyclonal antibodies to quantify Fus3, and monoclonal antibodies to quantify Myc-tagged Kss1 (Kss1-Myc). Upon normalization to a loading control, changes in phosphorylation or total protein can be calculated. However, because it is necessary to probe blots once for phosphorylated protein, and again for total protein levels, the stoichiometry of protein phosphorylation cannot be calculated. This approach can give only the relative amount of protein phosphorylation. Furthermore, Fus3 is known to exist in both mono-phosphorylated and dually phosphorylated pools [155, 156], and the phospho-p44/42 antibody is able to detect, to an extent, mono-phosphorylated Fus3 in addition to dually phosphorylated Fus3 [157]. This is a concern because mono-phosphorylated Fus3 does not stimulate, but rather inhibits downstream signaling [156]. Results from this method, therefore, are only an approximation of kinase activation.

To illustrate the method, we measured Fus3 phosphorylation in wild-type and *bar1Δ* cells in response to a low (0.3 μM) and high (3 μM) dose of pheromone. In wild-type cells subjected to 0.3 μM pheromone, Fus3 reached ~80% of maximal phosphorylation achieved at the high dose by 5 minutes, and then phosphorylation slowly decreased to ~25% of maximum by 90 minutes. At 3 μM pheromone, Fus3 reached ~70% of maximal phosphorylation achieved at this dose by 5 minutes, and continued to increase, reaching the maximum at 90 minutes (Figure 3.1A, top graph). In contrast, *bar1Δ* cells subjected to 0.3 μM pheromone, Fus3 again reached ~80% of maximal phosphorylation by 5 minutes, but this level of phosphorylation was sustained through the duration of the experiment. Upon stimulation with 3 μM pheromone Fus3 reached ~60% of maximal phosphorylation by 5 minutes, and continued to increase, reaching the maximum at 60 minutes before beginning to decline by 90 minutes (Figure 3.1B, top graph). These data are consistent with the fact that Bar1 degrades α -factor and thereby dampens the downstream signal over time.

Part of the increase in Fus3 phosphorylation is due to an increase in Fus3 expression. To account for this we strip the blots and reprobe with Fus3 antibodies. In wild-type cells subjected to 0.3 μM pheromone, Fus3 abundance increased by ~100% by 30 minutes, and these levels remained constant through 90 minutes. At 3 μM pheromone, Fus3 was maximally increased by ~150% by 60 minutes, and this level was sustained through 90 minutes (Figure 3.1A, middle graph). Induction occurred at a similar rate for 30 minutes, whereafter cells treated with the low dose remained at ~80% of that induced by the high dose. Fus3 induction was similar in wild-type and *bar1Δ* cells (Figure 3.1B, middle graph). Therefore, this analysis indicates that Bar1 limits Fus3 phosphorylation, but not Fus3 induction, at low doses of pheromone.

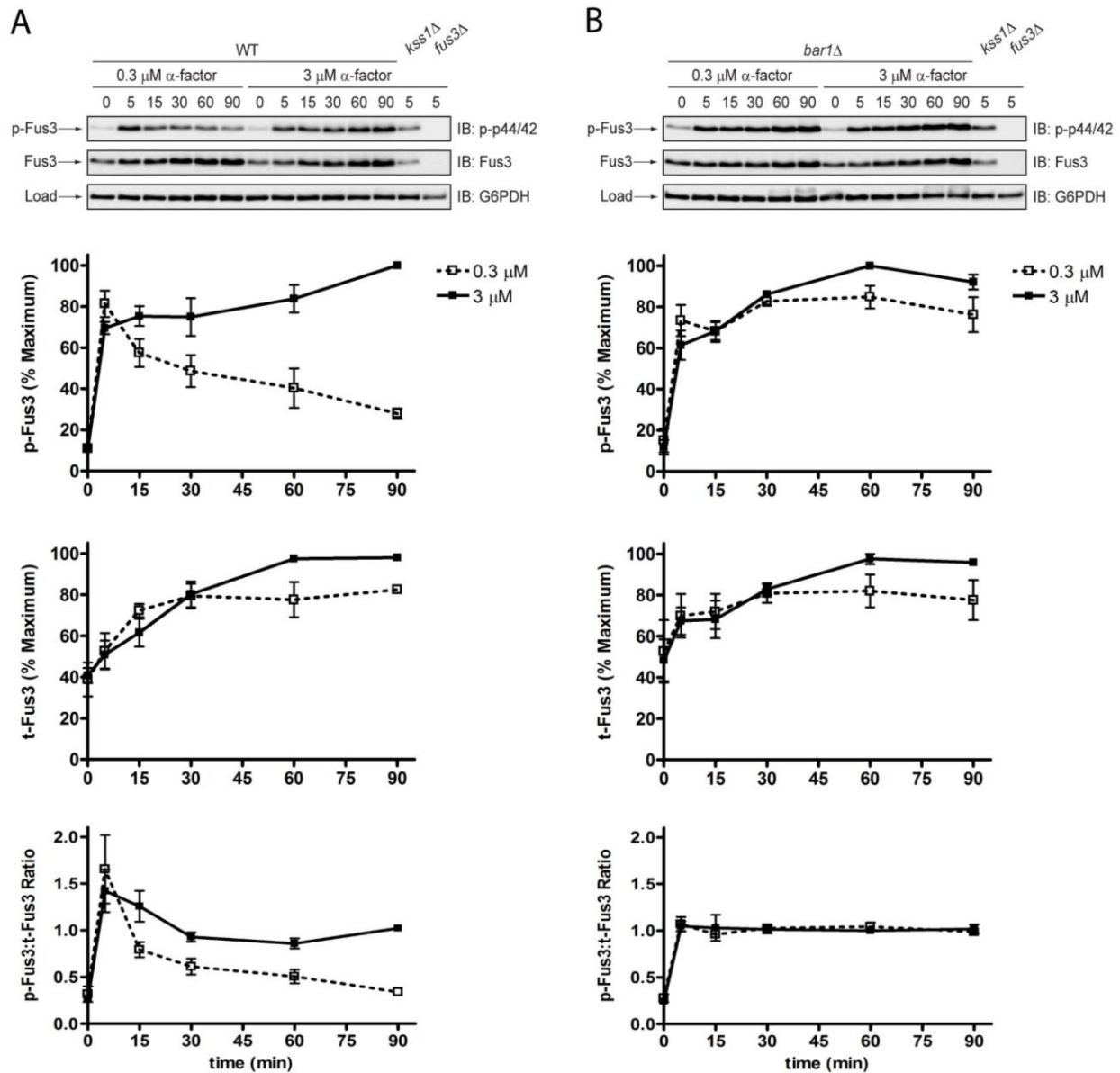


Figure 3.1 Phosphorylation of Fus3 by conventional SDS-PAGE and immunoblotting with phospho-p44-42 antibodies.

Western blot analysis of (A) wild-type cells or (B) *bar1Δ* cells treated with 0.3 μ M or 3 μ M α -factor mating pheromone were probed with phospho-p44/42 antibodies and total Fus3 antibodies. Phosphorylated Fus3 (top graphs) and total Fus3 (middle graphs) were plotted as % maximum signal on the blot. The phosphorylated Fus3 to total Fus3 ratio (bottom graphs) was calculated by dividing % maximum phosphorylated Fus3 by % maximum total Fus3. Data presented as mean \pm standard deviation, N = 3.

There are two schools of thought for how activated MAPK transmits the pheromone response. The first argues that the proportion of protein that is phosphorylated dictates pathway output. The second argues that the absolute amount of phosphorylated MAPK in the cell is more important. While we do not attempt to resolve this issue here, data from MAPK analyses can be interpreted in light of downstream outputs such as Ste12 phosphorylation, transcription induction, growth arrest, or mating efficiency.

We calculated the phosphorylated Fus3 to total Fus3 ratio for each dose of pheromone in wild-type and *bar1Δ* cells and plotted the ratio over time to demonstrate the differences between pheromone concentration and genotype. In wild-type cells, both doses of pheromone promoted rapid and robust phosphorylation of Fus3 by 5 minutes, while total Fus3 was only mildly induced, giving a ratio of ~1.5. Phosphorylation then declined in cells treated with the low dose, while Fus3 induction increased, thereby giving a ratio of <1 for the remainder of the experiment. In cells treated with the high dose, both phosphorylation and Fus3 induction continued to increase, giving a ratio of ~1 after 30 minutes (Figure 3.1A, bottom graph). In *bar1Δ* cells, phosphorylation increased proportionally with protein induction at both doses of pheromone, thus giving a ratio of 1 at all time points where pheromone was present (Figure 3.1B, bottom graph).

While Fus3 activation requires scaffolding by Ste5 in addition to activated Ste7 for its phosphorylation, Kss1 does not require binding to Ste5 for its phosphorylation [145]. Kss1 is also part of the filamentous growth MAPK pathway, and so has distinct roles from Fus3 [158, 159]. To understand differences between the activation of Fus3 and Kss1, we measured Kss1 phosphorylation in wild-type and *bar1Δ* cells in response to the low and high doses of pheromone as for Fus3 above. Commercial antibodies are not available for Kss1, so we used a C-

terminal 9xMyc-tagged version of Kss1, and probed with antibodies specific for the Myc tag to visualize Kss1. The same western blots used for the Fus3 analysis were probed for Kss1-Myc. The phospho-p44/42 antibody recognizes phosphorylated Kss1, so both MAPKs (as well as a third MAPK, Slt2) were simultaneously detected (Slt2 data not shown). After stripping the blots, we re-probed for total Fus3 and Kss1 simultaneously by combining both the total Fus3 antibody and the anti-Myc-tag antibody in the same solution. Because the data for both Fus3 and Kss1 were obtained from the same blots, the loading control was also the same for both proteins, and is presented in both Figure 3.1 and Figure 3.2.

In wild-type cells subjected to the low, 0.3 μ M dose of pheromone, Kss1 gave a nearly identical phosphorylation profile to that of Fus3. However, stimulation with the high, 3 μ M dose of pheromone promoted maximal Kss1 phosphorylation by 5 minutes, and this phosphorylation was sustained through 90 minutes (Figure 3.2A, top graph). In contrast, *bar1 Δ* cells subjected to the low dose for 5 minutes exhibited ~90% of maximal Kss1 phosphorylation attained by the high dose. Kss1 phosphorylation decreased to ~70% for the remainder of the experiment. At the high dose, *bar1 Δ* cells exhibited ~70% Kss1 phosphorylation from 5 minutes through 90 minutes (Figure 3.2B, top graph). These data also corroborate that *bar1 Δ* cells are supersensitive to pheromone, and Kss1, in addition to Fus3, is highly activated at lower doses of pheromone.

We next measured Kss1 protein levels in response to the low and high pheromone doses, immunoblotting for the Myc tag. In wild-type cells subjected to either the low or high dose of pheromone, Kss1 showed no induction through the duration of the experiment (Figure 3.2A, middle graph). In *bar1 Δ* cells subjected to the low dose exhibited modest induction at 5 minutes that then returned to base-line by 60 minutes. At the high dose, no induction was observed, and instead a slight reduction in Kss1 levels was observed by 90 minutes (Figure 3.2B, middle

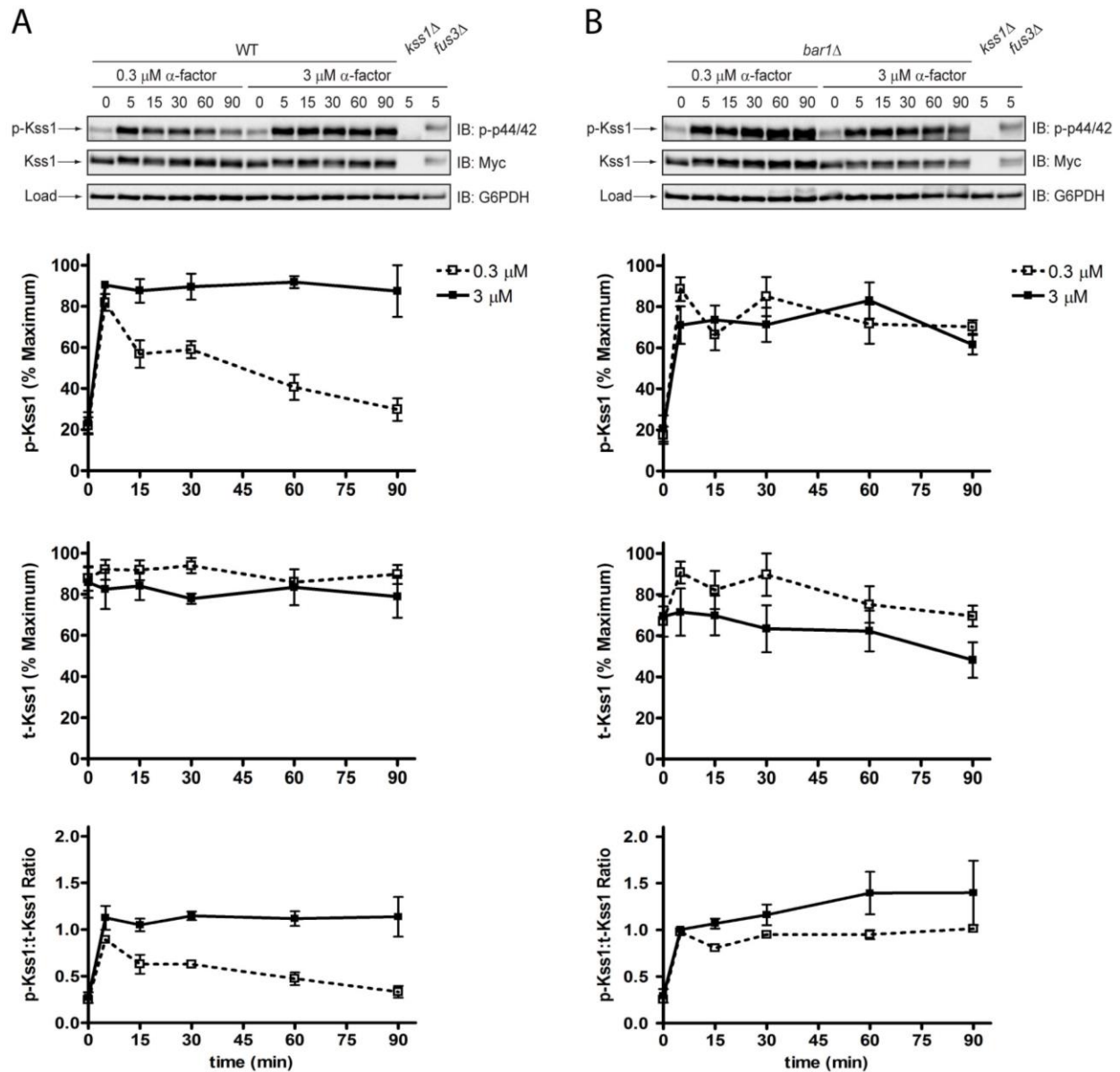


Figure 3.2 Phosphorylation of Kss1 by conventional SDS-PAGE and immunoblotting with phospho-p44-42 antibodies.

Western blot analysis of (A) wild-type cells or (B) *bar1* Δ cells treated with 0.3 μ M or 3 μ M α -factor mating pheromone were probed with phospho-p44/42 antibodies and anti-Myc tag antibodies to identify Kss1. Phosphorylated Kss1 (top graphs) and total Kss1 (middle graphs) were plotted as % maximum signal on the blot. The phosphorylated Kss1 to total Kss1 ratio (bottom graphs) was calculated by dividing % maximum phosphorylated Kss1 by % maximum total Kss1. Data presented as mean \pm standard deviation, N = 3.

graph). These data indicate that like Fus3, the increased pheromone sensitivity of *bar1Δ* cells results in increased phosphorylation of Kss1 at lower doses of pheromone rather than an increase in Kss1 induction.

We also calculated the phosphorylated Kss1 to total Kss1 ratio for each dose of pheromone in wild-type and *bar1Δ* cells and plotted the ratio over time as done for Fus3 above. In wild-type cells, both doses of pheromone promoted maximal phosphorylation of Kss1 by 5 minutes. The gradual dephosphorylation of Kss1 with no Kss1 induction resulted in a ratio of 1 at 5 minutes that was gradually reduced to 0.25 by 90 minutes. In contrast, the high dose promoted sustained phosphorylation and no induction, resulting in a ratio of ~1 at all times where pheromone was present (Figure 3.2A, bottom graph). In *bar1Δ* cells, Kss1 phosphorylation was sustained from 5 minutes through 90 minute at both doses of pheromone, and there was no substantial induction at either dose of pheromone, thus giving a ratio of near 1 at all time points where pheromone was present (Figure 3.2B, bottom graph).

Analysis by conventional immunoblotting with phospho-specific antibodies allows reliable comparison of different mutant strains and different doses of stimulus. This offers a more cost-effective alternative to the more-expensive Phos-tag approach when information on individual phospho-species is not required. The following section describes the use of Phos-tag gel electrophoresis to measure and calculate the stoichiometry of MAPK phosphorylation.

MAPK activation measured by Phos-tag SDS-PAGE and immunoblotting

Phosphate-binding tag, or Phos-tag is a divalent-metal-coordinating small molecule that has a high affinity for phosphorylated serine, threonine, and tyrosine [160, 161]. By adding Phos-tag and a divalent metal (e.g., Mn^{2+} or Zn^{2+}) to acrylamide gels, the electrophoretic mobility of phosphorylated proteins is slowed, thereby separating phosphorylated species from non-

phosphorylated species. Importantly, the number of bands is proportional to the number of phosphorylation events on the protein. Probing with antibodies specific for the protein of interest (e.g., Fus3) reveals all phosphorylated and non-phosphorylated protein species on the same blot. This allows a ratiometric quantification of each phospho-species. We have used Phos-tag SDS-PAGE and immunoblotting to identify, quantify, and assign a negative-regulatory role to the mono-phosphorylated form of Fus3 [156], and to characterize dose-to-duration signaling as a mechanism for the MAPK, Hog1 [126].

To illustrate the data that can be collected by the Phos-tag method, we reanalyzed the samples used with phospho-specific antibodies above (Figure 3.1). As shown in Figure 3.3, we observed clear separation of the dually phosphorylated, mono-phosphorylated, and non-phosphorylated Fus3 species (Figure 3.3, top). By adding the band intensities in each lane and dividing out each band from the total amount, we calculated the percent of total Fus3 in a given phosphorylated state. At the low dose of pheromone, ~30% of Fus3 was dually phosphorylated, and ~25% of Fus3 was mono-phosphorylated. Phosphorylation declined after 5 minutes, with slightly more of the mono-phosphorylated species than the dually phosphorylated species (Figure 3.3A, top graph). These results are consistent with the model that Fus3 is first dually phosphorylated, and then singly dephosphorylated [156]. At the high pheromone dose, the dually phosphorylated species persisted at higher levels for longer, and exceeded the mono-phosphorylated pool until 30 minutes. The mono-phosphorylated species increased steadily from 15 to 90 minutes, while the dually phosphorylated species decreased (Figure 3.3A, second graph), again consistent with a conversion from dual- to mono-phosphorylated species. These data also indicate that the increase observed by conventional immunoblotting (Figure 3.1A, top graph) is due in part to the increase in mono-phosphorylated Fus3.

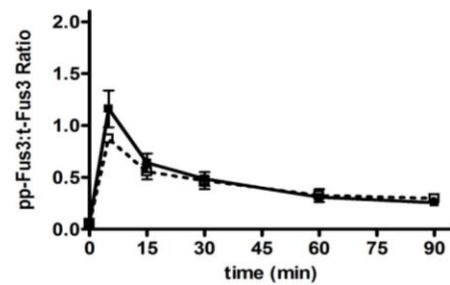
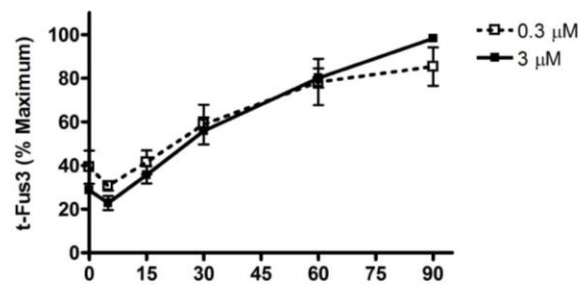
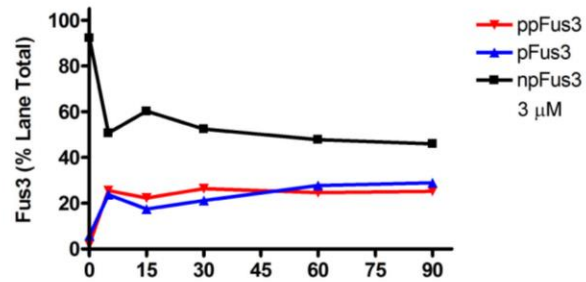
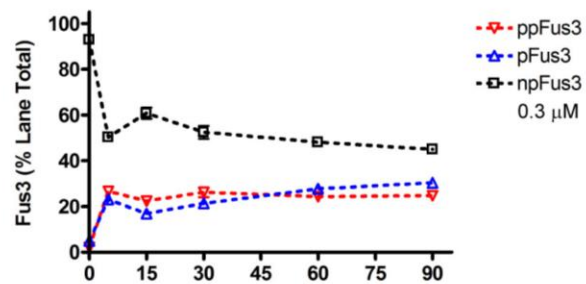
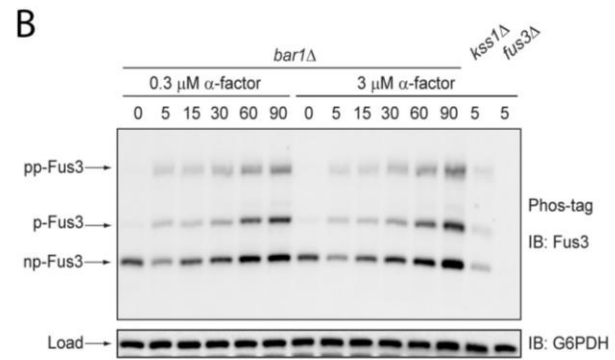
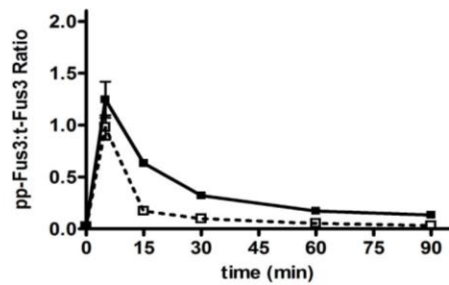
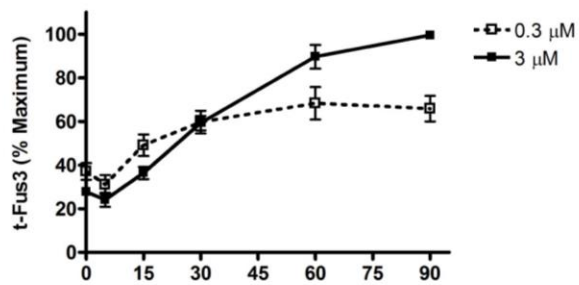
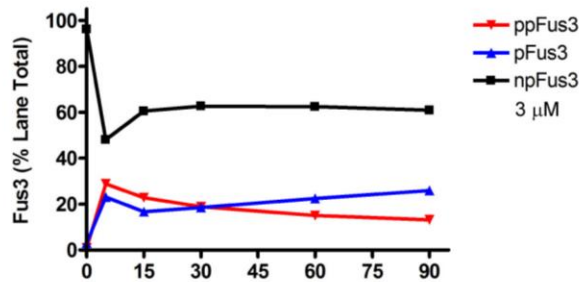
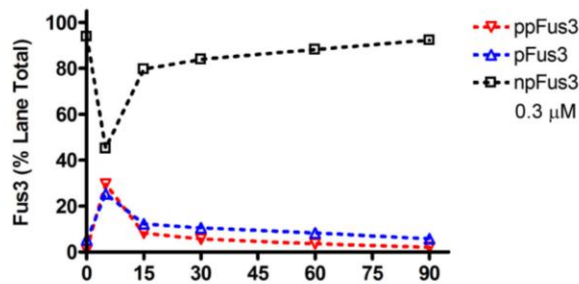
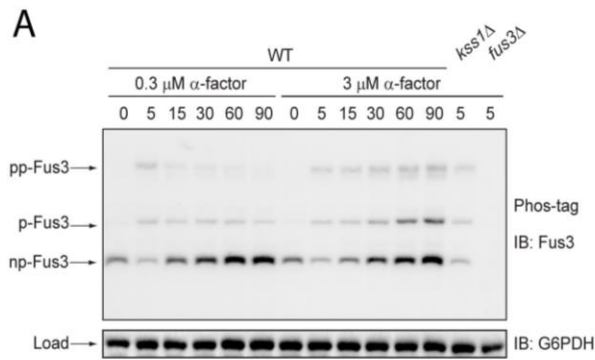


Figure 3.3 Phosphorylation of Fus3 by Phos-tag SDS-PAGE and immunoblotting with Fus3 antibodies.

Phos-tag western blot analysis of (A) wild-type cells or (B) *bar1Δ* cells treated with 0.3 μM or 3 μM α-factor mating pheromone were probed with total Fus3 antibodies to identify dually phosphorylated (pp-Fus3), mono-phosphorylated (p-Fus3), and non-phosphorylated Fus3 (np-Fus3). pp-Fus3, p-Fus3, and np-Fus3 (first and second graphs) were plotted as % of lane total. Total Fus3 (third graphs) were plotted as lane total as % maximum signal on the blot. The dually phosphorylated Fus3 to total Fus3 ratio (bottom graphs) was calculated by dividing the % dually phosphorylated Fus3 by % total Fus3. Data presented as mean ± standard deviation, N = 3.

In *bar1Δ* cells, pheromone stimulation at the low and high dose gave nearly identical results. Both phosphorylated species increased by 5 minutes to levels observed in wild-type cells, but the dually phosphorylated species persisted for 90 minutes, while the mono-phosphorylated species steadily increased (Figure 3.3B, top and second graph). These data are consistent with the supersensitivity of *bar1Δ* cells [151, 152].

We next analyzed Fus3 induction by plotting the total intensity of all bands in each lane as a percent of the maximum total signal on the blot (Figure 3.3 third graphs). We observed similar results to those obtained by conventional MAPK immunoblotting (Figure 3.1 middle graphs), however induction appeared to be stronger in the high dose in wild-type cells, and both doses in *bar1Δ* cells when analyzed by the Phos-tag method. This could be due in part to the stripping required in the conventional immunoblot analysis.

Finally, we compared the fully active, dually phosphorylated Fus3 to total Fus3 ratio. Wild-type cells gave a similar profile to that obtained from conventional immunoblotting for both doses of pheromone (Figure 3.1A, bottom graph), with the exception that both curves were shifted down by a factor of 0.25, and the high dose continued to decline after 30 minutes (Figure 3.3, bottom graph). In *bar1Δ* cells, we found that the profile for both doses was similar to the high dose in wild-type cells (Figure 3.3B, bottom graph). The rapid onset of dually phosphorylated Fus3 by 5 minutes and lack of induction at that time increases the ratio to ~1, but sustained activation and induced total Fus3 then drive the ratio down to 0.5 by 15 minutes and gradually to ~0.25 by 90 minutes. This is in opposition to the data obtained from conventional immunoblotting, where the ratio was increased to 1 by 5 minutes and remained there through 90 minutes (Figure 3.1B, bottom graph). The discrepancies observed between the two methods could be due to the fact that the phospho-p44/42 antibody recognizes both the dually

phosphorylated MAPK as well as the mono-phosphorylated species [157]. Overall, the trends in Fus3 phosphorylation are similar to those observed by conventional immunoblotting (Figure 3.1, top graphs), however with the Phos-tag method, the actual percent phosphorylated protein is revealed, in addition to the individual phospho-species.

Activation of Kss1 has not previously been analyzed by the Phos-tag method. As conventional immunoblotting identified differences between the phosphorylation and induction of Fus3 and Kss1, we also probed the Phos-tag blots used to analyze Fus3 with the anti-Myc tag antibodies in order to visualize Kss1. Blots were simultaneously probed with Fus3 and Myc-tag primary antibodies raised in different host species, and then probed with secondary antibodies conjugated to different fluorophores. Multi-channel fluorescence imaging allowed simultaneous detection of all phospho-species of both proteins. As with the conventional immunoblots above, the loading controls for the Phos-tag blots are the same, and are shown in both Figure 3.3 and Figure 3.4.

Phos-tag analysis of Kss1 likewise revealed clear separation of the dually phosphorylated, mono-phosphorylated, and non-phosphorylated species (Figure 3.4, top). The low dose of pheromone promoted dual phosphorylation of ~60% of Kss1, twice that observed for Fus3. Dual phosphorylation then declined steadily, reaching basal levels by 90 minutes. Whereas Fus3 mono-phosphorylation increased to ~25%, Kss1 mono-phosphorylation increased to ~15% and was sustained through 90 minutes (Figure 3.4A, top graph). As with the low dose, the high dose of pheromone promoted dual phosphorylation of ~60% of Kss1 by 5 minutes, and this phosphorylation slowly declined to ~50% by 90 minutes. Mono-phosphorylated slowly increased to ~20% by 90 minutes (Figure 3.4A, second graph). In contrast to Fus3, the dually phosphorylated species of Kss1 always existed in a higher proportion than mono-phosphorylated

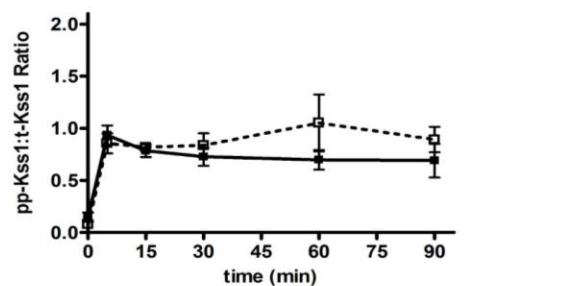
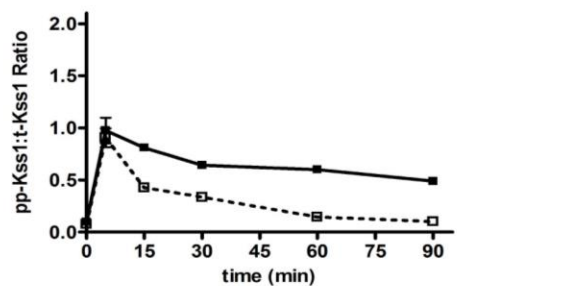
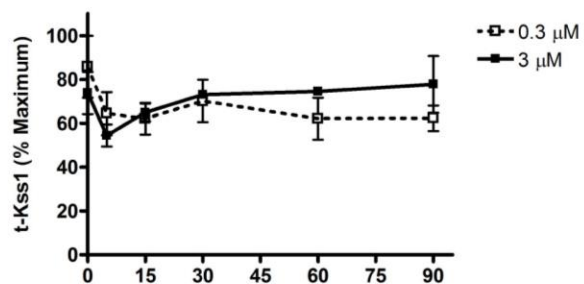
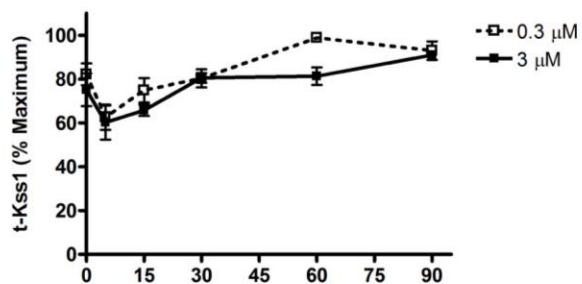
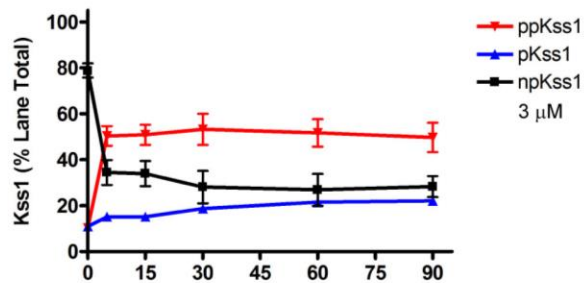
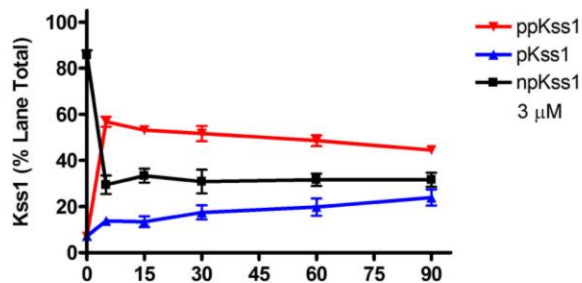
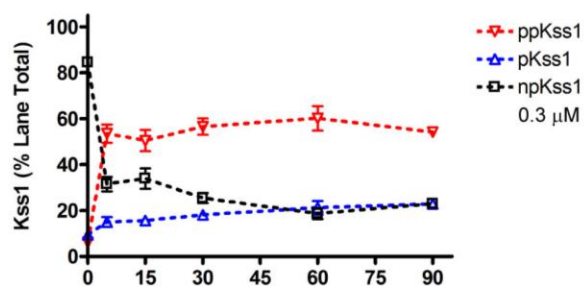
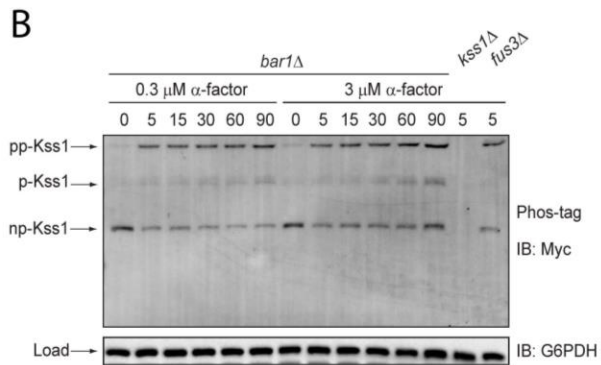
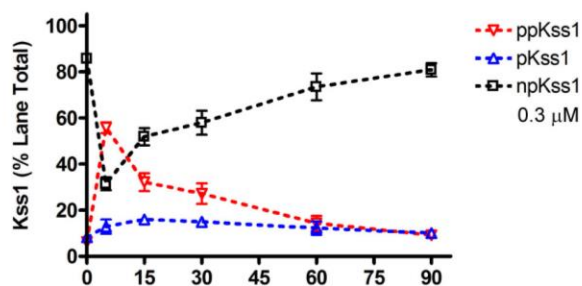
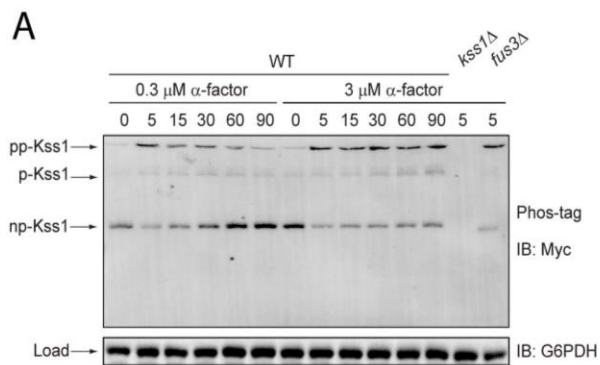


Figure 3.4 Phosphorylation of Kss1-Myc by Phos-tag SDS-PAGE and immunoblotting with Myc-Tag antibodies.

Phos-tag western blot analysis of (A) wild-type cells or (B) *bar1Δ* cells treated with 0.3 μM or 3 μM α -factor mating pheromone were probed with anti-Myc tag antibodies to identify dually phosphorylated (pp-Kss1), mono-phosphorylated (p-Kss1), and non-phosphorylated Kss1 (np-Kss1). pp-Kss1, p-Kss1, and np-Kss1 (first and second graphs) were plotted as % of lane total. Total Kss1 (third graphs) were plotted as lane total as % maximum signal on the blot. The dually phosphorylated Kss1 to total Kss1 ratio (bottom graphs) was calculated by dividing the % dually phosphorylated Kss1 by % total Kss1. Data presented as mean \pm standard deviation, N = 3.

Kss1. In *bar1Δ* cells, as with Fus3, pheromone stimulation at both doses gave nearly identical results for Kss1 phospho-species. Both phosphorylated species increased by 5 minutes to levels observed in wild-type cells, but with persistence of the dually phosphorylated species through 90 minutes. The mono-phosphorylated species again slowly increased to ~20% as in wild-type cells treated with the high dose of pheromone (Figure 3.4B, top and second graph). Thus, results for Kss1 obtained by the Phos-tag method are consistent with those obtained by conventional immunoblotting (Figure 3.2).

We next analyzed Kss1 induction as done for Fus3 above. We observed a small reduction in protein abundance by 5 minutes that then recovered to basal levels by 30 minutes in both wild-type and *bar1Δ* cells (Figure 3.4, third graphs). That there is relatively little change in the abundance of Kss1 over time is consistent with the findings obtained by conventional immunoblotting (Figure 3.2, middle graphs).

Finally, we compared the fully active, dually phosphorylated Kss1 to total Kss1 ratio. As observed for Fus3, wild-type cells gave a similar profile for Kss1 to that obtained from conventional immunoblotting for both doses of pheromone (Figure 3.2A, bottom graph). Again, both curves were shifted down by a factor of 0.25 (Figure 3.4A, bottom graph). In *bar1Δ* cells, we found that the profile for both doses was similar the profiles obtained by conventional immunoblotting, within error (Figure 3.4B, bottom graph).

We conclude that the use of phospho-specific antibodies allows reliable comparison of different mutant strains at different doses of stimulus. However, the Phos-tag method has several important advantages. First, the method allows easy detection of individual phospho-species, including the non-phosphorylated species, after probing with just one antibody. This allows ratiometric quantification of each phospho-species to give a precise measurement of the

percentage of phosphorylated protein in relation to the non-phosphorylated protein—a feature that is severely lacking in conventional immunoblotting with the phospho-specific antibody and total protein antibody. Second, the data provided by the Phos-tag method allows for more detailed mutational analysis, providing information on how individual phospho-species change in mutants of the protein of interest, or other proteins. For example, Phos-tag analysis of Fus3 in mutants lacking the upstream kinase Ste7, scaffolding protein Ste5, or phosphatase Msg5, revealed a mechanism of negative regulation attributed specifically to the mono-phosphorylated species of Fus3 [156]. Third, when used to analyze samples from a time course, the Phos-tag method allows kinetic tracking of each phospho-species, a feature that is lacking by many other methods, save for quantitative mass spectrometry, which may still give skewed results depending on the location of phosphorylation sites, and becomes very costly when used for time course analyses. Finally, quantitative measurement of phosphorylation over a range of stimulus concentrations and time has been extremely useful in developing mathematical models to represent the dynamics and regulation of signaling pathways [126, 156]. Such models can be used to predict the behavior of mutational or environmental perturbations to the pathway, and implemented as part of iterative, prediction-experimentation tests for understanding biological systems. Our previous Phos-tag analysis of Fus3 used this process to reveal a mechanism of negative regulation attributed specifically to the mono-phosphorylated species of Fus3 [156].

The major draw-back to the Phos-tag method is that some proteins simply give poor separation of phospho-species. Individual phospho-species from larger, and/or more-heavily phosphorylated proteins are more difficult to separate by the Phos-tag method, and may result in a band smear that changes position with the phosphorylation state, as with the yeast Ste11 MAPKKK adaptor protein, Ste50. While Ste50 is slightly smaller than a MAPK, it possesses

five phosphorylation sites, and migrates as a quantifiable smear through a Phos-tag gel [126]. Scrupulous optimization of gel conditions specific for Ste50 may yield better separation of individual phospho-species, and the necessity for protein-specific optimization is one factor to consider when deciding to use the Phos-tag method. Another consideration is the availability of antibodies specific for the protein of interest. If no such antibody is available, it is possible to use a tagged version of the target protein. Tag size will affect the electrophoretic mobility of the protein, and small epitope tags should be favored to maximize the separation potential. With optimized conditions, the Phos-tag method is clearly ideal for the analysis of MAPKs and other small proteins with few potential phosphorylation states, and future advances may make possible the analysis of larger, more highly phosphorylated proteins.

Transcriptional activity reporter assays

Activation of Fus3 and Kss1 leads to phosphorylation of the transcription factor Ste12, which induces a number of genes required for mating. Among the most strongly induced genes is *FUS1*, which is also highly specific to the pheromone response [63]. Accordingly, the *FUS1* promoter is widely used as a reporter of pathway activation [64, 150]. The *FUS1* promoter has been fused to reporter genes that encode β -galactosidase and fluorescent proteins (e.g., GFP), as well as drug resistance and nutritional markers.

The β -galactosidase transcriptional reporter assay using the P_{FUS1} -LacZ construct has been the gold standard. An increase in β -galactosidase expression can be detected by cleavage of a suitable substrate. Colorimetric reagents such as ONPG required cell lysis and are no longer widely used, having been replaced by the cell permeable substrate FDG [150]. As shown in Figure 3.5A, after exposure to pheromone for 1.5 hours, wild-type cells reach a maximum response at $\sim 30 \mu\text{M}$, with an EC_{50} of $\sim 1 \mu\text{M}$. Cells lacking the α -factor protease Bar1, respond at

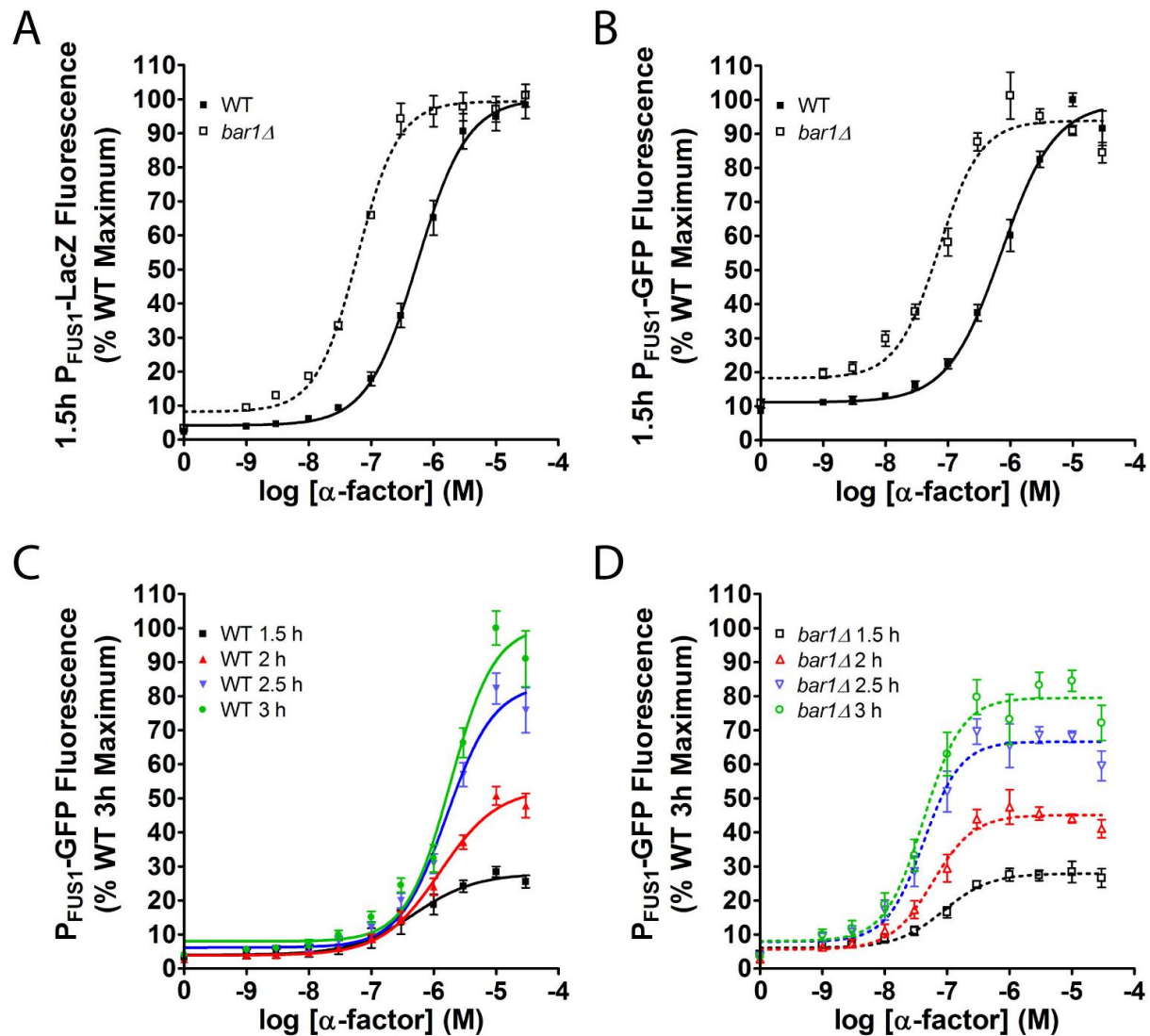


Figure 3.5 Pheromone-induced gene transcription assays

Dose-response curves for transcriptional output in response to α -factor mating pheromone. After 1.5 hours of pheromone stimulation of wild-type and $bar1\Delta$ cells, similar results are obtained by (A) the P_{FUS1} -LacZ and (B) the P_{FUS1} -GFP reporter. Increasing the incubation time in the P_{FUS1} -GFP reporter system increases the maximum response in (C) wild-type cells and (D) $bar1\Delta$ cells, without changing the EC_{50} . Data are presented as mean \pm standard deviation, N = 4.

10-fold lower concentrations of pheromone. Similar results are observed using an alternative construct where the *FUS1* promoter drives expression of GFP (Figure 3.5B). A notable difference between the two assays is that the P_{FUS1} -GFP assay exhibits higher basal signaling in both the wild-type and *bar1Δ* strain. This difference is likely due to a lower relative fold change in fluorescence in the P_{FUS1} -GFP assay.

As shown in Figure 3.5C and D, with longer incubation time, the maximum GFP signal continues to increase, reaching approximately four times the maximum signal observed at 1.5 hours. Notably, the EC_{50} does not change appreciably over time in either the wild-type or the *bar1Δ* strain. As the maximal signal increases over time, the fold increase in fluorescence relative to basal signal also increases. At 1.5 hours, the GFP signal over basal is ~10-fold. At 3 hours this increases to ~15-fold. Overall, this is lower than the increase in fluorescence obtained in a P_{FUS1} -LacZ assay; at 1.5 hours, the fluorescence increase over basal is ~25-fold. Therefore, P_{FUS1} -LacZ has a higher signal to noise range than P_{FUS1} -GFP. This sensitivity is the primary advantage of the P_{FUS1} -LacZ assay. Another advantage is that β -galactosidase does not have as long of a maturation time as GFP. Indeed, GFP takes, on average, 60 minutes to fully mature *in vitro* [162, 163]. Reading the P_{FUS1} -GFP assay at the same time point as the P_{FUS1} -LacZ assay, is therefore observing the transcriptional activity slightly in the past.

The P_{FUS1} -GFP assay does possess several advantages, however. One advantage of using P_{FUS1} -GFP is that multiple time points can be measured in the same experiment. One can simply measure the OD_{600} and fluorescence, continue incubating the plate, and measure again as often as is desired. To do a comparable experiment using the P_{FUS1} -LacZ approach, one plate per time point is required, since the growth conditions and cell integrity are compromised by the addition of the fluorescent substrate solution. As the fluorescent substrate is relatively expensive, time

course experiments by P_{FUS1} -LacZ can quickly become costly. Another advantage to using the P_{FUS1} -GFP system is that cell membrane integrity remains intact throughout the experiment. This becomes important, for example, in studying conditions of environmental stress. Certain stressors, such as changes in pH, can alter the activity of the β -galactosidase enzyme upon cell permeabilization, thereby altering the amount of fluorescent product produced. Intact cells are efficient in maintaining a physiological pH, and a GFP-based assay will give a more accurate fluorescent signal.

Conclusions

Here, we have reviewed two methods for measuring MAPK phosphorylation and two measures of transcriptional induction in pheromone-treated cells. We illustrated the utility of each method by comparing the activity of wild-type and *bar1* Δ mutant strains.

Based on our experience, we consider the Phos-tag SDS-PAGE and immunoblotting method to be superior to conventional immunoblotting with phospho-specific antibodies. Phos-tag permits the separation of all three phospho-species of MAPKs—dually phosphorylated, mono-phosphorylated, and non-phosphorylated. Ratiometric quantification of these phospho-species throughout a time course offers phospho-dynamics information that can be used to better understand the regulatory mechanisms at play in signal transduction pathways. This information is more informative than that obtained by conventional immunoblotting because phospho-specific MAPK antibodies do not distinguish between the two phosphorylated species. Still, immunoblotting with phospho-specific antibodies is convenient, and can provide information about the relative sensitivity of various mutants to pheromone.

We also compared two methods for monitoring the transcriptional activity of the pheromone response pathway—the β -galactosidase-based P_{FUS1} -LacZ assay and the fluorescent protein-based P_{FUS1} -GFP assay. We found that both assays are able to provide comparable results, and each assay has its advantages. The β -galactosidase-based assay has higher sensitivity (i.e., higher fold change in signal) than the GFP-based assay, and is advantageous when a higher dynamic range is required. The GFP-based assay is more economical, can be easily monitored over time, and is less susceptible to conditions that interfere with enzyme activity.

The methods described herein are applicable not only to the yeast system, but to MAPK pathways in other organisms. The assays can be adapted to monitor other signaling systems for biological characterization or drug discovery.

CHAPTER 4 – GENERAL DISCUSSION AND CONCLUSIONS

In situations of life or death, decisions must be made to favor survival. In a cell, the decision to respond to environmental insults, such as osmotic stress, outweigh the decision to procreate. Here, we have uncovered a new piece of the puzzle that is the cross-pathway coordination of the environmental stress response with pheromone response signaling in yeast. We identified 2-hydroxy BCAA derivatives as metabolites that serve as second messengers to inhibit the mating response during osmotic stress (Figure 4.1). As second messengers, these molecules are likely used to amplify the signal of osmotic stress so that necessary cellular resources are diverted toward responding to the stress and away from reproductive functions. We determined that Hog1 is required for the production of these second messengers, and that Gpa1 is phosphorylated by Elm1 as a consequence of their production. However, we were unable to identify the molecular target of these new second messengers. Further experiments in yeast to determine the target molecule(s) that interact with these second messengers, as well as the mechanism by which Hog1 promotes their production will be key in fully understanding this new stress-response axis, as well as in identifying potential new target molecules for pharmacological control of the stress response in a mammalian system.

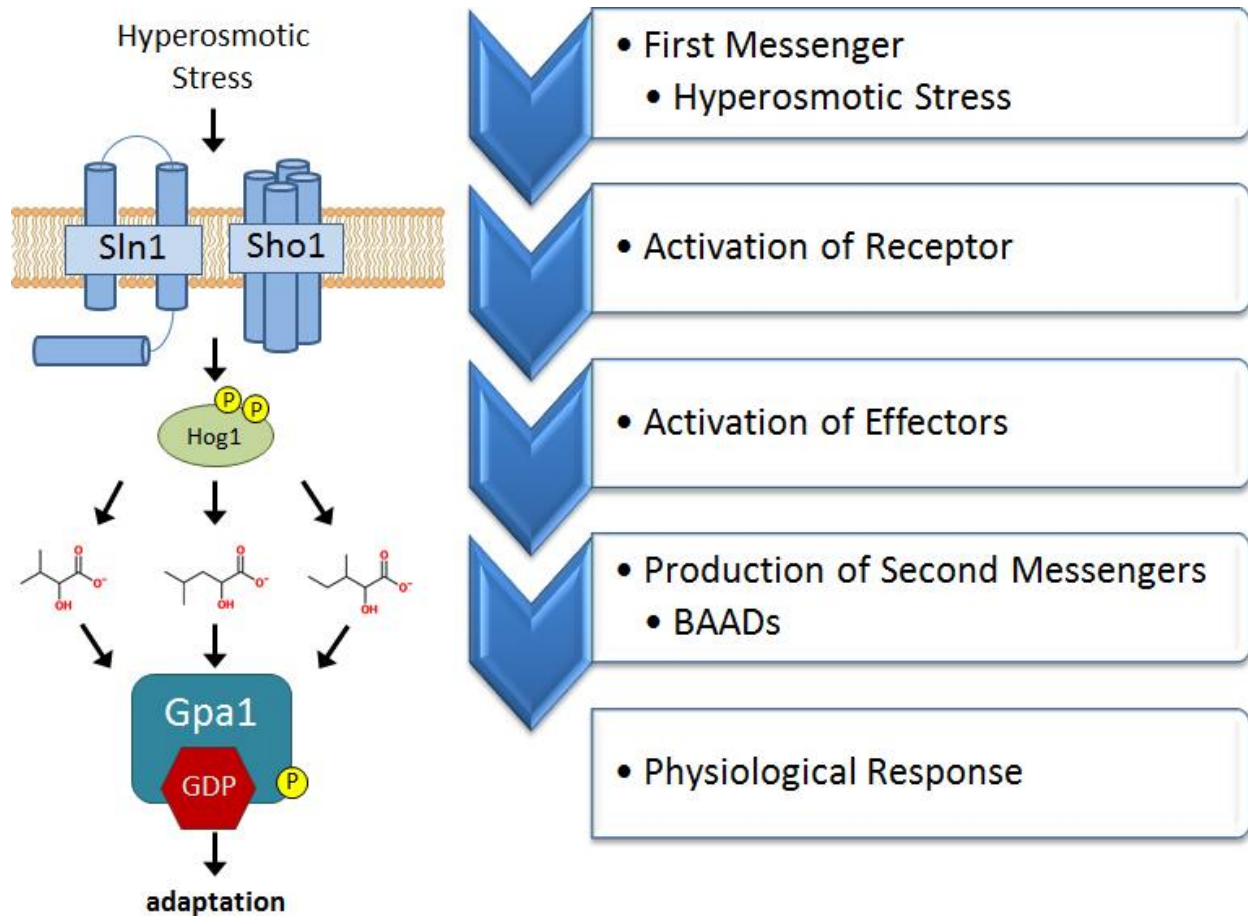


Figure 4.1 Model of BCAA derivatives as second messengers for osmotic stress.

In our model, hyperosmotic stress serves as the first messenger stimulus that activates the osmosensors of the HOG pathway, Sln1 and Sho1. Receptor activation then leads to activation of the effector, Hog1. Hog1 then increases production of the BCAA derivative second messengers by an as yet unknown mechanism. These second messengers then promote the phosphorylation of Gpa1 and the adaptive response of mating pathway signal dampening.

Future Directions

Determine the molecular target of the BCAA derivative second messengers

We have demonstrated that BCAA derivatives promote phosphorylation of Gpa1, so it is likely that they target some component of the G protein signaling complex (i.e., G α , G $\beta\gamma$, the GPCR, RGS protein, the kinase, or the phosphatase). We have ruled out the G α subunit by ^{15}N - ^1H 2D NMR (Figure 2.7), one of the most conclusive tests for protein-ligand binding. We have also determined that the kinase responsible for phosphorylating Gpa1 during osmotic stress is the AMPKK Elm1 (Figure 2.8).

If Elm1 were the target of the BCAA derivatives, we would expect to see less transcriptional dampening in response to osmotic stress or ectopic addition of BCAA derivatives in cells lacking Elm1. However, ablation of any Gpa1 phosphorylation by deletion of all three AMPKKs did not result in any substantial increase in the maximum response to mating pheromone and KCl or mating pheromone and BCAA derivatives. At lower concentrations of pheromone, the response was higher in cells lacking AMPKKs compared to wild-type cells, consistent with reduced Gpa1 phosphorylation. At intermediate concentrations of pheromone, KCl still dampened transcription, but BCAA derivatives had comparatively little effect alter the response to BCAA derivatives (Figure 2.10). These results are largely inconclusive insofar as implicating Elm1 as the target for BCAA derivatives. Further studies using purified Elm1 are necessary to identify it as the target, or rule it out.

Expression of Elm1 that was codon-optimized for *E. coli* resulted in high protein yield, but this protein was largely in the insoluble fraction of the lysate. Purification from the insoluble fraction is possible, but may not yield active protein. Further optimization of this purification process and validation of protein activity by *in vitro* kinase assays for Elm1 autophosphorylation

would be needed before experiments to identify Elm1 as the BCAA derivative target can be carried out. Alternatively, Elm1 can be purified from yeast. The GST-tagged library contains GST-Elm1 under control of the inducible GAL1 promoter [164]. Elm1 is a relatively low-abundance protein in yeast [54, 165], so inducible expression in this system will allow for higher protein yield. The GST epitope tag will allow for easy protein purification as done previously [83].

Once purified, Elm1 interaction with BCAA derivatives could be tested for in a number of ways. The hypothesis is that binding of BCAA derivatives to Elm1 would promote better kinase activity. One way to test this is to assay for increased Elm1 autophosphorylation in the presence of BCAA derivatives compared to that observed in the absence of BCAA derivatives, using the kinase-dead Elm1^{K117R} mutant as a negative control. A more rigorous test of direct binding of BCAA derivatives to Elm1 would be fast quantitative cysteine reactivity (fQCR) [166]. This approach uses increasing temperature to expose cysteine residues protected within the protein to bulk solvent. Solvent exposure enables these cysteine residues to then be labeled with the fluorescent thiol compound. The relative change in protein conformation can then be monitored over a range of temperatures by measuring the fluorescence. The midpoint of thermal unfolding (T_m) is then calculated and compared between treated and untreated protein samples. Elm1 possesses 14 cysteine residues in its primary structure, so would be a protein amenable to this approach. Alternatively, isothermal titration calorimetry (ITC) could be employed, and would allow for determination of specific binding constants.

Other components of the G protein complex could be assayed for interaction with BCAA derivatives much in the same way as described for Elm1 above. Purification of Ste4/Ste18 (G $\beta\gamma$) [167] and Sst2 (RGS) [168] is possible. It should be noted, however, that proper controls must be

used to account for the acidic nature of the BCAA derivatives. Optimization of buffering conditions is necessary to be sure that any effects observed are specific to the BCAA derivatives, and not due to decreased pH.

Once the target of the BCAA derivatives is identified, further mechanistic studies can be carried out to identify how the second messenger-target interaction promotes Gpa1 phosphorylation and/or reduced MAPK pathway activation. Potential mechanisms include increased phosphorylation by increased kinase activity of Elm1 (discussed above), and decreased MAPK activation through increased affinity for the RGS and increased affinity for G $\beta\gamma$, as both of these mechanisms would promote the “off” state of the pathway. With purified Gpa1, Sst2, and Ste4/Ste18, surface plasmon resonance (SPR) experiments could be conducted in the presence and absence of BCAA derivatives to assess changes in binding affinities between Gpa1 and Ste4/Ste18, Gpa1 and Sst2, or even all three components together. Elucidation of the molecular target of the BCAA derivatives will provide information necessary for the development of new potential therapeutic strategies in managing the detrimental aspects of the response to cell stress.

Determine the mechanism by which Hog1 promotes BCAA derivative production

Our metabolomics study shows that Hog1 is required for the dramatic increase in BCAA derivatives observed upon osmotic stress. However, we have so far been unable to find a specific role for Hog1 in promoting BCAA catabolism. We attempted to identify a role for Hog1 in phosphorylating the branched-chain amino acid transaminase enzymes, Bat1 and Bat2, by mutating potential MAPK consensus phosphorylation sites to the non-phosphorylatable residue alanine, and using Phos-tag SDS-PAGE and immunoblotting to detect changes in phosphorylation between the mutants and wild-type cells in the presence or absence of osmotic

stress. We found no significant difference in the phosphorylation profiles of the Bat1 and Bat2 mutants compared to the wild-type versions upon KCl stimulation (Figure 2.5). Likewise, we saw no clear change in the abundance of either Bat1 or Bat2 upon KCl stimulation. As Bat1 and Bat2 regulate the first step in BCAA catabolism (Figure 2.4A), it seemed that those enzymes would be the most logical target for regulation by phosphorylation by Hog1. As this was not the case, it may be prudent to widen the scope of potential mechanisms that might account for Hog1-dependent production of BCAA derivatives.

Our metabolomics analysis compared wild-type and Hog1-deficient cells. Therefore, it is unclear whether Hog1 catalytic activity or the binding of Hog1 to other proteins is required for the production of BCAA derivatives. Indeed, catalytically inactive MAPKs can still bind to and regulate transcription factors [169, 170]. To determine how Hog1 contributes to BCAA derivative production, first it should be determined whether Hog1 binding or kinase activity drives production of BCAA derivatives. To this end, targeted metabolite analysis by mass spectrometry or NMR could be employed to measure BCAA derivatives in a pharmacologically inhibitable ('ATP-analog-sensitive') Hog1 mutant (Hog1^{T100A}), a Hog1-deficient mutant (*hog1Δ*), and wild type cells in the presence and absence of osmotic stress. If Hog1 catalytic activity is required for increased BCAA catabolism, then upon osmotic stress, a decrease in BCAA derivatives in the Hog1^{T100A} samples as compared to wild type, and similar levels as compared to *hog1Δ* samples should be observed. If Hog1 binding, and not catalytic activity is required, then upon osmotic stress, BCAA derivative levels in the Hog1^{T100A} samples should be similar to that observed in wild-type cells, and increased as compared to *hog1Δ* samples.

Next, to identify proteins that interact with Hog1 upon osmotic stress, the bacterial biotin ligase BirA can be fused to Hog1. Subsequent biotinylation of proximal proteins upon osmotic

stress can be detected by mass spectrometry. Hog1 interaction studies have been done in the past, but not using this method. An advantage to the BirA approach is that it can capture transient interactions that can be missed in other assays, such as co-immunoprecipitation. This may reveal new Hog1-interacting proteins, some of which may be involved in BCAA catabolism.

Another possible mechanism by which Hog1 could promote BCAA derivative production is through transcriptional regulation of BCAA catabolic enzymes. We have shown that Bat1 and Bat2 levels do not change in response to osmotic stress (Figure 2.5). However, other components of the Ehrlich pathway or alternative oxidoreductase enzymes may be transcriptionally regulated by Hog1. Indeed, several genes are upregulated on the same short time scale in which we observe increased BCAA derivative production and Gpa1 phosphorylation. A meta-analysis of an in-depth microarray analysis of wild-type and *hog1Δ* cells subjected to osmotic stress for various amounts of time [171] reveals that there are 40 genes whose expression is increased greater than 2-fold by 20 minutes after osmotic stress in wild-type cells, but not in *hog1Δ* cells (Figure 4.2). Of these 40 genes, 8 are oxidoreductases (*ALD2*, *TKL2*, *ALD4*, *YML131W*, *ARI1*, *THI4*, *GRX7*, and *GRX1*), and Ald2 and Ald4 are involved in the Ehrlich pathway. It is possible that one or more of these genes is responsible for producing the BCAA derivative second messengers. To follow up on this analysis, protein levels should be measured by western blotting. Subsequently, a direct role of these proteins in BCAA derivative production can be confirmed by deletion of the gene of interest, followed by measuring BCAA derivative levels by targeted metabolomics as described above. Determining the mechanism by which Hog1 upregulates BCAA catabolism in response to osmotic stress will likely be translatable to stress-response MAPK systems in humans.

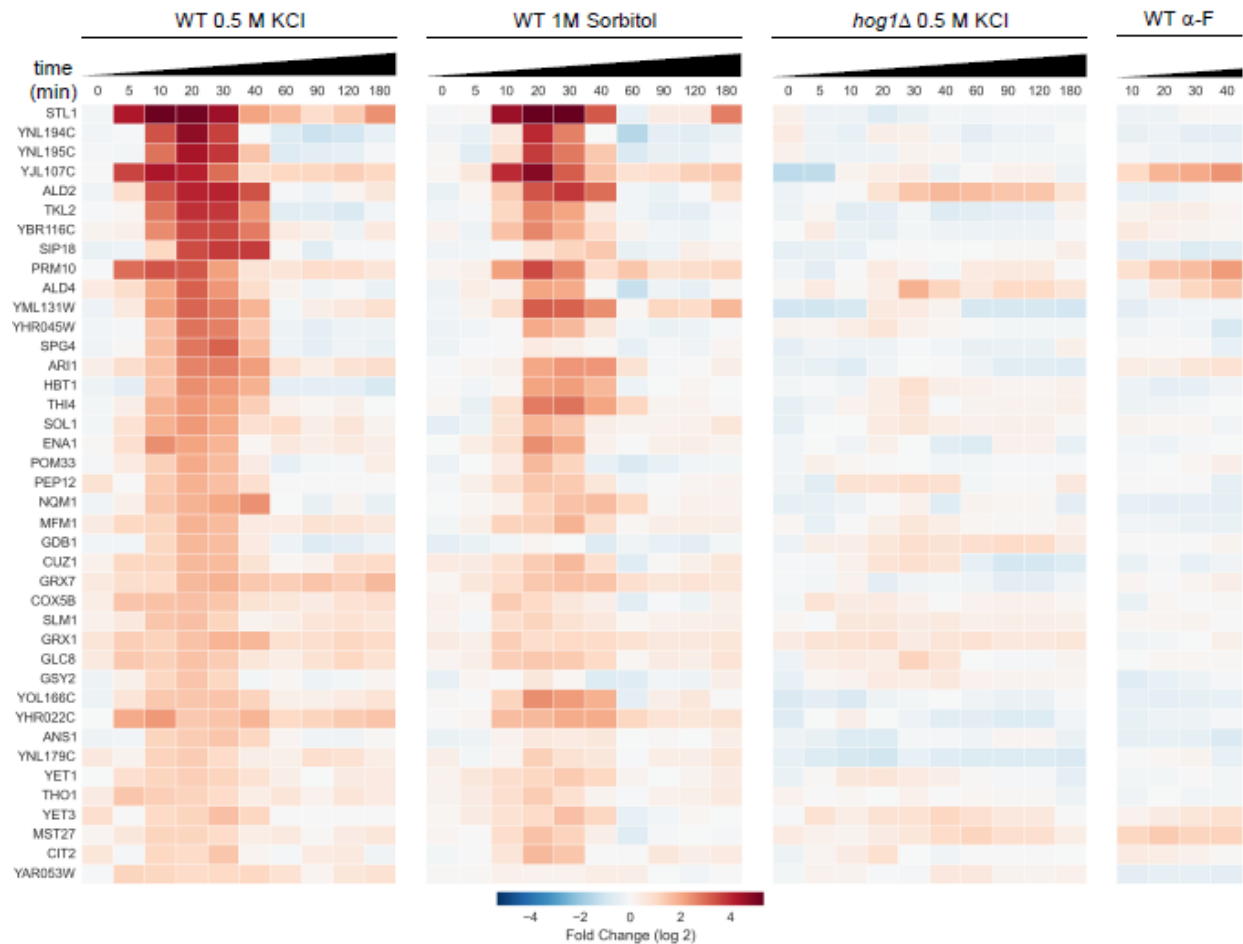


Figure 4.2 Osmotic stress-dependent, Hog1-dependent gene transcription.

Meta-analysis of microarray data [171] reveals that 40 genes increase at least 2-fold by 20 minutes in response to osmotic stress by 0.5 M KCl in wild-type cells, but not in *hog1Δ* cells. Similar expression changes were observed upon osmotic stress by a comparable 1 M sorbitol stimulation. Mating pheromone (α -F) was used as a negative control.

Broader applications of this research

Molecules generated from amino acid metabolism are some of the most common signaling agents in physiological systems. Serotonin, the neurotransmitter responsible for good mood and well-being, is derived from tryptophan. Dopamine, norepinephrine, epinephrine are derived from tyrosine. Dopamine is responsible for reward-associated behavior and motor control, and norepinephrine and epinephrine control the autonomic nervous system. Glutamate acts as an excitatory neurotransmitter, and its derivative, gamma-aminobutyric acid (GABA) is the principle inhibitory neurotransmitter. Interestingly, all of the aforementioned amino acid derivatives are ligands for GPCRs, emphasizing the interconnectedness of amino acid metabolism and G protein signaling. Next, I will discuss how BCAAs and their derivatives can also behave as signaling molecules in cell growth, and their potential as therapeutics.

BCAAs as signaling molecules

The most prominently up-regulated BCAA metabolite in our metabolomics analysis was the 2-hydroxy carboxylic acid derivative of leucine (HIC). HIC was also found to be the most bioactive of the three BCAA derivatives. This is consistent with the known role of leucine as a signaling molecule. Leucine promotes cell growth through protein synthesis and mitochondrial biogenesis [172]. Amino acids, particularly leucine, stimulate growth signaling through the mTOR pathway by promoting the active state of Rag-family small GTPases [173, 174], which then bind to Raptor, recruiting the mTORC1 complex to endomembrane compartments containing the activator, Rheb [173]. In yeast, the Exit from G₀ Complex (EGOC), containing the Rag GTPase ortholog, Gtr1, is positively regulated in leucine-rich conditions by leucyl-tRNA synthetase, increasing TORC1 activity [175]. Conversely, EGOC is negatively regulated by the

Seh1-associated (SEA) complex (GATOR in mammals) through increased GTP hydrolysis activity of Gtr1 under leucine-starvation conditions, which decreases TORC1 activity [176].

While much is known about the role of leucine as a signaling molecule in normal growth and in disease states, there is no real consensus on whether leucine or, more broadly, BCAA supplementation as a whole is beneficial or detrimental to overall health [177]. Indeed, performance athletes frequently make use of BCAA supplementation to promote muscle growth and recovery, and to prevent delayed-onset muscle soreness [178, 179]. Other studies show that high levels of circulating BCAAs in combination with a high-fat diet can promote insulin insensitivity and diabetes [74, 180]. Further, tissue-specific differences in BCAA metabolism exist among different cancers. Two *Kras*-driven cancers, pancreatic ductal adenocarcinoma (PDAC) and non-small cell lung carcinoma (NSCLC), exhibit opposing preferences in utilizing BCAAs for tumor growth; BCAA uptake is largely unchanged in PDAC compared to normal pancreatic cells, whereas NSCLC displays enhanced BCAA uptake compared to normal lung cells [181]. To add further to this complexity, BCAA supplementation has been shown to improve chemotherapeutic efficacy in inhibiting hepatocellular cancer stem cell growth [182, 183]. Clearly, there is still much to be learned to fully understand the extent to which BCAAs and their metabolites act to regulate the growth and meet the energy demands of cells.

BCAA metabolites as signaling molecules

It is becoming more apparent that BCAA metabolites play equally, or even more, important roles in cells as the BCAAs themselves. Indeed, 2-ketoisocaproate (KIC), the product of leucine transamination, can promote TORC1 activity as effectively as leucine in both yeast and skeletal muscle [102, 184]. Interestingly, this effect is specific to leucine and KIC in yeast, as the other BCAAs, valine and isoleucine, and their keto acid metabolites, 2-ketoisovalerate,

and 2-keto-3-methylvalerate, respectively, do not promote TORC1 activity [102]. These findings are in line with our results that the 2-hydroxy derivative leucine, HIC exhibits the greatest increase in abundance and ability to dampen pheromone signaling.

2-hydroxy acids are tolerated for use as dietary supplements, and can indeed promote growth. The analogs of each BCAA, 2-keto acid, and 2-hydroxy acid were tested for their ability to increase body mass in rats and chicks, and it was found that the L-isoforms of each 2-keto acid and 2-hydroxy acid similarly promoted growth in both species, albeit to a lesser capacity than that of the L-BCAA [185]. However, there do appear to be specific functions for 2-hydroxy acids. Compared to leucine, administration of HIC during and after the immobilization period of limb casting in rats was shown to improve atrophied muscle recovery upon cast removal [186]. In soccer athletes, HIC supplementation for 4 weeks led to increased lean body mass and reduced delayed-onset muscle soreness after intense exercise compared to placebo groups [187]. Clearly, BCAA derivatives confer a clinical significance, yet remain poorly understood overall. We have identified a new function for 2-hydroxy BCAA derivatives, and the identification of their mechanism of action could serve to identify new therapeutic targets and applications.

Potential application of BCAA derivatives to stress-related cell damage: ischemia-reperfusion injury as an example

Cardiovascular disease (CVD) is the most prevalent cause of death in the United States. Of the 85.6 million Americans affected by CVD, an estimated 7.6 million have suffered myocardial infarction (MI) [188]. Ischemia resulting from MI induces cell stress and damage due to poor nutrient delivery, and timely coronary reperfusion is the only proven way to limit infarct size. Paradoxically, reperfusion of ischemic tissue is known to cause rapid cell damage and death by both apoptosis and necrosis, termed lethal ischemia-reperfusion injury (IRI) [189-192]. The

extent to which IRI occurs has a significant impact on the survival of the affected individual. Therefore, limiting cell damage and retaining myocardial function has been the objective of many studies dedicated to understanding the molecular mechanisms by which IRI occurs [192-196]. Factors found to contribute to the severity of IRI include generation of reactive oxygen species, induction of inflammatory responses, and fluxes in pH and osmolarity [191, 194]. Activation of AMPK, and the MAPKs, JNK and p38, by these conditions permits an adaptive response leading to cardioprotection [39, 40, 80, 196, 197]. Furthermore, signaling through GPCRs promotes stress adaptation and cardioprotection by suppressing apoptosis through Akt and MAPK signaling [4, 195].

Our work here considers the effects of 2-hydroxy acids on mediating the response to osmotic stress. Given the known activation of Hog1 in osmotic and oxidative stress, it is probable that these 2-hydroxy acids are also produced in response to those stresses in mammals through p38 or JNK signaling, and future experiments should aim to determine if this is true. If so, 2-hydroxy acids could be used as protective therapeutics during ischemia and ischemia-reperfusion injury following myocardial or cerebrovascular infarction. Indeed, 2-keto acids derived from BCAAs were found to inhibit necrosis induced by the oxidative stress associated with IRI [198]. Similarly, studies aimed at identifying changes in myocardial metabolism in infarcted and failing mouse hearts did detect the valine-derived 2-hydroxy acid (HIV) in mice that underwent trans-aortic constriction (TAC) to induce heart failure, or coronary ligation to induce MI. HIV showed a nominal increase in experimental, but not sham mice after 8 weeks of TAC, as well as after 5 days of induced MI [76]. However, metabolites were not measured directly following MI to study the early events following ischemia, nor was a model of ischemia-reperfusion injury explored where blood flow was restored after MI. Additional experiments in

this area should be conducted to determine the extent to which BCAA derivatives might play a role in mediating the stress response in the heart or brain.

Concluding remarks

As we search for a more complete understanding of how cells receive and respond to signals in their environment, we continue to find new connections between signaling pathways. It is clear that these pathways are not isolated systems, and are instead part of interwoven networks that, amazingly, maintain the fidelity necessary to execute the appropriate response to a given signal. In this dissertation, I have identified a new component of the network that responds to osmotic stress, whereby BCAA catabolism produces second messengers to reduce signaling for cell reproduction and to permit stress adaptation. Deregulated cross-talk between network components can lead to disease. Therefore, it is important that the mechanisms by which this new BCAA catabolism component acts are identified and the potential for 2-hydroxy BCAA derivatives as drug lead compounds is explored.

REFERENCES

1. Johnson, G.L. and R. Lapadat, *Mitogen-activated protein kinase pathways mediated by ERK, JNK, and p38 protein kinases*. Science, 2002. **298**(5600): p. 1911-2.
2. Sugden, P.H. and A. Clerk, *Regulation of the ERK subgroup of MAP kinase cascades through G protein-coupled receptors*. Cell Signal, 1997. **9**(5): p. 337-51.
3. Kiel, C. and L. Serrano, *Challenges ahead in signal transduction: MAPK as an example*. Curr Opin Biotechnol, 2012. **23**(3): p. 305-14.
4. Nagiec, M.J. and H.G. Dohlman, *Checkpoints in a Yeast Differentiation Pathway Coordinate Signaling during Hyperosmotic Stress*. PLoS Genet, 2012. **8**(1).
5. Clement, S.T., G. Dixit, and H.G. Dohlman, *Regulation of Yeast G Protein Signaling by the Kinases That Activate the AMPK Homolog Snf1*. Science Signaling, 2013. **6**(291).
6. Rask-Andersen, M., M.S. Almen, and H.B. Schiøth, *Trends in the exploitation of novel drug targets*. Nat Rev Drug Discov, 2011. **10**(8): p. 579-90.
7. Arshavsky, V.Y., T.D. Lamb, and E.N. Pugh, Jr., *G proteins and phototransduction*. Annu Rev Physiol, 2002. **64**: p. 153-87.
8. Buck, L. and R. Axel, *A novel multigene family may encode odorant receptors: a molecular basis for odor recognition*. Cell, 1991. **65**(1): p. 175-87.
9. Chandrashekar, J., et al., *The receptors and cells for mammalian taste*. Nature, 2006. **444**(7117): p. 288-94.
10. Marinissen, M.J. and J.S. Gutkind, *G-protein-coupled receptors and signaling networks: emerging paradigms*. Trends Pharmacol Sci, 2001. **22**(7): p. 368-76.
11. Linder, M.E., et al., *Purification and characterization of Go alpha and three types of Gi alpha after expression in Escherichia coli*. J Biol Chem, 1990. **265**(14): p. 8243-51.
12. Noel, J.P., H.E. Hamm, and P.B. Sigler, *The 2.2 Å crystal structure of transducin-alpha complexed with GTP gamma S*. Nature, 1993. **366**(6456): p. 654-63.
13. Coleman, D.E., et al., *Structures of active conformations of Gi alpha 1 and the mechanism of GTP hydrolysis*. Science, 1994. **265**(5177): p. 1405-12.
14. Sprang, S.R., *G protein mechanisms: insights from structural analysis*. Annu Rev Biochem, 1997. **66**: p. 639-78.
15. Ross, E.M. and T.M. Wilkie, *GTPase-activating proteins for heterotrimeric G proteins: regulators of G protein signaling (RGS) and RGS-like proteins*. Annu Rev Biochem, 2000. **69**: p. 795-827.

16. Berman, D.M., T. Kozasa, and A.G. Gilman, *The GTPase-activating protein RGS4 stabilizes the transition state for nucleotide hydrolysis*. J Biol Chem, 1996. **271**(44): p. 27209-12.
17. Wedegaertner, P.B., P.T. Wilson, and H.R. Bourne, *Lipid Modifications of Trimeric G Proteins*. Journal of Biological Chemistry, 1995. **270**(2): p. 503-506.
18. Song, J. and H.G. Dohlman, *Partial Constitutive Activation of Pheromone Responses by a Palmitoylation-Site Mutant of a G Protein α Subunit in Yeast*. Biochemistry, 1996. **35**(47): p. 14806-14817.
19. Marotti, et al., *Direct Identification of a G Protein Ubiquitination Site by Mass Spectrometry*. Biochemistry, 2002. **41**(16): p. 5067-5074.
20. Torres, M.P., et al., *G Protein Mono-ubiquitination by the Rsp5 Ubiquitin Ligase*. Journal of Biological Chemistry, 2009. **284**(13): p. 8940-8950.
21. Manganello, J.M., et al., *Protein Kinase A-mediated Phosphorylation of the Ga13 Switch I Region Alters the Ga β 13-G Protein-coupled Receptor Complex and Inhibits Rho Activation*. Journal of Biological Chemistry, 2003. **278**(1): p. 124-130.
22. Navarro, L., et al., *Identification of a Molecular Target for the Yersinia Protein Kinase A*. Molecular Cell, 2007. **26**(4): p. 465-477.
23. Kozasa, T. and A.G. Gilman, *Protein Kinase C Phosphorylates G12 α and Inhibits Its Interaction with G β γ* . Journal of Biological Chemistry, 1996. **271**(21): p. 12562-12567.
24. Shi, J., B. Zemaitaitis, and N.A. Muma, *Phosphorylation of Ga11 Protein Contributes to Agonist-Induced Desensitization of 5-HT2A Receptor Signaling*. Molecular Pharmacology, 2007. **71**(1): p. 303-313.
25. Hausdorff, W.P., et al., *Tyrosine phosphorylation of G protein alpha subunits by pp60c-src*. Proceedings of the National Academy of Sciences, 1992. **89**(13): p. 5720-5724.
26. Glick, J.L., et al., *RGSZ1, a Gz-selective Regulator of G Protein Signaling Whose Action Is Sensitive to the Phosphorylation State of Gza*. Journal of Biological Chemistry, 1998. **273**(40): p. 26008-26013.
27. Hildebrandt, J.D., *Role of subunit diversity in signaling by heterotrimeric G proteins*. Biochem Pharmacol, 1997. **54**(3): p. 325-39.
28. Le Page, S.L., Y. Bi, and J.A. Williams, *CCK-A receptor activates RhoA through G alpha 12/13 in NIH3T3 cells*. Am J Physiol Cell Physiol, 2003. **285**(5): p. C1197-206.
29. Berthet, J., T.W. Rall, and E.W. Sutherland, *The relationship of epinephrine and glucagon to liver phosphorylase. IV. Effect of epinephrine and glucagon on the reactivation of phosphorylase in liver homogenates*. J Biol Chem, 1957. **224**(1): p. 463-75.

30. Sutherland, E.W. and T.W. Rall, *Fractionation and characterization of a cyclic adenine ribonucleotide formed by tissue particles*. J Biol Chem, 1958. **232**(2): p. 1077-91.
31. Levitzki, A., *From epinephrine to cyclic AMP*. Science, 1988. **241**(4867): p. 800-6.
32. Smith, M., G.I. Drummond, and H.G. Khorana, *Cyclic Phosphates. IV. Ribonucleoside-3',5' Cyclic Phosphates. A General Method of Synthesis and Some Properties*. J. Am. Chem. Soc., 1961. **83**(3): p. 698-706.
33. Hokin, M.R. and L.E. Hokin, *Enzyme secretion and the incorporation of P32 into phospholipides of pancreas slices*. J Biol Chem, 1953. **203**(2): p. 967-77.
34. Lapetina, E.G. and R.H. Michell, *A membrane-bound activity catalysing phosphatidylinositol breakdown to 1,2-diacylglycerol, D-myoinositol 1:2-cyclic phosphate and D-myoinositol 1-phosphate. Properties and subcellular distribution in rat cerebral cortex*. Biochem J, 1973. **131**(3): p. 433-42.
35. Berridge, M.J., *Rapid accumulation of inositol trisphosphate reveals that agonists hydrolyse polyphosphoinositides instead of phosphatidylinositol*. Biochem J, 1983. **212**(3): p. 849-58.
36. Rasmussen, H., et al., *Calcium ion as second messenger*. Clin Endocrinol (Oxf), 1976. **5 Suppl**: p. 11S-27S.
37. Nishimoto, S. and E. Nishida, *MAPK signalling: ERK5 versus ERK1/2*. EMBO Rep, 2006. **7**(8): p. 782-6.
38. Johnson, G.L., *Defining MAPK interactomes*. ACS Chem Biol, 2011. **6**(1): p. 18-20.
39. Cuadrado, A. and A.R. Nebreda, *Mechanisms and functions of p38 MAPK signalling*. Biochem J, 2010. **429**(3): p. 403-17.
40. Gasch, A.P., et al., *Genomic Expression Programs in the Response of Yeast Cells to Environmental Changes*. Molecular Biology of the Cell, 2000. **11**(12): p. 4241-4257.
41. Zhang, Y. and F. Chen, *Reactive oxygen species (ROS), troublemakers between nuclear factor-kappaB (NF-kappaB) and c-Jun NH(2)-terminal kinase (JNK)*. Cancer Res, 2004. **64**(6): p. 1902-5.
42. Miermont, A., et al., *Severe osmotic compression triggers a slowdown of intracellular signaling, which can be explained by molecular crowding*. Proc Natl Acad Sci U S A, 2013. **110**(14): p. 5725-30.
43. Burg, M.B., J.D. Ferraris, and N.I. Dmitrieva, *Cellular response to hyperosmotic stresses*. Physiol Rev, 2007. **87**(4): p. 1441-74.

44. Ko, B.C., et al., *Fyn and p38 signaling are both required for maximal hypertonic activation of the osmotic response element-binding protein/tonicity-responsive enhancer-binding protein (OREBP/TonEBP)*. J Biol Chem, 2002. **277**(48): p. 46085-92.
45. Kino, T., et al., *Brx mediates the response of lymphocytes to osmotic stress through the activation of NFAT5*. Sci Signal, 2009. **2**(57): p. ra5.
46. Ho, S.N., *The role of NFAT5/TonEBP in establishing an optimal intracellular environment*. Arch Biochem Biophys, 2003. **413**(2): p. 151-7.
47. Deng, R., et al., *Oxidative stress markers induced by hyperosmolarity in primary human corneal epithelial cells*. PLoS One, 2015. **10**(5): p. e0126561.
48. Willermain, F., et al., *Origins and consequences of hyperosmolar stress in retinal pigmented epithelial cells*. Front Physiol, 2014. **5**: p. 199.
49. Van Ness-Otunnu, R. and J.B. Hack, *Hyperglycemic crisis*. J Emerg Med, 2013. **45**(5): p. 797-805.
50. Baskurt, O.K. and H.J. Meiselman, *Blood rheology and hemodynamics*. Semin Thromb Hemost, 2003. **29**(5): p. 435-50.
51. Brocker, C., D.C. Thompson, and V. Vasiliou, *The role of hyperosmotic stress in inflammation and disease*. Biomol Concepts, 2012. **3**(4): p. 345-364.
52. Giaever, G., et al., *Functional profiling of the Saccharomyces cerevisiae genome*. Nature, 2002. **418**(6896): p. 387-91.
53. Mnaimneh, S., et al., *Exploration of Essential Gene Functions via Titratable Promoter Alleles*. Cell, 2004. **118**(1): p. 31-44.
54. Ghaemmaghami, S., et al., *Global analysis of protein expression in yeast*. Nature, 2003. **425**(6959): p. 737-41.
55. Sopko, R., et al., *Mapping pathways and phenotypes by systematic gene overexpression*. Mol Cell, 2006. **21**(3): p. 319-30.
56. Huh, W.K., et al., *Global analysis of protein localization in budding yeast*. Nature, 2003. **425**(6959): p. 686-91.
57. Dohlman, H.G. and J.W. Thorner, *Regulation of G protein-initiated signal transduction in yeast: paradigms and principles*. Annu Rev Biochem, 2001. **70**: p. 703-54.
58. Han, J., et al., *A MAP kinase targeted by endotoxin and hyperosmolarity in mammalian cells*. Science, 1994. **265**(5173): p. 808-11.
59. Alvaro, C.G. and J. Thorner, *Heterotrimeric G Protein-coupled Receptor Signaling in Yeast Mating Pheromone Response*. J Biol Chem, 2016. **291**(15): p. 7788-95.

60. Blumer, K.J., J.E. Reneke, and J. Thorner, *The STE2 gene product is the ligand-binding component of the alpha-factor receptor of Saccharomyces cerevisiae*. J Biol Chem, 1988. **263**(22): p. 10836-42.
61. Bardwell, L., *A walk-through of the yeast mating pheromone response pathway*. Peptides, 2005. **26**(2): p. 339-50.
62. Printen, J.A. and G.F. Sprague, Jr., *Protein-protein interactions in the yeast pheromone response pathway: Ste5p interacts with all members of the MAP kinase cascade*. Genetics, 1994. **138**(3): p. 609-19.
63. Hagen, D.C., G. McCaffrey, and G.F. Sprague, Jr., *Pheromone response elements are necessary and sufficient for basal and pheromone-induced transcription of the FUS1 gene of Saccharomyces cerevisiae*. Mol Cell Biol, 1991. **11**(6): p. 2952-61.
64. Erdman, S., et al., *Pheromone-regulated genes required for yeast mating differentiation*. J Cell Biol, 1998. **140**(3): p. 461-83.
65. Hohmann, S., *Osmotic Stress Signaling and Osmoadaptation in Yeasts*. Microbiology and Molecular Biology Reviews, 2002. **66**(2): p. 300-372.
66. Posas, F. and H. Saito, *Osmotic activation of the HOG MAPK pathway via Ste11p MAPKKK: scaffold role of Pbs2p MAPKK*. Science, 1997. **276**(5319): p. 1702-5.
67. Tatebayashi, K., et al., *Transmembrane mucins Hkr1 and Msb2 are putative osmosensors in the SHO1 branch of yeast HOG pathway*. EMBO J, 2007. **26**(15): p. 3521-33.
68. Ota, I.M. and A. Varshavsky, *A yeast protein similar to bacterial two-component regulators*. Science, 1993. **262**(5133): p. 566-9.
69. Saito, H. and F. Posas, *Response to hyperosmotic stress*. Genetics, 2012. **192**(2): p. 289-318.
70. Tebani, A., et al., *Omics-Based Strategies in Precision Medicine: Toward a Paradigm Shift in Inborn Errors of Metabolism Investigations*. Int J Mol Sci, 2016. **17**(9).
71. Evans, A.M., et al., *Integrated, nontargeted ultrahigh performance liquid chromatography/electrospray ionization tandem mass spectrometry platform for the identification and relative quantification of the small-molecule complement of biological systems*. Anal Chem, 2009. **81**(16): p. 6656-67.
72. Koek, M.M., et al., *Quantitative metabolomics based on gas chromatography mass spectrometry: status and perspectives*. Metabolomics, 2011. **7**(3): p. 307-328.
73. Wishart, D.S., *Quantitative metabolomics using NMR*. TrAC Trends in Analytical Chemistry, 2008. **27**(3): p. 228-237.

74. Newgard, C.B., et al., *A branched-chain amino acid-related metabolic signature that differentiates obese and lean humans and contributes to insulin resistance*. *Cell Metab*, 2009. **9**(4): p. 311-26.
75. Suhre, K., *Metabolic profiling in diabetes*. *J Endocrinol*, 2014. **221**(3): p. R75-85.
76. Sansbury, B.E., et al., *Metabolomic Analysis of Pressure-overloaded and Infarcted Mouse Hearts*. *Circ Heart Fail*, 2014.
77. Marcobal, A., et al., *A metabolomic view of how the human gut microbiota impacts the host metabolome using humanized and gnotobiotic mice*. *ISME J*, 2013. **7**(10): p. 1933-43.
78. He, X., et al., *Gut Microbiota and Nonalcoholic Fatty Liver Disease: Insights on Mechanism and Application of Metabolomics*. *Int J Mol Sci*, 2016. **17**(3): p. 300.
79. Griffin, J.L., X. Wang, and E. Stanley, *Does our gut microbiome predict cardiovascular risk? A review of the evidence from metabolomics*. *Circ Cardiovasc Genet*, 2015. **8**(1): p. 187-91.
80. Wullschleger, S., R. Loewith, and M.N. Hall, *TOR signaling in growth and metabolism*. *Cell*, 2006. **124**(3): p. 471-84.
81. Hardie, D.G., F.A. Ross, and S.A. Hawley, *AMPK: a nutrient and energy sensor that maintains energy homeostasis*. *Nat Rev Mol Cell Biol*, 2012. **13**(4): p. 251-62.
82. Shin, S., et al., *ERK2 Mediates Metabolic Stress Response to Regulate Cell Fate*. *Mol Cell*, 2015. **59**(3): p. 382-98.
83. Torres, M.P., et al., *Cell Cycle-Dependent Phosphorylation and Ubiquitination of a G Protein A Subunit*. *Journal of Biological Chemistry*, 2011. **286**(23): p. 20208-20216.
84. Isom, Daniel G., et al., *Protons as Second Messenger Regulators of G Protein Signaling*. *Molecular Cell*, 2013. **51**(4): p. 531-538.
85. Sutherland, C.M., et al., *Elm1p Is One of Three Upstream Kinases for the Saccharomyces cerevisiae SNF1 Complex*. *Current Biology*, 2003. **13**(15): p. 1299-1305.
86. Tappa, S., et al., *PPI phosphatase-binding motif in Reg1 protein of Saccharomyces cerevisiae is required for interaction with both the PPI phosphatase Glc7 and the Snf1 protein kinase*. *Cellular Signalling*, 2010. **22**(7): p. 1013-1021.
87. Elbing, K., Rhonda R. McCartney, and Martin C. Schmidt, *Purification and characterization of the three Snf1-activating kinases of Saccharomyces cerevisiae*. *Biochemical Journal*, 2006. **393**(Pt 3): p. 797-805.
88. Hong, S.-P. and M. Carlson, *Regulation of Snf1 Protein Kinase in Response to Environmental Stress*. *Journal of Biological Chemistry*, 2007. **282**(23): p. 16838-16845.

89. Winkler, A., et al., *Heat stress activates the yeast high-osmolarity glycerol mitogen-activated protein kinase pathway, and protein tyrosine phosphatases are essential under heat stress*. Eukaryot Cell, 2002. **1**(2): p. 163-73.
90. Panadero, J., et al., *A downshift in temperature activates the high osmolarity glycerol (HOG) pathway, which determines freeze tolerance in Saccharomyces cerevisiae*. J Biol Chem, 2006. **281**(8): p. 4638-45.
91. Haghazari, E. and W.-D. Heyer, *The Hog1 MAP kinase pathway and the Mec1 DNA damage checkpoint pathway independently control the cellular responses to hydrogen peroxide*. DNA Repair, 2004. **3**(7): p. 769-776.
92. Hickman, M.J., D. Spatt, and F. Winston, *The Hog1 mitogen-activated protein kinase mediates a hypoxic response in Saccharomyces cerevisiae*. Genetics, 2011. **188**(2): p. 325-38.
93. Hao, N., et al., *A systems-biology analysis of feedback inhibition in the Sho1 osmotic-stress-response pathway*. Current biology, 2007. **17**(8): p. 659-667.
94. Orij, R., et al., *In vivo measurement of cytosolic and mitochondrial pH using a pH-sensitive GFP derivative in Saccharomyces cerevisiae reveals a relation between intracellular pH and growth*. Microbiology, 2009. **155**(Pt 1): p. 268-78.
95. Miesenböck, G., D.A. De Angelis, and J.E. Rothman, *Visualizing secretion and synaptic transmission with pH-sensitive green fluorescent proteins*. Nature, 1998. **394**(6689): p. 192-5.
96. Fiehn, O., *Metabolomics--the link between genotypes and phenotypes*. Plant Mol Biol, 2002. **48**(1-2): p. 155-71.
97. Hounsa, C.G., et al., *Role of trehalose in survival of Saccharomyces cerevisiae under osmotic stress*. Microbiology, 1998. **144** (Pt 3): p. 671-80.
98. Albertyn, J., et al., *GPD1, which encodes glycerol-3-phosphate dehydrogenase, is essential for growth under osmotic stress in Saccharomyces cerevisiae, and its expression is regulated by the high-osmolarity glycerol response pathway*. Mol Cell Biol, 1994. **14**(6): p. 4135-44.
99. Hazelwood, L.A., et al., *The Ehrlich pathway for fusel alcohol production: a century of research on Saccharomyces cerevisiae metabolism*. Appl Environ Microbiol, 2008. **74**(8): p. 2259-66.
100. Hazelwood, L.A., et al., *A new physiological role for Pdr12p in Saccharomyces cerevisiae: export of aromatic and branched-chain organic acids produced in amino acid catabolism*. FEMS Yeast Res, 2006. **6**(6): p. 937-45.

101. Schoondermark-Stolk, S.A., et al., *Bat2p is essential in Saccharomyces cerevisiae for fusel alcohol production on the non-fermentable carbon source ethanol*. FEMS Yeast Res, 2005. **5**(8): p. 757-66.
102. Kingsbury, J.M., N.D. Sen, and M.E. Cardenas, *Branched-Chain Aminotransferases Control TORC1 Signaling in Saccharomyces cerevisiae*. PLoS Genet, 2015. **11**(12): p. e1005714.
103. Hiroaki, H., *Recent applications of isotopic labeling for protein NMR in drug discovery*. Expert Opin Drug Discov, 2013. **8**(5): p. 523-36.
104. Hao, N., et al., *Regulators of G protein signaling and transient activation of signaling: experimental and computational analysis reveals negative and positive feedback controls on G protein activity*. J Biol Chem, 2003. **278**(47): p. 46506-15.
105. Michell, R.H., et al., *The stimulation of inositol lipid metabolism that accompanies calcium mobilization in stimulated cells: defined characteristics and unanswered questions*. Philos Trans R Soc Lond B Biol Sci, 1981. **296**(1080): p. 123-38.
106. Harper, A.E., R.H. Miller, and K.P. Block, *Branched-chain amino acid metabolism*. Annu Rev Nutr, 1984. **4**: p. 409-54.
107. Strauss, K.A., E.G. Puffenberger, and D.H. Morton, *Maple Syrup Urine Disease*, in *GeneReviews(R)*, R.A. Pagon, et al., Editors. 1993: Seattle (WA).
108. Tavares, R.G., et al., *Inhibition of glutamate uptake into synaptic vesicles of rat brain by the metabolites accumulating in maple syrup urine disease*. J Neurol Sci, 2000. **181**(1-2): p. 44-9.
109. Funchal, C., et al., *Reduction of glutamate uptake into cerebral cortex of developing rats by the branched-chain alpha-keto acids accumulating in maple syrup urine disease*. Neurochem Res, 2004. **29**(4): p. 747-53.
110. Amaral, A.U., et al., *Alpha-ketoisocaproic acid and leucine provoke mitochondrial bioenergetic dysfunction in rat brain*. Brain Res, 2010. **1324**: p. 75-84.
111. Sgaravatti, A.M., et al., *Inhibition of brain energy metabolism by the alpha-keto acids accumulating in maple syrup urine disease*. Biochim Biophys Acta, 2003. **1639**(3): p. 232-8.
112. Villani, G.R., et al., *"Classical organic acidurias": diagnosis and pathogenesis*. Clin Exp Med, 2016.
113. Adeva-Andany, M.M., et al., *Enzymes involved in branched-chain amino acid metabolism in humans*. Amino Acids, 2017.
114. Huang, Y., et al., *Branched-chain amino acid metabolism in heart disease: an epiphenomenon or a real culprit?* Cardiovasc Res, 2011. **90**(2): p. 220-3.

115. Sun, H., et al., *Catabolic Defect of Branched-Chain Amino Acids Promotes Heart Failure*. *Circulation*, 2016. **133**(21): p. 2038-49.
116. Brachmann, C.B., et al., *Designer deletion strains derived from *Saccharomyces cerevisiae* S288C: a useful set of strains and plasmids for PCR-mediated gene disruption and other applications*. *Yeast*, 1998. **14**(2): p. 115-32.
117. Wach, A., et al., *New heterologous modules for classical or PCR-based gene disruptions in *Saccharomyces cerevisiae**. *Yeast*, 1994. **10**(13): p. 1793-808.
118. Hentges, P., et al., *Three novel antibiotic marker cassettes for gene disruption and marker switching in *Schizosaccharomyces pombe**. *Yeast*, 2005. **22**(13): p. 1013-9.
119. Gietz, R.D. and R.A. Woods, *Transformation of yeast by lithium acetate/single-stranded carrier DNA/polyethylene glycol method*. *Methods Enzymol*, 2002. **350**: p. 87-96.
120. Storici, F. and M. Resnick, *The Delitto Perfetto Approach to In Vivo Site-Directed Mutagenesis and Chromosome Rearrangements with Synthetic Oligonucleotides in Yeast*. *Methods in Enzymology*, 2006. **409**: p. 329-345.
121. Funakoshi, M. and M. Hochstrasser, *Small epitope-linker modules for PCR-based C-terminal tagging in *Saccharomyces cerevisiae**. *Yeast*, 2009. **26**(3): p. 185-92.
122. Cormack, B.P., et al., *Yeast-enhanced green fluorescent protein (yEGFP): a reporter of gene expression in *Candida albicans**. *Microbiology*, 1997. **143** (Pt 2): p. 303-11.
123. Siekhaus, D.E. and D.G. Drubin, *Spontaneous receptor-independent heterotrimeric G-protein signalling in an RGS mutant*. *Nat Cell Biol*, 2003. **5**(3): p. 231-5.
124. Sikorski, R.S. and P. Hieter, *A system of shuttle vectors and yeast host strains designed for efficient manipulation of DNA in *Saccharomyces cerevisiae**. *Genetics*, 1989. **122**(1): p. 19-27.
125. Dohlman, H.G., et al., *Pheromone action regulates G-protein alpha-subunit myristoylation in the yeast *Saccharomyces cerevisiae**. *Proc Natl Acad Sci U S A*, 1993. **90**(20): p. 9688-92.
126. English, J.G., et al., *MAPK feedback encodes a switch and timer for tunable stress adaptation in yeast*. *Sci Signal*, 2015. **8**(359): p. ra5.
127. Sha, W., et al., *Metabolomic profiling can predict which humans will develop liver dysfunction when deprived of dietary choline*. *FASEB J*, 2010. **24**(8): p. 2962-75.
128. Dehaven, C.D., et al., *Organization of GC/MS and LC/MS metabolomics data into chemical libraries*. *J Cheminform*, 2010. **2**(1): p. 9.

129. Maly, J. and K.A. Crowhurst, *Expression, purification and preliminary NMR characterization of isotopically labeled wild-type human heterotrimeric G protein α_{i1}* . *Protein Expr Purif*, 2012. **84**(2): p. 255-64.
130. Courchesne, W.E., R. Kunisawa, and J. Thorner, *A putative protein kinase overcomes pheromone-induced arrest of cell cycling in *S. cerevisiae**. *Cell*, 1989. **58**(6): p. 1107-19.
131. Elion, E.A., P.L. Grisafi, and G.R. Fink, *FUS3 encodes a *cdc2+*/CDC28-related kinase required for the transition from mitosis into conjugation*. *Cell*, 1990. **60**(4): p. 649-64.
132. Gartner, A., K. Nasmyth, and G. Ammerer, *Signal transduction in *Saccharomyces cerevisiae* requires tyrosine and threonine phosphorylation of FUS3 and KSS1*. *Genes Dev*, 1992. **6**(7): p. 1280-92.
133. Stevenson, B.J., et al., *Constitutive mutants of the protein kinase STE11 activate the yeast pheromone response pathway in the absence of the G protein*. *Genes Dev*, 1992. **6**(7): p. 1293-304.
134. Zhou, Z., et al., *Pheromone-induced signal transduction in *Saccharomyces cerevisiae* requires the sequential function of three protein kinases*. *Mol Cell Biol*, 1993. **13**(4): p. 2069-80.
135. Avruch, J., *MAP kinase pathways: the first twenty years*. *Biochim Biophys Acta*, 2007. **1773**(8): p. 1150-60.
136. Pei, Y., S. Dong, and B.L. Roth, *Generation of designer receptors exclusively activated by designer drugs (DREADDs) using directed molecular evolution*. *Curr Protoc Neurosci*, 2010. **Chapter 4**: p. Unit 4 33.
137. Dong, S., S.C. Rogan, and B.L. Roth, *Directed molecular evolution of DREADDs: a generic approach to creating next-generation RASSLs*. *Nat Protoc*, 2010. **5**(3): p. 561-73.
138. Dowell, S.J. and A.J. Brown, *Yeast assays for G-protein-coupled receptors*. *Receptors Channels*, 2002. **8**(5-6): p. 343-52.
139. Minic, J., et al., *Functional expression of olfactory receptors in yeast and development of a bioassay for odorant screening*. *FEBS J*, 2005. **272**(2): p. 524-37.
140. Minic, J., et al., *Yeast system as a screening tool for pharmacological assessment of g protein coupled receptors*. *Curr Med Chem*, 2005. **12**(8): p. 961-9.
141. Fujita, K., et al., *Yeast pheromone signaling pathway as a bioassay to assess the effect of chemicals on mammalian peptide hormones*. *Ecotoxicol Environ Saf*, 2003. **56**(3): p. 358-66.
142. Dohlman, H.G. and J. Thorner, *REGULATION OF G PROTEIN-INITIATED SIGNAL TRANSDUCTION IN YEAST: Paradigms and Principles*. *Annual Review of Biochemistry*, 2001. **70**(1): p. 703-754.

143. Wang, Y. and H.G. Dohlman, *Pheromone signaling mechanisms in yeast: a prototypical sex machine*. Science, 2004. **306**(5701): p. 1508-9.
144. Choi, K.Y., et al., *Ste5 tethers multiple protein kinases in the MAP kinase cascade required for mating in S. cerevisiae*. Cell, 1994. **78**(3): p. 499-512.
145. Kusari, A.B., et al., *A conserved protein interaction network involving the yeast MAP kinases Fus3 and Kss1*. J Cell Biol, 2004. **164**(2): p. 267-77.
146. Janke, C., et al., *A versatile toolbox for PCR-based tagging of yeast genes: new fluorescent proteins, more markers and promoter substitution cassettes*. Yeast, 2004. **21**(11): p. 947-62.
147. Hoffman, G.A., T.R. Garrison, and H.G. Dohlman, *Endoproteolytic processing of Sst2, a multidomain regulator of G protein signaling in yeast*. J Biol Chem, 2000. **275**(48): p. 37533-41.
148. Schneider, C.A., W.S. Rasband, and K.W. Eliceiri, *NIH Image to ImageJ: 25 years of image analysis*. Nat Methods, 2012. **9**(7): p. 671-5.
149. Janes, K.A., *An analysis of critical factors for quantitative immunoblotting*. Sci Signal, 2015. **8**(371): p. rs2.
150. Hoffman, G.A., T.R. Garrison, and H.G. Dohlman, *Analysis of RGS proteins in Saccharomyces cerevisiae*. Methods Enzymol, 2002. **344**: p. 617-31.
151. Chan, R.K. and C.A. Otte, *Isolation and genetic analysis of Saccharomyces cerevisiae mutants supersensitive to G1 arrest by a factor and alpha factor pheromones*. Mol Cell Biol, 1982. **2**(1): p. 11-20.
152. Chan, R.K. and C.A. Otte, *Physiological characterization of Saccharomyces cerevisiae mutants supersensitive to G1 arrest by a factor and alpha factor pheromones*. Mol Cell Biol, 1982. **2**(1): p. 21-9.
153. MacKay, V.L., et al., *The Saccharomyces cerevisiae BAR1 gene encodes an exported protein with homology to pepsin*. Proc Natl Acad Sci U S A, 1988. **85**(1): p. 55-9.
154. Choi, Y.J., et al., *Saccharomyces cerevisiae Ste5 is important for induction and substrate specificity of Fus3 MAP kinase in the pheromone signaling pathway*. Mol Cells, 2000. **10**(3): p. 301-8.
155. Bhattacharyya, R.P., et al., *The Ste5 scaffold allosterically modulates signaling output of the yeast mating pathway*. Science, 2006. **311**(5762): p. 822-6.
156. Nagiec, M.J., et al., *Signal inhibition by a dynamically regulated pool of monophosphorylated MAPK*. Mol Biol Cell, 2015. **26**(18): p. 3359-71.

157. Hur, J.Y., et al., *Quantitative profiling of dual phosphorylation of Fus3 MAP kinase in Saccharomyces cerevisiae*. Mol Cells, 2008. **26**(1): p. 41-7.
158. Roberts, R.L. and G.R. Fink, *Elements of a single MAP kinase cascade in Saccharomyces cerevisiae mediate two developmental programs in the same cell type: mating and invasive growth*. Genes Dev, 1994. **8**(24): p. 2974-85.
159. Cook, J.G., L. Bardwell, and J. Thorner, *Inhibitory and activating functions for MAPK Kss1 in the S. cerevisiae filamentous-growth signalling pathway*. Nature, 1997. **390**(6655): p. 85-8.
160. Kinoshita, E., et al., *Phosphate-binding tag, a new tool to visualize phosphorylated proteins*. Molecular & Cellular Proteomics, 2006. **5**(4): p. 749-757.
161. Kinoshita-Kikuta, E., et al., *Label-free kinase profiling using phosphate affinity polyacrylamide gel electrophoresis*. Molecular & Cellular Proteomics, 2007. **6**(2): p. 356-366.
162. Reid, B.G. and G.C. Flynn, *Chromophore formation in green fluorescent protein*. Biochemistry, 1997. **36**(22): p. 6786-91.
163. Tsien, R.Y., *The green fluorescent protein*. Annu Rev Biochem, 1998. **67**: p. 509-44.
164. Zhu, H., et al., *Global analysis of protein activities using proteome chips*. Science, 2001. **293**(5537): p. 2101-5.
165. Kulak, N.A., et al., *Minimal, encapsulated proteomic-sample processing applied to copy-number estimation in eukaryotic cells*. Nat Methods, 2014. **11**(3): p. 319-24.
166. Isom, D.G., et al., *A miniaturized technique for assessing protein thermodynamics and function using fast determination of quantitative cysteine reactivity*. Proteins, 2011. **79**(4): p. 1034-47.
167. Zhu, M., et al., *Pheromone- and RSP5-dependent ubiquitination of the G protein beta subunit Ste4 in yeast*. J Biol Chem, 2011. **286**(31): p. 27147-55.
168. Apanovitch, D.M., et al., *Sst2 is a GTPase-activating protein for Gpa1: purification and characterization of a cognate RGS-Galpha protein pair in yeast*. Biochemistry, 1998. **37**(14): p. 4815-22.
169. Alepuz, P.M., et al., *Osmostress-induced transcription by Hot1 depends on a Hog1-mediated recruitment of the RNA Pol II*. The EMBO journal, 2003. **22**(10): p. 2433-2442.
170. Cook, K.E. and E.K. O'Shea, *Hog1 controls global reallocation of RNA Pol II upon osmotic shock in Saccharomyces cerevisiae*. G3 (Bethesda), 2012. **2**(9): p. 1129-36.

171. O'Rourke, S.M. and I. Herskowitz, *Unique and redundant roles for HOG MAPK pathway components as revealed by whole-genome expression analysis*. Mol Biol Cell, 2004. **15**(2): p. 532-42.
172. Duan, Y., et al., *The role of leucine and its metabolites in protein and energy metabolism*. Amino Acids, 2016. **48**(1): p. 41-51.
173. Sancak, Y., et al., *The Rag GTPases bind raptor and mediate amino acid signaling to mTORC1*. Science, 2008. **320**(5882): p. 1496-501.
174. Kim, E., et al., *Regulation of TORC1 by Rag GTPases in nutrient response*. Nat Cell Biol, 2008. **10**(8): p. 935-45.
175. Bonfils, G., et al., *Leucyl-tRNA synthetase controls TORC1 via the EGO complex*. Mol Cell, 2012. **46**(1): p. 105-10.
176. Panchaud, N., M.P. Peli-Gulli, and C. De Virgilio, *Amino acid deprivation inhibits TORC1 through a GTPase-activating protein complex for the Rag family GTPase Gtr1*. Sci Signal, 2013. **6**(277): p. ra42.
177. Yao, K., et al., *Leucine in Obesity: Therapeutic Prospects*. Trends Pharmacol Sci, 2016. **37**(8): p. 714-27.
178. Shimomura, Y., et al., *Nutraceutical effects of branched-chain amino acids on skeletal muscle*. J Nutr, 2006. **136**(2): p. 529S-532S.
179. Howatson, G., et al., *Exercise-induced muscle damage is reduced in resistance-trained males by branched chain amino acids: a randomized, double-blind, placebo controlled study*. J Int Soc Sports Nutr, 2012. **9**: p. 20.
180. White, P.J., et al., *Branched-chain amino acid restriction in Zucker-fatty rats improves muscle insulin sensitivity by enhancing efficiency of fatty acid oxidation and acyl-glycine export*. Mol Metab, 2016. **5**(7): p. 538-51.
181. Mayers, J.R., et al., *Tissue of origin dictates branched-chain amino acid metabolism in mutant Kras-driven cancers*. Science, 2016. **353**(6304): p. 1161-5.
182. Nishitani, S., et al., *Branched chain amino acid suppresses hepatocellular cancer stem cells through the activation of mammalian target of rapamycin*. PLoS One, 2013. **8**(11): p. e82346.
183. Sugiyama, K., L. Yu, and N. Nagasue, *Direct effect of branched-chain amino acids on the growth and metabolism of cultured human hepatocellular carcinoma cells*. Nutr Cancer, 1998. **31**(1): p. 62-8.
184. Yoshizawa, F., et al., *Tissue-specific regulation of 4E-BP1 and S6K1 phosphorylation by alpha-ketoisocaproate*. J Nutr Sci Vitaminol (Tokyo), 2004. **50**(1): p. 56-60.

185. Boebel, K.P. and D.H. Baker, *Comparative utilization of the alpha-keto and D- and L-alpha-hydroxy analogs of leucine, isoleucine and valine by chicks and rats*. J Nutr, 1982. **112**(10): p. 1929-39.
186. Lang, C.H., et al., *Chronic alpha-hydroxyisocaproic acid treatment improves muscle recovery after immobilization-induced atrophy*. Am J Physiol Endocrinol Metab, 2013. **305**(3): p. E416-28.
187. Mero, A.A., et al., *Effects of alpha-hydroxy-isocaproic acid on body composition, DOMS and performance in athletes*. J Int Soc Sports Nutr, 2010. **7**: p. 1.
188. Mozaffarian, D., et al., *Heart Disease and Stroke Statistics-2015 Update: A Report From the American Heart Association*. Circulation, 2014.
189. Braunwald, E. and R.A. Kloner, *Myocardial reperfusion: a double-edged sword?* J Clin Invest, 1985. **76**(5): p. 1713-9.
190. Yellon, D.M. and D.J. Hausenloy, *Myocardial reperfusion injury*. N Engl J Med, 2007. **357**(11): p. 1121-35.
191. Piper, H.M., D. García-Dorado, and M. Ovize, *A fresh look at reperfusion injury*. Cardiovasc Res, 1998. **38**(2): p. 291-300.
192. McCully, J.D., et al., *Differential contribution of necrosis and apoptosis in myocardial ischemia-reperfusion injury*. Am J Physiol Heart Circ Physiol, 2004. **286**(5): p. H1923-35.
193. Maroko, P.R. and E. Braunwald, *Effects of metabolic and pharmacologic interventions on myocardial infarct size following coronary occlusion*. Acta Med Scand Suppl, 1976. **587**: p. 125-36.
194. Hausenloy, D.J. and D.M. Yellon, *Myocardial ischemia-reperfusion injury: a neglected therapeutic target*. J Clin Invest, 2013. **123**(1): p. 92-100.
195. Hausenloy, D.J. and D.M. Yellon, *New directions for protecting the heart against ischaemia-reperfusion injury: targeting the Reperfusion Injury Salvage Kinase (RISK)-pathway*. Cardiovasc Res, 2004. **61**(3): p. 448-60.
196. Heidbreder, M., et al., *Remote vs. ischaemic preconditioning: the differential role of mitogen-activated protein kinase pathways*. Cardiovasc Res, 2008. **78**(1): p. 108-15.
197. Morrison, A. and J. Li, *PPAR-gamma and AMPK--advantageous targets for myocardial ischemia/reperfusion therapy*. Biochem Pharmacol, 2011. **82**(3): p. 195-200.
198. Dong, W., et al., *Keto acid metabolites of branched-chain amino acids inhibit oxidative stress-induced necrosis and attenuate myocardial ischemia-reperfusion injury*. J Mol Cell Cardiol, 2016. **101**: p. 90-98.